Fabrication of Sub 5-nm Plasmonic Nano-gap Nanostructures for Extreme Confinement of Optical Fields

Jeetendra Gour[1], **Sebastian Beer**[1], **Stefan Nolte**[1,2], **Uwe Zeitner**[1,2]

1. Institute of Applied Physics, Friedrich Schiller University Jena, Albert-Einstein-Str. 15, 07745 Jena, Germany
2. Fraunhofer Institute for Applied Optics and Precision Engineering IOF, Albert-Einstein-Str. 7, 07745 Jena, Germany

E-mail: jeetendra.gour@uni-jena.de

Squeezing light into nanometric volumes or confining it into nanometer-wide gaps in plasmonic metals can lead to extreme field enhancements, nonlinear optical effects, and optically induced electron tunneling. However, it has not been readily accessible to experimentalists due to the lack of reliable technology to realize uniform nano-gaps with sub-5 nm resolution. In this work, we use a combination of atomic layer deposition [1] and ion beam etching based planarization technique to obtain a reliable definition of the gap-size in a periodic gold grating.

In the paper, we introduce the technology process to realize structures with gap sizes in the sub-5 nm range and present our results demonstrating 3 nm wide, vertically oriented gaps in 1D grating structures in 30 nm thick gold films. The scanning electron microscope image in Fig. 1(a) shows a top view of the realized 1D nano-gap array . The scanning transmission electron micrograph in Fig. 1 (b) shows high resolution bright field cross-section of the nano-gap confirming sub-5nm vertical gaps. The process is very flexible and we are working on its application for the realization of plasmonic antenna structures of various lateral geometries with sub-5nm gaps.

The fabricated nano-gap structures are intended to be used for the investigation of the nonlinear optical processes such as wavelength conversion [2], optically induced electron tunneling and nonlinear resonance effects [3]. Further potential applications could be found in near field imaging, optical switching etc.
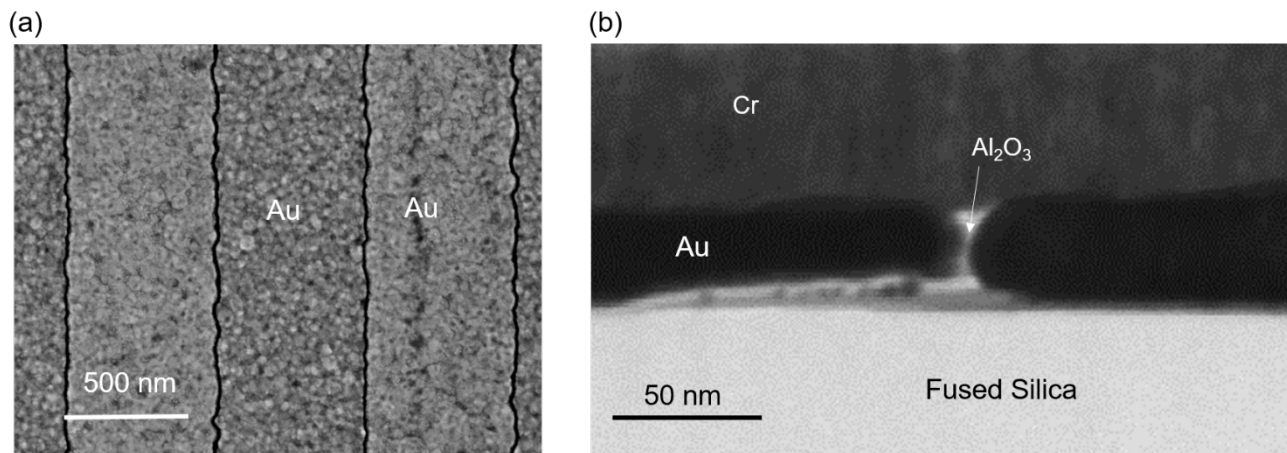

Fig. 1 (a) Top scanning electron micrograph of sub-5 nm nano-gap grating structures (Period=600 nm). (b)High resolution TEM image of the nano-gap cross-section.

References

[1] Chen, X., Park, HR., Pelton, M. et al. 2013. *Atomic layer lithography of wafer-scale nanogap arrays for extreme confinement of electromagnetic waves.* Nat Commun 4, 2361.

[2] Nezami,MS.,Yoo, D.,Hajisalem,G., Oh, SH. et. al. 2016. *ACS Photonics 3 (8)*, 1461-1467.

[3] Kley, EB., et al. 2006. *Nonlinear resonance effects on thin micro structured aluminum metal gratings by high power fs-laser pulses.* Proc. of SPIE Vol. 6149 614902-1.

Geometry optimization of the magnetic Purcell factor in high index dielectric nanostructures

Y. Brûlé[1], P. Wiecha[2], A. Cuche[3], V. Paillard[3], G. Colas des Francs[1]

1. *Laboratoire Interdisciplinaire Carnot de Bourgogne, ICB-CNRS, Université de Bourgogne Franche-Comté, 21000 Dijon, France,*
2. *Laboratoire d'Analyse et d'Architecture des Systèmes, LAAS-CNRS, Université de Toulouse, 31031 Toulouse, France*
3. *Centre d'Élaboration de Matériaux et d'Études Structurales, CEMES-CNRS, Université de Toulouse, 31055 Toulouse, France*
yoann.brule@u-bourgogne.fr

The coupling of the magnetic part of light to atoms is much weaker than the electric one. Hence, the development of novel applications based on magnetic response in the optical regime, such as negative-index metamaterials [1] or efficient nanoantennas [2], requires to focus on the engineering of the magnetic Local Density Of States (LDOS).
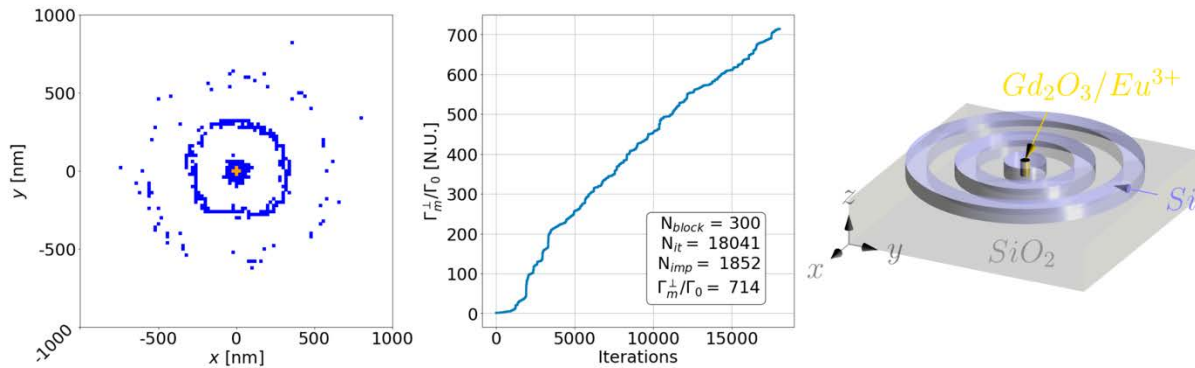

Fig. 1 Left : XY-plane projection of the optimized structure (orange : fixed core emitter, blue : Si nanopillars), Center : Evolution of the magnetic Purcell factor through the optimization iterations, Right : Scheme of the configuration extrapolated from the optimized nanostructure.

In this work, we use evolutionary algorithms coupled to the Green's Dyadic Method (GDM) in order to optimize the geometry of planar silicon dielectric nanoantennas for controlling the emission rate of magnetic (MD) or electric (ED) dipolar emitters (so-called Purcell factor) [3,4]. Depending on the nature and orientation of the dipoles, different optimized shapes are obtained, all presenting regular and periodical features. To summarize, we distinguish different behaviours in the near- and far-field zones of the dipolar emitter. In the far-field, we observe circular gratings for all the configurations. As far as the near-field zone is concerned, we observe strong differences for ED and MD emitters, with the presence or not of a Si core, that depends on both the dipole nature and orientation. Similar configurations have been guessed in the literature but our work reveals that they are close to be optimal. We determine the dimensions of a feasible 100 nm thickness planar dielectric silicon nanoantenna deposited on a glass substrate that leads to a $2 \cdot 10^3$ enhancement of the spontaneous decay rate of the magnetic dipolar transition in Eu^{3+} ions. Finally, to go beyond the "black box" optimization, we also discuss the physical origin of the obtained designs thanks to modal analysis but also in relation to the deterministic design approach recently developed by Mignuzzi *et al.* in [5].

This work paves the way toward a better comprehension of the interaction between quantum emitters and high index dielectric nanoantennas and could lead to innovative applications such as optical negative-index metamaterials or quantum technological components.

References

[1] Shalaev, V. 2007, *Optical negative-index metamaterials,* Nat. Photonics **1**, 41.
[2] Bidault, S. *et al*, 2019, *Dielectric nanoantennas to manipulate solid-state light emission*, J. Appl. Phys. **126**, 094104.
[3] Wiecha, P. *et al*, 2022, *"pyGDM" -python toolkit for nano-optics full-field simulations*, Comput. Phys. Commun. **270**, 108142.
[4] Brûlé, Y. *et al*, 2022, *Magnetic and electric Purcell factor control through geometry optimization of high index dielectric nanostructure*, in prep., arXiv:2201.01734.
[5] Mignuzzi, S. *et al*, 2019, *Nanoscale design of the local density of optical states,* Nano Lett., **19**, 1613.

Imaging-Based Hydrogen Sensing Based on Fano-like Spatial Distribution of Transmission in a Metal−Insulator−Metal Plasmonic Doppler Grating

Yi-Ju Chen[1], Fan-Cheng Lin[2], Ankit Kumar Singh[1], Lei Ouyang[1,3,4], Jer-Shing Huang[1,2,3,5,6]

1. Leibniz Institute of Photonic Technology, Albert-Einstein Straße 9, 07745 Jena, Germany
2. Department of Chemistry, National Tsing Hua University, Hsinchu 30013, Taiwan
3. Institute of Physical Chemistry and Abbe Center of Photonics, Friedrich-Schiller-Universität Jena, Helmholtzweg 4, D-07743 Jena, Germany
4. State Key Laboratory of Biogeology and Environmental Geology, Faculty of Materials Science and Chemistry, China University of Geosciences, Wuhan 430074, China
5. Research Center for Applied Sciences, Academia Sinica, Taipei 11529, Taiwan
6. Department of Electrophysics, National Yang Ming Chiao Tung University, Hsinchu 30010, Taiwan
E-mail: yi.ju.chen@uni-jena.de

To cope with global warming on a long-term basis, the role of sustainable and renewable energy becomes more and more important. Hydrogen has been recognized as an alternative to fossil fuels and a potentially valuable tool for tackling climate change. Due to the low explosion concentration (4%), using hydrogen requires a robust and sensitive sensor to monitor the concentration or detect the leakage of hydrogen. Optical hydrogen sensing methods are better than electrical methods because they are free from spark generation and feasible for remote optical readout. Conventional spectroscopic nanosensors require broadband excitation and spectrometers, rendering the devices bulky and complex. An alternative is the monochromatic imaging-based sensor, which observes the optical response of a series of spatially varying nanostructures such that the spatial intensity distribution provides the analytical signal. In this case, the setup only requires an imaging system and a smartly designed platform to report the spatial distribution of analytical optical signals. [1-2]

In this work, a spatial intensity-based hydrogen sensing platform is presented based on Fano-like spatial distribution of the transmission in a Pd-Al$_2$O$_3$-Au metal-insulator-metal plasmonic Doppler grating (MIM-PDG) (Fig.1a). [3] Due to the mode interference inside the MIM-PDG, a spatial Fano-like transmission intensity profile can be observed at a single frequency (Fig.1b). Upon hydrogen absorption, the spatial transmission profiles changes (Fig. 1c). By analyzing the spatial profile with a non-spectral parametric Fano resonance model, the coupling and damping parameters of the Fano resonance under different hydrogen concentrations can be obtained to establish a calibration curve for quantitative analysis. Increasing the hydrogen absorption can lead to three different responses of the presented MIM-PDG platform, namely increasing, decreasing, and unchanged transmission. While the first two cases are useful for quantification of hydrogen absorption, the third case represents hydrogen insensitive gratings, which provide stable optical response resistive to hydrogen absorption and can serve as a reference signal under fluctuating hydrogen concentration.
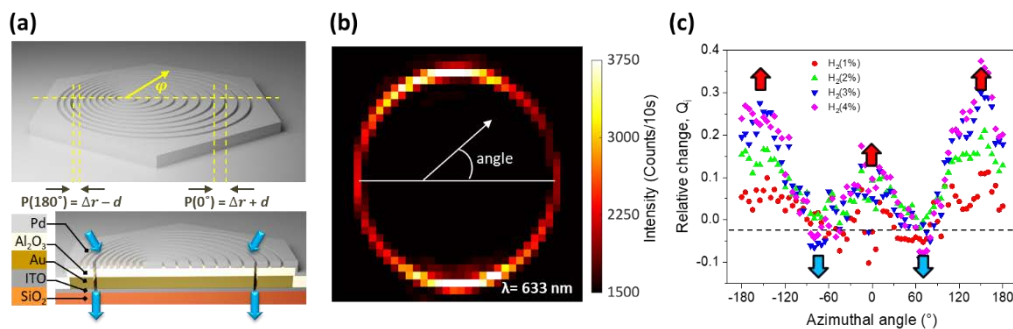

Fig. 1 (a) The geometry and cross section of the Pd-Al$_2$O$_3$-Au MIM-PDG structure on an ITO coated coverslip. Only one circular ring is completely milling until the ITO layer. Rest rings are only milled into the Pd layer. The grating period continuously changes with the in-plane azimuthal angle (φ) from the largest period ($\Delta r + d$) at $\varphi = 0°$ to the smallest period ($\Delta r - d$) at $\varphi = 180°$. (b) Monochromatic transmission intensity image of the MIM-PDG illuminated by an unpolarized source at 633 nm. (c) Changes in the transmission intensity relative to 0% hydrogen as functions of azimuthal angle for 1% (red), 2% (green), 3% (blue), and 4% (cyan) hydrogen concentrations. The red (blue) arrows mark the azimuthal angles, at which the transmission intensity increases (decreases) with increasing concentration of hydrogen.

References

[1] See, K.-M. *et al.* 2017 *Nanoscale* **9**, 10811-10819.
[2] Lin, F.-C. *et al.* 2019 *Anal. Chem.* **91**, 9382-9387.
[3] Chen, Y.-J. *et al.* 2021 *Adv. Opt. Mater.* **9**, 2100869.

Chiral Scatterometry on Gold-Nanohelicoid-on-Mirror Structures

Yilin Chen, Jianfang Wang[*]

Department of Physics, The Chinese University of Hong Kong, Shatin, Hong Kong SAR, China

E-mail: jfwang@phy.cuhk.edu.hk

Chiral molecules and nanostructures exhibiting unique chiroptical responses are promising materials for applications in sensing, optical data storage, and displays [1]. Plasmonic chiral nanostructures demonstrate a diverse chiral response as plasmons scatter and absorb circularly polarized light (CPL) differently. Chiral scatterometry of chiral nanoparticles has been used to characterize their chiroptical properties [2]. Herein we focus on the effect of the dielectric properties of substrates on the chiroptical scattering of gold nanohelicoids (GNHs). The GNHs were synthesized by a seed-mediated growth method. They show distinct spectral and structural handedness. The scattering g-factor signals of the GNHs-on-substrate structures were measured by single-particle differential dark-field scattering upon transfer of the GNHs from silica substrates to gold films (Fig. 1a,b). The large localized electromagnetic enhancements can be achieved with the single GNHs separated from the gold film by a thin dielectric layer, resulting in larger differential scattering (Fig. 1c). The degree of scattering g-factor of the GNH-on-mirror structures was up to 6 times larger than that for the ensemble (Fig. 1d). Averaging over the L-handed and D-handed GNHs with random orientations on gold films also showed good mirror symmetry. We systematically studied the chiral scattering properties and the plasmonic modes of the GNH-on-mirror structures. Our results of the substrate-based optical chirality in chiral nanosystems shed new light on chiral light–matter interactions at substrate–nanostructure interfaces.
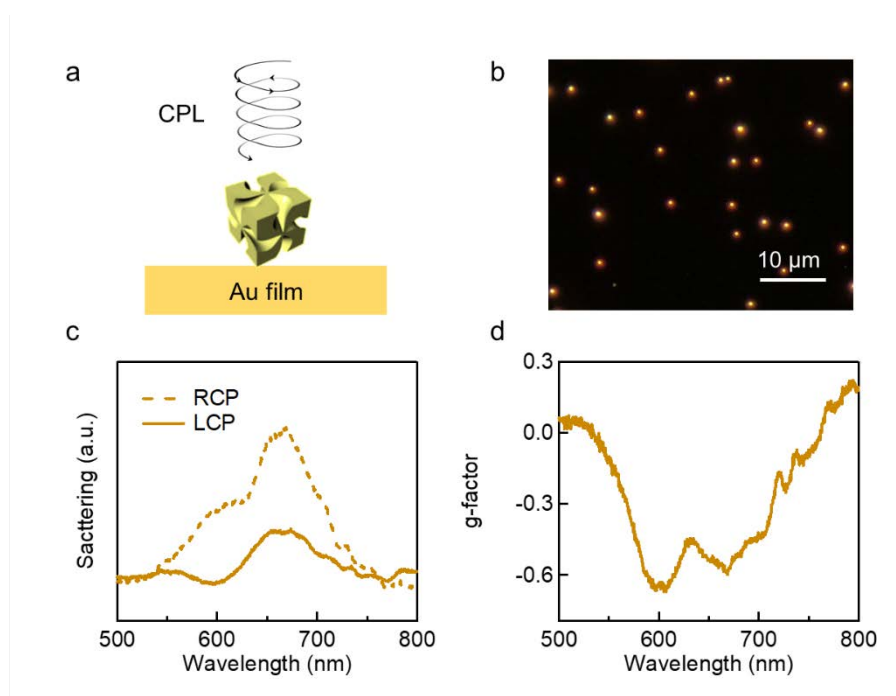

Fig. 1 (a) Schematic diagram and (b) dark-field scattering image of the GNH-on-mirror structures under CPL. (c) Measured scattering spectra under left- (solid) and right-handed CPL (dashed) and (d) calculated scattering g-factor of the GNH-on-mirror structure with a 1-nm-thickness dielectric spacer.

References

[1] Lee H. E.; Ahn H. Y.; Mun J.; Lee, Y. Y.; Kim, M.; Cho, N. H.; Chang K.; Kim W. S.; Rho J.; Nam, K. T. 2018. *Nature*, 556, 360.
[2] Karst J.; Cho N. H.; Kim H.; Lee H. E.; Nam K. T.; Giessen, H.; Hentschel, M. 2019. *ACS nano*, 13, 8659.

THz Band-stop Filter using a Bragg Grating

Seyedali Dehghanian[1,] **Levi Smith**[1,] **Thomas Darcie**[1]

1. Department of Electrical and Computer Engineering, University of Victoria, Victoria, BC V8P 5C2, Canada

E-mail: adehghanian@uvic.ca

The terahertz region of electromagnetic spectrum has become a significant research area due to its various applications in science. Effective terahertz wave filtering in systems requires integrated THz System-On-Chip (TSoC) components. A low-loss, low-distortion and low-pulse-dispersion TSoC has been demonstrated using Photoconductive Switch (PCS) devices bonded directly to a Coplanar Strip-line (CPS) transmission line defined using photolithography on 1μm-thin Si_3N_4 membrane [1]. Based on this capability, it is now possible to develop different components for the TSoC. Here, a novel THz Bragg Grating (TBG) integrated into the CPS transmission line is presented to reject specific spectral components from a THz-bandwidth transmitted pulse. The Bragg frequency was selected to be 0.8 THz.

Previous studies have demonstrated the operation of band-stop filters in the THz frequency range, working at a center frequency of 600 GHz. To characterize these filters, they were embedded in a micro-strip line attached to photoconductive switches that serve as THz emitters and detectors [2]. Some studies have also been conducted to filter THz specific spectrum using other materials such as graphene or silicon [3,4]. This work focuses on developing integrated, compact and efficient TSoC technologies in which guided-wave THz systems replace the current free-space THz systems.

Fig. 1 Structure of TBG integrated in CPS transmission line.

Here we analyze a structure compatible with experimental fabrication. A 200 nm layer of gold (Au) was applied to a Si_3N_4 membrane. There are N identical cascaded sections of length $\Lambda = \lambda_B/2\sqrt{e_{eff}}$ in the proposed THz Bragg filter (TBG). The length of the TBG restricts increasing the number of sections because a longer structure introduces more attenuation. We set N to be 10, 20, and 40 to represent of longer filters. Fig.1 illustrates the total structure and unit cell: each units cell consists of two quarter wave sections, $L_o = \Lambda/4$, and Z_o, and one half wave section, $L_1 = \Lambda/2$, and Z_1. The system was modelled using a cascade of two-port ABCD transmission matrices for lossy transmission lines. The cascaded ABCD matrices were then converted to S-parameters using standard methods to which was used to characterize the reflection coefficient (Fig. 2).
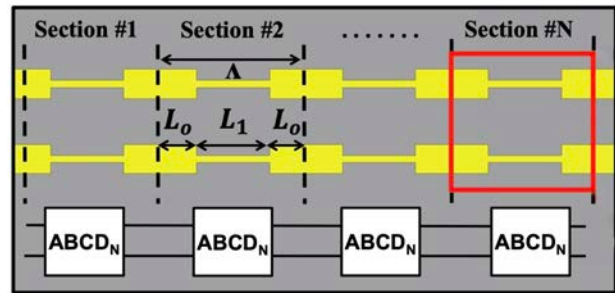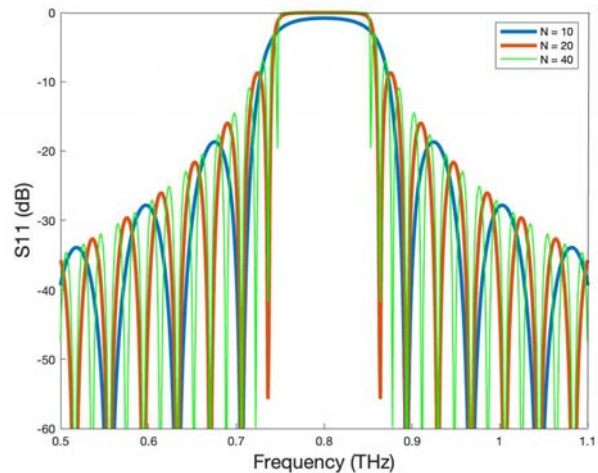

Fig. 2 Reflection coefficient of TBG for N equal to 10, 20 and 40

References

[1] Smith, R., & Darcie, T. (2019). Demonstration of a low-distortion terahertz system-on-chip using a CPS waveguide on a thin membrane substrate. Optics Express, 27(10), 13653. https://doi.org/10.1364/oe.27.013653

[2] Cunningham, J., Wood, C., Davies, A. G., Hunter, I., Linfield, E. H., & Beere, H. E. (2005, May 23). Terahertz frequency range band-stop filters. AIP Publishing. Retrieved February 11, 2022, from https://aip.scitation.org/doi/10.1063/1.1938255

[3] Ram, G. C., Sambaiah, P., Yuvaraj, S., & Kartikeyan, M. V. (2021, November 27). *Tunable bandstop filter using graphene in terahertz frequency band*. AEU - International Journal of Electronics and Communications. Retrieved February 11, 2022, from https://www.sciencedirect.com/science/article/pii/S1434841121004441

[4] Gao, W., Lee, W. S. L., Fumeaux, C., & Withayachumnankul, W. (2021, July 1). *Effective-medium-clad Bragg grating filters*. AIP Publishing. Retrieved February 11, 2022, from https://aip.scitation.org/doi/10.1063/5.0051310

Deep subwavelength control of circularly polarized light by using cathodoluminescence nanoscopy

Zheyu Fang[1*]

[1]School of Physics, State Key Laboratory for Mesoscopic Physics, Academy for Advanced Interdisciplinary Studies, Collaborative Innovation Center of Quantum Matter, and Nano-optoelectronics Frontier Center of Ministry of Education, Peking University, Beijing 100871

E-mail: zhyfang@pku.edu.cn

Circularly polarized light is crucial for the modern physics research. Highly integrated nanophotonic device further requires the fully control of circularly polarized light at nanoscale, which is limited via optical methods due to the optical diffraction limit. Here, we report several approaches to manipulate circularly polarized light emission at deep subwavelength scale by electron beam. Circularly polarized cathodoluminescence [1] and Smith-Purcell radiation can be generated via precise stimulation on metal or hybrid nanostructures, while the chirality and direction of emission can be actively controlled by shifting the electron impact position within 100 nm.

As a noninvasive technique, cathodoluminescence (CL) microscopy and spectroscopy with nanoscale resolution have been successfully utilized in the electromagnetic mode investigation of plasmonic nanostructures. The scanning electron beam functions as a local dipole source, enabling flexible and selectively mode excitation and control. Using chiral CL nanoscopy, we found new chiroptical effects that is hidden in the near-field of the achiral nanostructure and reported a selective manipulation of photon spin angular momentum at a deep subwavelength scale via electron-induced optical spin Hall effect (OSHE) in Au nanoantennas [2,3]. The steering of OSHE under electron excitation with nanoscale impinging position movement can be applied for a spin-dependent binary encoding.

Cathodoluminescence nanoscopy has been successfully used in the detection of local density of states in photonic nanostructure as well, which directly determines the radiative properties of quantum emitters as Purcell effect. By resolving radiated power into LCP and RCP contributions, chiral CL emissions are shown to directly render the chiral radiative LDOS that governs the radiative decay into either LCP or RCP channels [4], enabling the characterization of chiral light-matter interactions like chiral photon emissions. Furthermore, we can use CL nanoscopy to control the valley polarization in 2D transition metal dichalcogenides, tailor the optical properties of excitons [5].

These approaches may offer exciting opportunities for compact electron-driven source in opto-electronic circuits with switchable chirality and open new prospects at the interface of nanophotonic and quantum optics.

References

[1] Han, T. Y.; Zu, S.; Li, Z. W.; Jiang, M. L.; Zhu, X.; Fang, Z. Y., Reveal and Control of Chiral Cathodoluminescence at Subnanoscale. *Nano Letters* **2018,** *18* (1), 567-572.

[2] Zu, S.; Han, T. Y.; Jiang, M. L.; Lin, F.; Zhu, X.; Fang, Z. Y., Deep-Subwavelength Resolving and Manipulating of Hidden Chirality in Achiral Nanostructures. *Acs Nano* **2018,** *12* (4), 3908-3916.

[3] Chi, C.; Jiang, Q.; Liu, Z.; Zheng, L.; Jiang, M.; Zhang, H.; Lin, F.; Shen, B.; Fang, Z., Selectively steering photon spin angular momentum via electron-induced optical spin Hall effect. *Sci Adv* **2021,** *7* (18), eabf8011.

[4] Zu, S.; Han, T. Y.; Jiang, M. L.; Liu, Z. X.; Jiang, Q.; Lin, F.; Zhu, X.; Fang, Z. Y., Imaging of Plasmonic Chiral Radiative Local Density of States with Cathodoluminescence Nanoscopy. *Nano Letters* **2019,** *19* (2), 775-780.

[5] Zheng, L.; Liu, Z.; Liu, D.; Wang, X.; Li, Y.; Jiang, M.; Lin, F.; Zhang, H.; Shen, B.; Zhu, X.; Gong, Y.; Fang, Z., Deep subwavelength control of valley polarized cathodoluminescence in h-BN/WSe2/h-BN heterostructure. *Nat Commun* **2021,** *12* (1).

Fabry-Pérot Phonon Polaritons in Boron Nitride Nanotube Resonators

Cassandra Phillips, <u>Yi-Fang Lai</u>, Gilbert C. Walker*

Department of Chemistry, University of Toronto, 80 St. George Street, Toronto, Ontario M5S 3H6, Canada

*E-mail: gilbert.walker@utoronto.ca. Web: thewalkerlab.com

Phonon polaritons (PhPs) results from the coupling between optical photons and lattice vibrational phonons; PhPs offer extreme confinement of optical fields and strong dispersion in the mid-infrared spectral region [1]. This strong confinement can be used in SERS enhancement, driving reactions, sensor, hyperlensing, and other applications [2-6]. To study the propagation and interference of PhPs in a 1-D system, we employ scattering scanning near-field optical microscopy (s-SNOM), analytical, and computational techniques to describe the resonance behavior observed in boron nitride nanotubes (BNNTs), where strong optical anisotropy supports the propagation of volume-confined hyperbolic PhPs (HPhPs) [7-9].

We observe that, in BNNTs of a sufficiently small length, the reflected standing waves from both terminals strongly interfere with one another, leading to large constructive enhancement at select wavelengths through Fabry-Pérot interference (Fig. 1). The resonance of HPhPs results in the discretization of the dispersion relationship, and their intensity can be nicely simulated both analytically and computationally using a Fabry-Pérot model. The 1-D nano-resonant behavior illustrates methods to increase and localize field strength at positions on a BNNT nanotube.
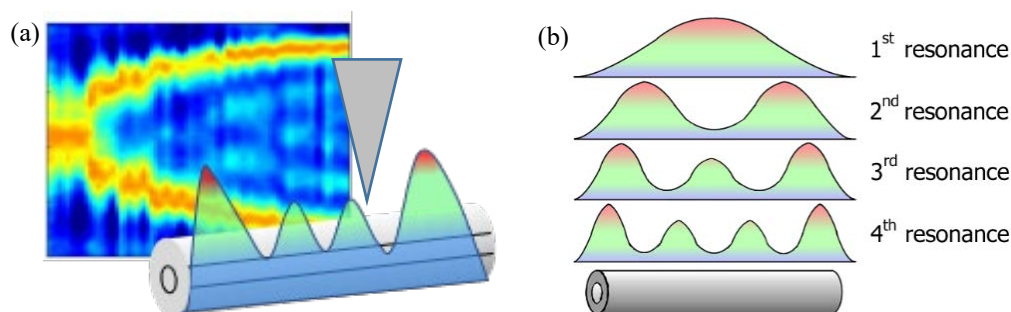

Fig. 1 (a) Experimental spatiospectral image of the imaginary optical response of a short (0.88 μm) BNNT in the mid-IR region, along with a schematic illustration of an AFM probe imaging the volume-confined PhPs via the scattered nearfield. (b) Schematic showing the appearance of discretized, increasing resonant modes in a BNNT.

References

[1] Basov, D. N.; Fogler, M. M.; Abajo, F. J. G. de. 2016. *Science*, 354 (6309)
[2] Caldwell, J. D.; Lindsay, L.; Giannini, V.; Vurgaftman, I.; Reinecke, T. L.; Maier, S. A.; Glembocki, O. J. Low-Loss. 2015. *Nanophotonics*, 4 (1), 44–68.
[3] Barnes, W. L. 2006. *J. Opt. A: Pure Appl. Opt.*, 8 (4), S87–S93.
[4] Sanvitto, D.; Kéna-Cohen, S. 2016. *Nature Mater*, 15 (10), 1061–1073.
[5] Park, S.-M.; Lee, K. S.; Kim, J.-H.; Yeon, G. J.; Shin, H.-H.; Park, S.; Kim, Z. H. 2020. *J. Phys. Chem. Lett.*, 11 (21), 9313–9320.
[6] Qiu, L.; Mandal, A.; Morshed, O.; Meidenbauer, M. T.; Girten, W.; Huo, P.; Vamivakas, A. N.; Krauss, T. D. 2021. *J. Phys. Chem. Lett.*, 12 (20), 5030–5038.
[7] Poddubny, A.; Iorsh, I.; Belov, P.; Kivshar, Y. 2013. *Nat. Photonics*, 7 (12), 948–957.
[8] Zapata-Rodríguez, C. J.; Miret, J. J.; Vuković, S.; Belić, M. R. 2013. Opt. Express, OE, 21 (16), 19113–19127.
[9] Ferrari, L.; Wu, C.; Lepage, D.; Zhang, X.; Liu, Z. 2015. *Prog. Quantum Electron.*, 40, 1–40.

Investigating Spectrum of Double Nanoholes with Different Aperture and Gap Sizes

Behnam Khosravi[1], **Reuven Gordon**[2]

1. University of Victoria, 3800 Finnerty Road, Victoria, BC, Canada
2. University of Victoria, 3800 Finnerty Road, Victoria, BC, Canada
E-mail: rgordon@uvic.ca

Double nanoholes in metallic films can be used for trapping nano particles and single molecules in the gap between the holes. An incident laser beam on the holes, induces plasmonic resonances that create a force in the gap. The force brings in the particle and leads to a change in refractive index and transmission spectrum.

The resonance frequencies in the transmission spectrum depend on the size of the holes and the gap width in between. By tailoring these dimensions, the peaks can be shifted towards the desired frequency. These peaks are due to the wedge and gap plasmonic resonances in the structure [1]. In order to maximize the transmission changes during trapping of a particle, the laser wavelength should be at a slope in the transmission spectrum of the structure. An increase or decrease in the transmission can be observed when the particle is trapped.

The fabrication process involves colloidal nanolithography with polystyrene nanospheres and gold deposition on a glass surface, which forms double nano holes shown in Fig. 1A with a gap width of a few nanometers [2]. Nanospheres with different sizes and etching times were used to make holes with different gap widths.

The model used in FDTD simulations consists of two holes and a gap in between, on a gold layer on glass. The holes are filled with water and a nanoparticle was placed in the gap. Enlarging the holes diameter redshifts the peaks for hole resonances. By changing the gap width, the gap resonance shifts correspondingly. Transmission spectrum of a double nanohole with hole diameter of 150 nm is shown in Fig. 1B.
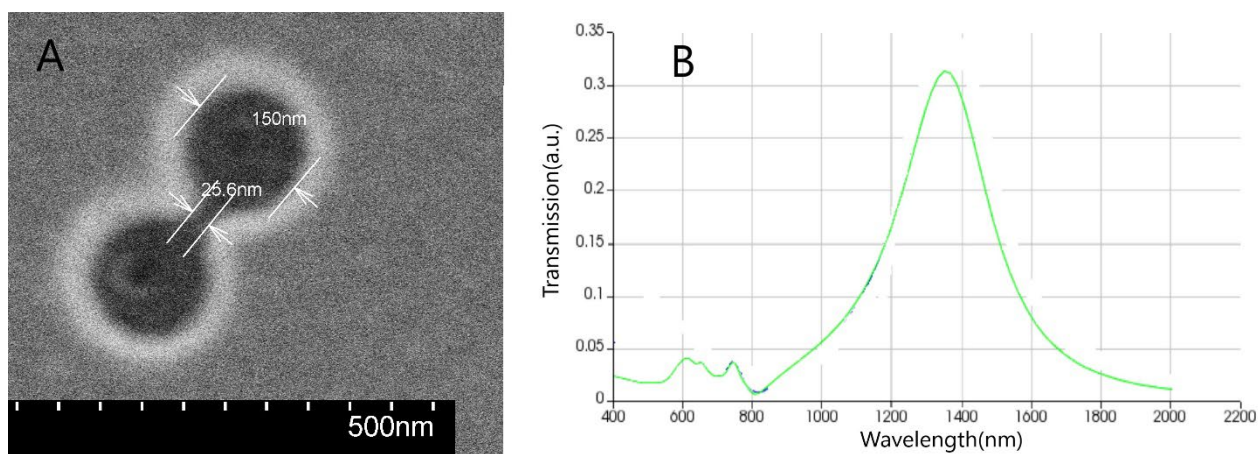

Fig. 1. A) SEM image of a double nanohole on a 70nm thick gold layer. B) FDTD simulation of transmission spectrum through a double nano hole of the same size as Fig. 1 (A).

The optical setup used for trapping nanoparticles, used a vertical sample placement and a novel cross-polarized-reflection geometry. The holes on the sample surface were visible using an infrared LED and a CMOS camera. The laser beam observed in the camera, comes from the reflection from the sample surface. This reflection-based method simplifies the alignment of microscope lenses and sample placement. A polarizing beam splitter have been used to observe the polarization change of the laser beam reflection from double nanoholes.

References
[1] Chen Y, Kotnala, A,Yu L,Zhang J, Gordon R, 2015, *Opt. Express*, 23, 30227-30236.
[2] Ravindranath AL, Shariatdoust MS, Mathew S, Gordon R, 2019, *Opt. Express*, 27, 16184-16194.

Digital harmonic holographic microscope for the study of nanostructures in nonlinear regime

Serena Goldmann[1], **Samuel Grésillon**[1], **Ignacio Izeddin**[1], **Valentina Krachmalnicoff**[1], **Gilles Tessier**[2], **Yannick De Wilde**[1],

1. Institut Langevin, ESPCI Paris, Université PSL, CNRS, 75005 Paris, France
2. Institut de la Vision – Sorbonne Université, 17 rue Moreau, 75012, Paris
E-mail : serena.goldmann@espci.fr

Digital holography is an imaging technique that enables a 3-dimensional reconstruction of the electromagnetic field scattered by an object in both amplitude and phase. We demonstrated its use in microscopy for the full 3-D mapping of the scattered field from single nanostructures such as nano-antennas [1] and near-field probes [2], while detecting the scattered field at the same frequency as the laser excitation. Since second harmonic generation (SHG) is a coherent process, SHG light can also be used to generate interferences and holograms [3, 4].

Here, we describe the development of a harmonic holographic microscope. We apply SHG holography to nanoparticles and plasmonic nanostructures in order to obtain single-shot measurements of their second harmonic 3D radiation pattern and to map intensity and phase variations near the sample. Using e.g. the angular spectrum representation of optical fields [5], and assuming propagation in homogeneous media, the knowledge of the scattered field (amplitude and phase) in a given plane allows it to be calculated in any other plane, i.e. in 3D, by numerical back-propagation.

Since both the amplitude and the phase have to be measured to fully characterize the field in a plane, we chose to focus on digital holography. The holographic setup is designed as an off-axis Mach Zehnder interferometer (Fig 1.a). The incoming beam, generated by a Ti:Sapphire femtosecond laser oscillator, is divided into a reference and a sample arm. The reference beam efficiently generates SHG in a BBO doubling crystal, while the sample beam yields SHG in the sample itself. The beams are then recombined to interfere on an EM-CCD camera (Fig 1.b). Back-propagation algorithms are computed and applied to the resulting hologram. Thus, we obtain the second harmonic radiation diagram of the sample via the 3-dimensional reconstruction of the SHG field generated by the sample excited by fs laser pulses.

In addition to providing 3D reconstruction, the harmonic holography microscope also benefits from an interferometric amplification effect [6], making the method particularly well suited to measure the weak SHG signal produced by nanostructures.
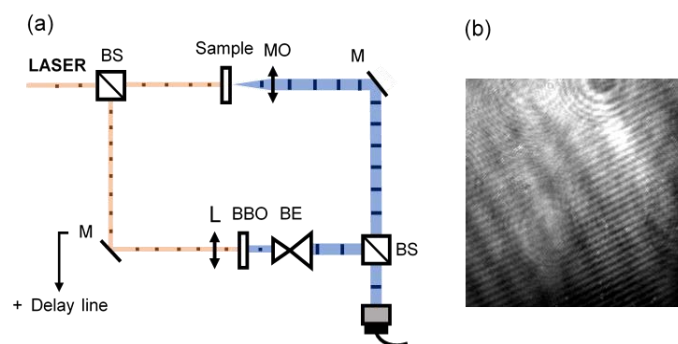
Fig 1.(a) Experimental setup schematics: BS, beam splitter, MO, microscope objective, M, mirror, L, lens, BBO, beta-barium borate crystal, BE, beam expander (b) Hologram

References

[1] Suck, S. Y.; Collin, S.; Bardou, N.; De Wilde, Y.; Tessier, G. 2011. *Optics Letters,* 36, 849−851
[2] Rahbany, N., Izeddin, I., Krachmalnicoff, V., Carminati, R., Tessier, G., De Wilde, Y. 2018. *ACS Photonics*, 5, 1539-1545.
[3] Pu Y., Centurion M., Psaltis D. 2008. *Applied Optics*, 47, A103-A110.
[4] Shaffer E., Pavillon N., Kühn J., Depeursinge C. 2009. *Optics Letters*, 34, 2450-2452.
[5] Novotny, L., and Hecht, B. *Principles of Nano-optics.* 2006. Cambridge University Press.
[6] Gross, M., Atlan, M. 2007. *Optics Letters,* 32, 909-911.

WS$_2$-Flake-Sandwiched, Au-Nanodisk-Enabled High-Quality Fabry–Pérot Nanoresonators for Photoluminescence Modulation

He Huang, **Shasha Li**, **Jianfang Wang**[*]

Department of Physics, The Chinese University of Hong Kong, Shatin, Hong Kong SAR, China

E-mail: jfwang@phy.cuhk.edu.hk

The increasing demand for compact and high-performance photonic devices drives the development of optical resonators with nanoscale sizes and ultrahigh quality (Q) factors. Fabry–Pérot (FP) resonators, one of the most widely-employed optical resonators, can support ultrahigh Q factors in the simple structure, which is particularly attractive for applications in lasers, filters, and ultrasensitive sensors. However, the construction of FP resonators with both nanoscale sizes and high Q factors still faces great challenges [1,2]. Herein we demonstrate the construction of FP nanoresonators with a piece of WS$_2$ flake sandwiched between Au nanodisks (NDs) and a Au film (Fig. 1a,b). The atomically flat surfaces of the WS$_2$ flake and the Au NDs benefit mirror alignment and boost Q the factor up to 76. The single-Au-ND-enabled nanoresonators can support FP resonance modes with different orders in the visible region. We systematically studied the optical properties and formation mechanism of the high-quality FP modes. The FP modes were further hybridized with excitons in the WS$_2$ flake spacer, allowing the modulation of the WS$_2$ indirect bandgap emission (Fig. 1c,d). Our results combine the advantages of plasmonic nanoparticles with those of FP resonators, providing a promising platform for the development of compact nanophotonic devices such as tunable nanolasers, smart sensors, and photonic circuit elements.
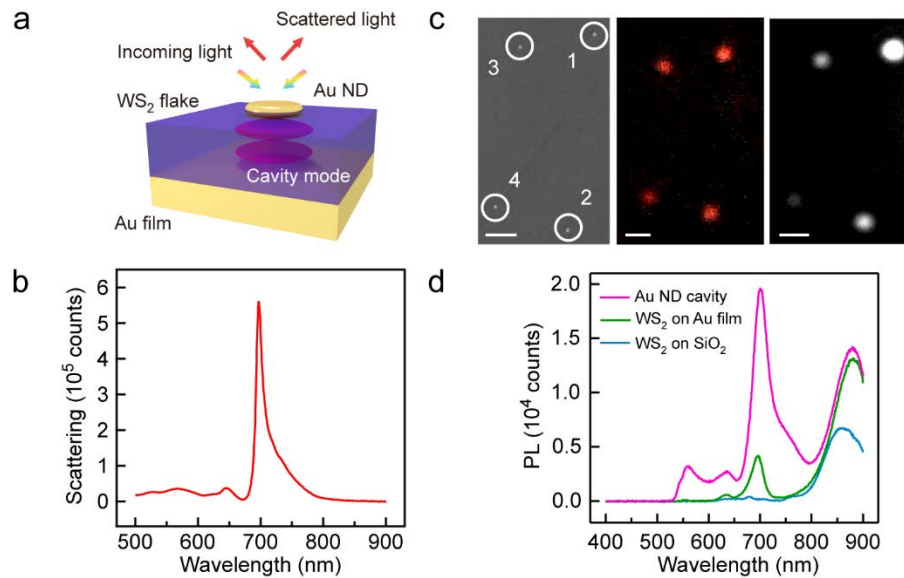

Fig. 1 (a) Schematic diagram of a single-Au-ND-enabled FP nanoresonator. The chromatic and red arrows indicate the incident and scattered light, respectively. The magenta oblate spheroids indicate the formation of standing waves in the cavity, leading to the excitation of the FP resonance. (b) Measured scattering spectrum of a nanoresonator. (c) Scanning electron microscopy (SEM) image (left), scattering image taken with a 695 nm longpass filter (middle), and photoluminescence (PL) image (right) of four Au-ND-enabled FP nanoresonators. The nanostructures are indicated by circles in the SEM image. The scale bars are 1 μm. (d) Measured PL spectra of different structures.

References

[1] Schmidt, M. A.; Lei, D. Y.; Wondraczek, L.; Nazabal, V.; Maier, S. A. 2012. *Nat. Commun.* 3, 1108.
[2] Casalis de Pury, A.; Zheng, X.; Ojambati, O. S.; Trifonov, A.; Grosse, C.; Kleemann, M. E.; Babenko, V.; Purdie, D.; Taniguchi, T.; Wantanabe, K.; Lombardo, A.; Vandenbosch, G. A. E.; Hofmann, S.; Baumberg, J. J. 2020. *Phys. Rev. Lett.* 124, 093901.

Manipulating the quantum field statistics of confine infrared fields via ultrafast modulation of vibrational polaritons

Johan F. Triana[1], **Felipe Herrera**[1,2]

1. *Departamento de Física, Universidad de Santiago de Chile, Santiago, Chile*
2. *ANID-Millennium Institute for Research in Optics, Chile*
E-mail: johan.triana@usach.cl

Demonstrations of strong and ultrastrong light-matter interaction in mid-infrared resonators have stimulated the search for control schemes that can be used to prepare target material and photonics states for a variety of applications in chemistry [1]. We propose a scheme for modifying the photon number and field quadrature statistics of a confined mid-IR electromagnetic field by modulating the vacuum frequency with femtosecond UV pulses [2]. The scheme relies on the transient modification of the carrier density of the field-confining materials and strong coupling between the confined field and an ensemble of molecular vibrations. We study variations of the Mandel Q-factor and squeezing over sub-picosecond timescales by modulating the cavity frequency ~15%, resulting in squeezing factors of order ~1 dB for a system initially prepared in the stationary ground and lower polariton states [3]. We relate the predicted variations of quantum field statistics to the type of dipolar structure and anharmonicity of the molecular vibrations. Our work can stimulate the design of novel infrared devices at room temperature for applications in quantum metrology and quantum information processing.

References
[1] F. Herrera and J. Owrutsky. 2020. *J. Chem. Phys.* 152, 100902
[2] J.F. Triana, F.J. Hernández and F. Herrera. 2020. *J. Chem. Phys.* 152, 234111
[3] J.F. Triana, F. Herrera. 2022. *New J. Phys.* 24, 023008

Analytic approach to reflection and transmission of surface polaritons

Wonjae Choi[1], **Q-Han Park**[2]

1,2. Department of Physics, Korea University, 145, Anam-ro, Seongbuk-gu, Seoul, Republic of Korea

E-mail: chldnjswo01@korea.ac.kr

Surface polaritons (SPs) such as graphene plasmons and exciton-polaritons are intrinsic electromagnetic modes strongly confined to a two-dimensional (2D) material. When SPs propagating along the 2D material meet a 1D boundary or a discontinuity, certain fractions of SPs become reflected and transmitted while the rest of them become scattered. This fundamental phenomenon occurs ubiquitously when conducting near-field microscopy experiments for 2D materials or designing planar optical devices such as graphene-based plasmonic waveguide [1]. Due to the improvement of computing power and the development of simulation programs, most studies resorted on numerical analysis of the problem. Even in theoretical efforts, due to the complexity of the scattering process, theoretical studies focused only on the specific case such as normal incidence [2-3]. Theoretical studies on general cases such as oblique incidence, despite of its importance, have not been reported until now. Although numerical calculations provide fast and efficient revenue to understand the physical properties of SPs, accessing analytic solutions is essential in understanding the general properties of the system.

In this work, we present an analytic study on obliquely incident SPs to a boundary like Fig. 1(a). In Fig. 1(a), two different 2D materials are bounded at $x=0$ and sandwiched between two optical media, and an SP is obliquely coming into the boundary from $x<0$. We derived an analytic solution by using the Wiener-Hopf method [4]. To verify the solution, we conducted a FEM simulation for obliquely incident SP in Fig. 1(b) by setting y-dependence to e^{iqy} (q: transverse momentum) and plotted the x-component of the electric field. We compared the absolute value of the x-component of the electric field on $z=0$ about simulation and theory in Fig. 1(c). Comparisons to 3D cases are given in Fig. 1(d), where we compared the solution with that of the Fresnel's equation for TM polarization. We find that this quasi-two-dimensional system shows slightly different features of reflection and transmission compared to those of Fresnel's equation. We provide an explanation underlying similarities and differences.
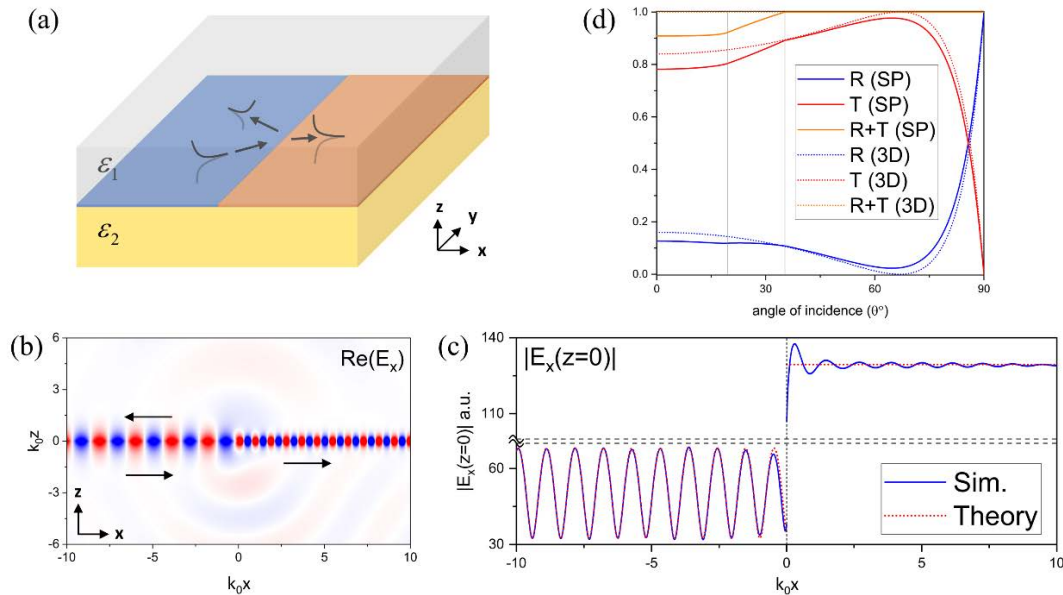

Fig. 1 (a): The geometry of the system. All materials are non-magnetic. Obliquely incident, reflected, and transmitted SPs are presented. (b): Simulated result for obliquely incident SP. (c): Comparison between simulation results and theory. (d): Reflectance, transmittance, and their sum for the case of Fig. 1(a) (solid line) and Fresnel's equation for TM polarization (dotted line).

In summary, we derived an analytic solution for obliquely incident SP and confirmed that the scattered fields make the difference between this system and the conventional three-dimensional system. We expect that this work will improve our fundamental understanding of reflection and transmission for SPs and provide insights when designing planar optical devices.

References

[1] Christensen, J., Manjavacas, A., Thongrattanasiri, S., Koppens, F. H., & García de Abajo, F. J. (2012). *ACS nano*, 6(1), 431-440.
[2] Siaber, S., Zonetti, S., & Sydoruk, O. (2019). *Journal of Optics*, 21(10), 105002.
[3] Rejaei, B., & Khavasi, A. (2015). *Journal of Optics*, 17(7), 075002.
[4] Margetis, D. (2020). *Journal of Mathematical Physics*, 61(6), 062901.

Double Nanohole Optical Tweezers Study of Conformation Changes of pr65

Samuel Mathew[1], **Ghazal Hajisalem**[1], **Elham Babaei**[1], **Michael Dobinson1**[1], **Reuven Gordon**[1]

Mohsin Naqvi[2], **Janet Kumita** [2]

1. Electrical and Computer Engineering, University of Victoria, Victoria BC, V8W 2Y2 Canada
2. Pharmacology, University of Cambridge, Cambridge, United Kingdom
E-mail: samuelmathew@uvic.ca

Pr65 is the 65 KDa structural subunit of protein phosphatase PP2A [1] implicated in enzyme action [1] and cancer [2]. Previous research, for example [1], suggests that the elastic properties of pr65 are crucial both for its function and characterization, yet a literature search of its elastic constant returns no result.

This study attempts to fill this gap. Furthermore, because the magnitude of external force found to produce measurable conformation changes in pr65 [1] is well within the range of force exerted by optical tweezers [3], it does this by trapping pr65 in a double nanohole (DNH) optical tweezers and analyzing the time series of the light intensities scattered by the trapped pr65. Two discrete jumps were observed, consistent with the fact that protein conformation change is subject to overcoming a free energy barrier [4].

Previous studies such as [1] show that pr65 unfolds under tension, and we attribute the observed jumps to the unfolding of pr65 due to electrostriction in the cusp of our double nanohole optical tweezers. We found that the change in the polarizability of pr65 following this unfolding is roughly 3.2×10^{-36} $Cm^{-2}V^{-1}$, and estimate that the flexural stiffness of pr65 in the regime of our experiment is about 50 mN/m, corresponding to a flexural oscillation frequency of about 0.30 cm^{-1}, comparable to 0.37 cm^{-1} predicted by [1] based on normal mode analysis. A snapshot of our results is shown in Figure 1 below.
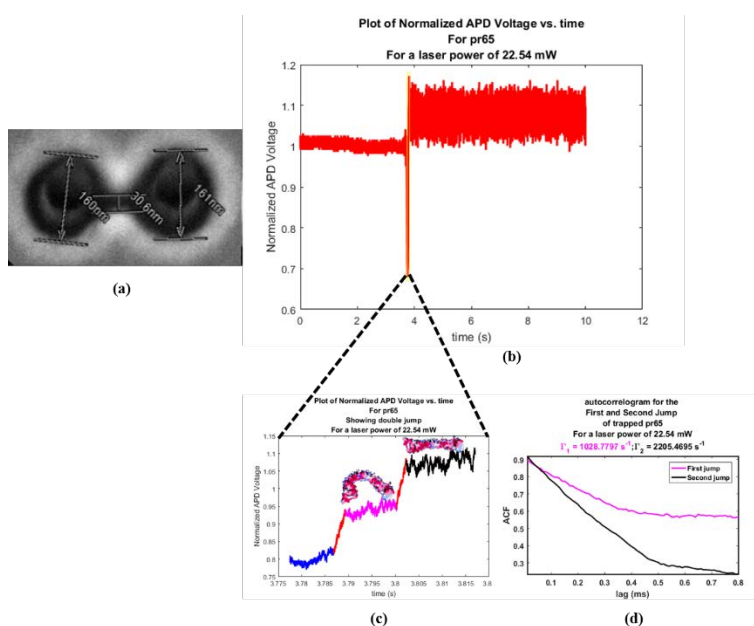

Fig. 1 (a) Double nanohole (DNH) aperture; (b) Time series of scattered intensity; (c) Zoom-in showing two discrete jumps; (d) Autocorrelograms of the time series for the first jump (magenta solid line) and the second jump (black solid line).

References

[1] A. Grinthal, I. Adamovic, B. K. M. Weiner and N. Kleckner, "PR65, the HEAT-repeat scaffold of phosphase PP2A, is an elastic connector that links force and catalysis," Proceedings of the National Academy of Sciences, vol. 107, no. 6, pp. 2467 - 2472, 2010.

[2] M. R. Groves, N. Hanlon, P. Turowski, B. A. Hemmings and D. Barford, "The structure of the protein phosphatase 2a pr65/a subunit reveals the," Cell, vol. 96, pp. 99 - 110, 1999.

[3] M. C. Williams, "Measuring Piconewton Forces," 2002. [Online]. Available: https://www.biophysics.org/Portals/0/BPSAssets/Articles/williams.pdf. [Accessed 7 February 2022].

[4] A. N. Naganathan, R. Perez-Jimenez, V. Muñoz and J. M. Sanchez-Ruiz, "Estimation of protein folding free energy barriers from calorimetric data by multi-model bayesian analysis," Phys. Chem. Chem. Phys, vol. 13, p. 17064 –17076, 2011.

Isolating Er3+-Doped Nanocrystals for single photon Sources at 1550 nm

Zohreh Sharifi[1], **Reuven Gordon**[2]

1. Department of Electrical Engineering, University of Victoria, Victoria, Canada
2. Department of Electrical Engineering, University of Victoria, Victoria, Canada
E-mail: rgordon@uvic.ca

Single-photon sources which can be created by isolation individual atoms and atom-like defects are required for quantum technologies. One of the promising choices for single photon sources are erbium ions which produce single photons at low-loss fiber optic wavelengths, but they have low emission rates. Gold double nanoholes (DNHs) can be used to enhance the emission of single erbium emitters. Here, we tune the size of DNHs to achieve the best enhancement to show visible emission from single nanocrystals at 1550 nm using an optical tweezers. We observe discrete levels of emission at 1550 nm for Erbium- doped nanocrystals with low numbers of emitters and demonstrate isolating single emitters.

In our previous work [1], we demonstrated that the plasmonic resonances of DNH apertures in a gold film can be tuned to much more enhancement of the erbium emitters emission compared to rectangular apertures [2]. Here, we use the same procedure and techniques to create DNH apertures with different cusp separations and use the same optical trapping setup to achieve more enhancement at 1550 nm.

Fig. 1 a) shows the emission 23.4 nm Yb–Er-doped NaYF4 nanocrystals using DNH apertures with varying average cusp separations. It illustrates how the size and shape of the aperture can affect the overall emission. Fig. 1 b) shows the emission at 1550 nm of single nanocrystals as measured with a 1 s integration time. It proves that the emission is separated into discrete levels. We attribute these levels to the discrete numbers of erbium emitters in the nanocrystals, from zero to six individual active emitters.
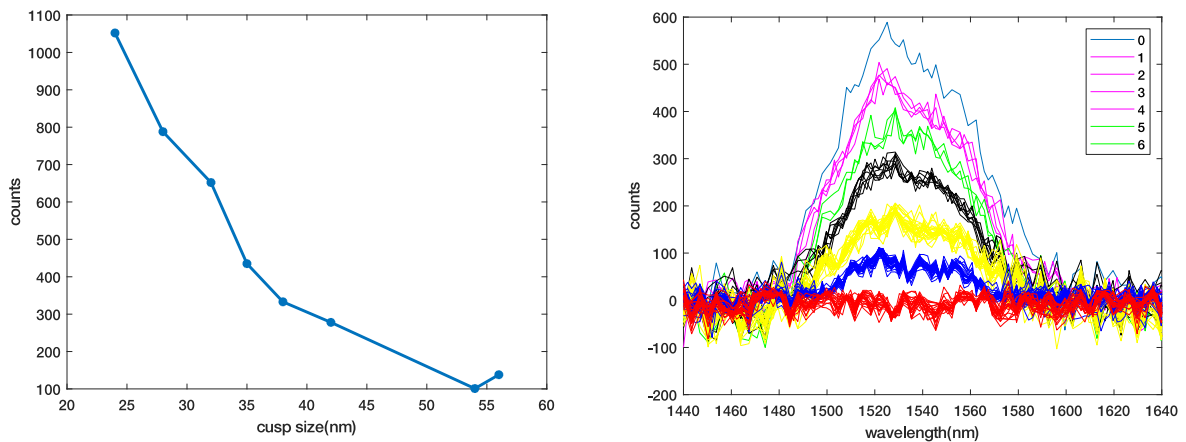

Fig. 1 a) Emission from 23.4 nm nanocrystals at 1550 nm for varying DNH cusp separations. b) Emission counts from nanocrystals showing discrete levels corresponding to different amounts of active erbium emitters. Collected by a spectrometer with 1 s acquisition time.

The discrete levels of emission can be used to identify and isolate single active emitters and is a step towards reliable production of single photon sources at 1550 nm, the low-loss fiber optic band.

References

[1] Sharifi, Z., Dobinson, M., Hajisalem, G., Shariatdoust, M.S., Frencken, A.L., van Veggel, F.C. and Gordon, R., 2021. *Isolating and enhancing single-photon emitters for 1550 nm quantum light sources using double nanohole optical tweezers*. The Journal of Chemical Physics, 154(18), p.184204.
[2] Alizadehkhaledi, A., Frencken, A.L., van Veggel, F.C. and Gordon, R., 2019. *Isolating nanocrystals with an individual erbium emitter: A route to a stable single-photon source at 1550 nm wavelength*. Nano Letters, 20(2), pp.1018-1022.

Enantioselective optical trapping by elliptical plasmonic nanoholes

Zhan-Hong Lin[1], Jiwei Zhang[2], Ankit Kumar Singh[1], Xiaofei Wu[1], and Jer-Shing Huang[1,3,4,5]

1. Leibniz Institute of Photonic Technology, Albert-Einstein Straße 9, 07745 Jena, Germany
2. MOE Key Laboratory of Material Physics and Chemistry under Extraordinary Conditions, and Shaanxi Key Laboratory of Optical Information Technology, School of Physical Science and Technology, Northwestern Polytechnical University, Xi'an 710129, China
3. Abbe Center of Photonics, Friedrich-Schiller University Jena, Jena, Germany
4. Research Center for Applied Sciences, Academia Sinica, 128 Sec. 2, Academia Road, Nankang District, 11529 Taipei, Taiwan
5. Department of Electrophysics, National Chiao Tung University, 1001 University Road, 30010 Hsinchu, Taiwan
E-mail: zhan-hong.lin@leibniz-ipht.de

Circular dichroism (CD) is one of the key chiral characteristics to distinguish chiral chemical or biological systems between their enantiomers. However, the sensitivity of analytical methods based on chiral light-matter interaction is usually low due to the size mismatch between the light helix and the size of molecular chiral domains. Plasmonic nanostructures offer the possibility to engineer optical near fields [1] and enhance light-matter interaction. Realization of efficient enhancement requires, however, the presence of target analyte in the area of the enhanced field, which is typically limited by free diffusion. Therefore, it is important to rationally design nanostructures to simultaneously provide plasmon-enhanced chiroptical field for CD [2, 3] and optical trapping force [4] to trap the target in the hotspot.

Here, we propose using elliptical nanoholes on an extended gold film as a simple yet effective achiral platform to demonstrate chiroptical analysis [5]. For a linearly polarized light, a well-designed elliptical nanohole can simultaneously generate chiral near-field for chiroptical analysis and act as a nano-optical trap to capture dielectric and plasmonic nanospheres (Fig. 1 a). The figure also shows two distinct optical potential (U_{xy}) landscapes of the same elliptical nanohole upon linear polarization illumination. Depending on the chirality (κ) of the nanoparticle, the in-plane trapping potential can be attractive (Fig. 1 b) or repulsive (Fig. 1 c) to the particle, making the elliptical nanohole an effective enantioselective optical trap.
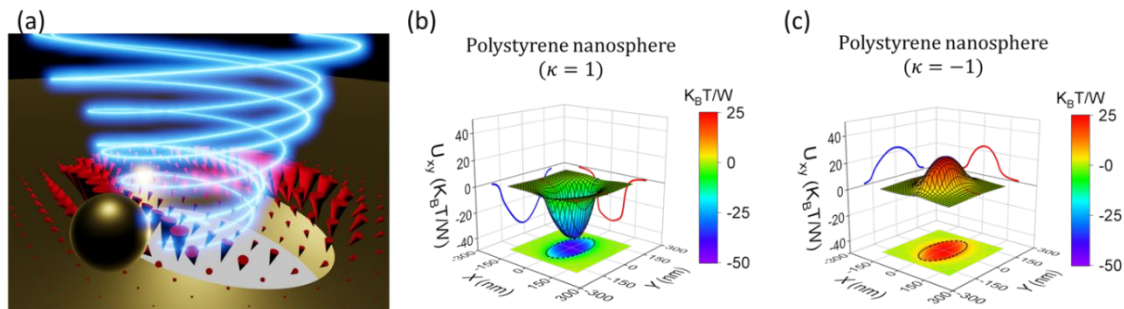

Fig. 1 Plasmonic optical trap by elliptical nanohole. (a) Schematic of the elliptical nanohole on the gold film. (b, c) Trapping potential contour maps of the in-plane optical force (F_x and F_y) exerted on a chiral PS nanosphere (diameter = 20 nm). The chirality parameter κ is ±1. The red and blue traces on the x-z and y-z projection planes are the cross-sectional potential cut by y = 0 and x = 0 planes. The black dashed lines on the x-y projection planes mark the boundaries of the elliptical nanohole. The calculations were made for an injected power in the aperture of 1 W.

Using this achiral platform with linearly polarized illumination, false chiroptical signals due to nanostructures can be eliminated. Moreover, the compatibility of the platform with typical optical microscopes is greatly improved because the problems due to the distortion of circularly polarized light by the optics of a microscope are avoided. The platform is ideal for sensitive chiroptical analysis in combination with nanoparticles-based solid-state extraction and pre-concentration, which further enhances chemical selectivity and sensitivity.

References
[1] Biagioni, P., Huang, J. -S., Duò, L., Finazzi, M., and Hecht, B., 2009 *Phys. Rev. Lett.* **102**, 256801.
[2] Schäferling, M., Dregely, D., Hentschel, M., and Giessen, H., 2012 *Phys. Rev. X* **2**, 031010.
[3] Lin, D. and Huang, J.-S., 2014 *Optics Express* **22**, 7434-7445.
[4] Juan, M. L., Gordon, R., Pang, Y., Eftekhari, F., and Quidant, R., 2009 *Nat. Phys.* **5**, 915-919.
[5] Lin, Z.-H., Zhang J., and Huang J.-S., 2021 *Nanoscale* **13**, 9185

Probing Raman active acoustic vibrations of single molecule protein: PR65

Elham Babaei[1], Ghazal Hajisalem[1], Burak Kaynak[2], Pemra Doruker[2], Mohsin M. Naqvi[3], Janet Kumita[3], Feng-Yu Wang[4], Jhih-Hong Cheng[4], Che-Min Wu[4], Shang-Hua Yang[4], Ivet Bahar[2], Laura Itzhaki[3], Reuven Gordon[1]

1. University of Victoria, Victoria, Canada
2. University of Pittsburgh, Pittsburgh, United States
3. University of Cambridge, Cambridge, United Kingdom
4. National Tsing Hua University, Hsinchu, Taiwan

E-mail: elhambabaei@uvic.ca

We demonstrate Extraordinary Acoustic Raman (EAR) vibrational modes of PR65. Two lasers have been used in order to sweep the beat frequency to excite the single molecule in the double nanohole optical tweezer setup. EAR spectrum shows that the modes of vibration are at frequencies: 11.1 GHz, 20.8 GHz, 31.5 GHz, 38.0 GHz which are in agreement with results of Anisotropic Network Model (ANM) simulation. This technique is label free and single molecule compared to other methods of characterization of proteins. Normal mode analysis (NMA) reveals that tumor suppressor protein phosphate 2A (PP2A) conformation fluctuation due to forces imposed from mechanical and chemical energy inputs is dominated by elastic deformation of its subunit PR65. Characterizing natural repeat proteins PR65 is of highest importance since they are involved in many cellular processes.
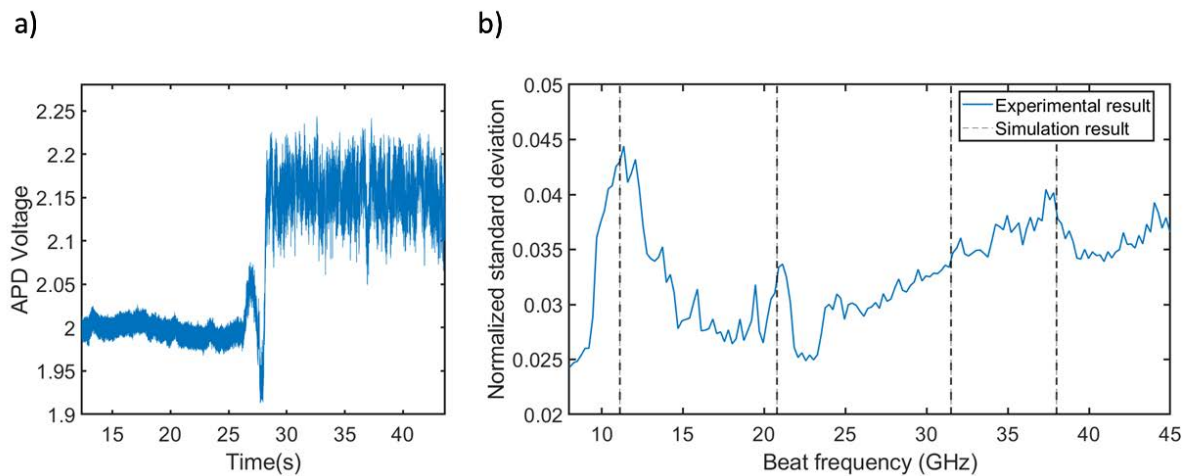
Fig. 1 a) Trapping event of PR65 using optical trapping setup. b) EARs of PR65. Solid lines are the experimental measurements and the dashed lines show the ANM results

References

[1] Wheaton, S., Gelfand, R.M. and Gordon, R., 2015. Probing the Raman-active acoustic vibrations of nanoparticles with extraordinary spectral resolution. Nature Photonics, 9(1), pp.68-72.
[2] DeWolf, T. and Gordon, R., 2016. Theory of acoustic Raman modes in proteins. Physical Review Letters, 117(13), p.138101.
[3] Kaynak, B.T., Bahar, I. and Doruker, P., 2020. Essential site scanning analysis: a new approach for detecting sites that modulate the dispersion of protein global motions. Computational and structural biotechnology journal, 18, pp.1577-1586.
[4] Kaynak, B.T., Zhang, S., Bahar, I. and Doruker, P., 2021. ClustENMD: efficient sampling of biomolecular conformational space at atomic resolution. Bioinformatics, 37(21), pp.3956-3958.

Coupling between Perovskite Quantum Dots in an Plasmonic Optical Tweezer

Parinaz Moazzezi[123], **Hao Zhang**[12], **Brett Henderson**[23], **Vishal Yeddu**[23], **Cristina Cordoba**[24], **Arthur Blackburn**[24], **Makhsud I. Saidaminov**[123], **Irina Paci**[23] and **Reuven Gordon**[12]

1. Department of Electrical and Computer Engineering, University of Victoria, 3800 Finnerty Road, Victoria, V8P 5C2, British Columbia, Canada
2. Centre for Advanced Materials & Related Technologies (CAMTEC), University of Victoria, 3800 Finnerty Road, Victoria, V8P 5C2, British Columbia, Canada
3. Department of Chemistry, University of Victoria, 3800 Finnerty Road, Victoria, V8P 5C2, British Columbia, Canada
4. Department of Physics and Astronomy, University of Victoria, 3800 Finnerty Road, Victoria, V8P 5C2, British Columbia, Canada

E-mail: rgordon@uvic.ca

All inorganic halide Perovskite ($CsPbBr_3$) nanocrystals (NCs) have efficient single photon emission and long coherence times which makes them of interest for quantum information application [1]. Their strong coupling also allows for non-classical emission, such as superfluorescence [2]. To understand the coupling better, it is of interest to study the coupling between two such emitters, and this may be used to create entangled states [3].

In this paper we measure the coupling between two PQDs by an optical tweezer trapping setup [4]. We sequentially trap two dots in a single trap and measure the change in emission wavelength and intensity. Fig 1. Shows the distribution of two-photon photoluminescence for single and double PQD trapping. Double PQD trapping is identified via jumps recorded on an avalanche photo diode. The emission intensity for double PQDs is more than double in comparison with single PQD trapping, and also there is systematic red-shift in the emission. The direct electronic coupling (left figure) does not explain the observed shift, and so other mechanisms are required to explain these results.
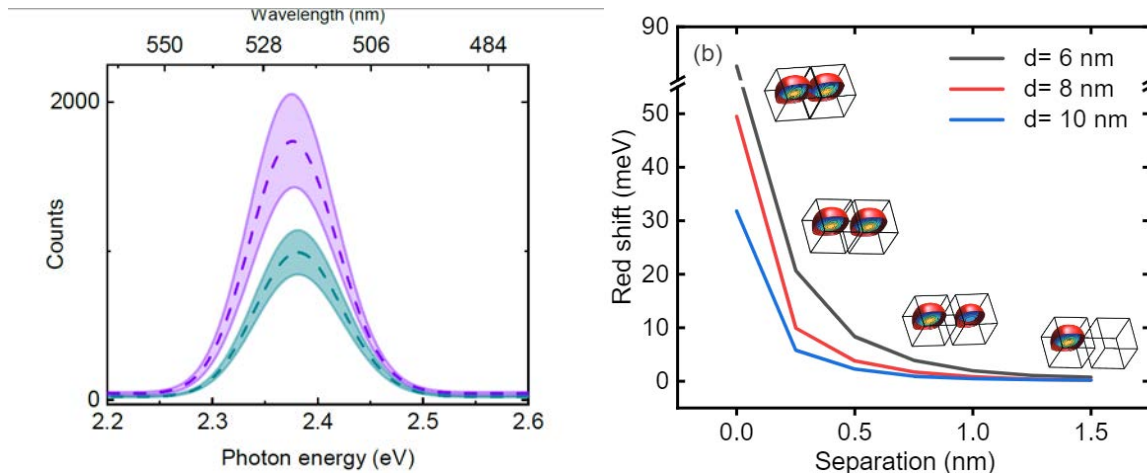

Fig. 1 (a) spectra of single dot trapping and double dots trapping. The areas filled with blue and green stands for the experiment data at each sampling (fit with Gauss function). The dotted line in red and black are fitted by Gauss function from multiple spectra. (b) Quantum calculation of energy shift. Inset shows the wavefunction distribution for the two dots.

References

[1] H. Utzat *et al.*, "Coherent single-photon emission from colloidal lead halide perovskite quantum dots.," *Science*, vol. 363, no. 6431, pp. 1068–1072, Mar. 2019, doi: 10.1126/science.aau7392.

[2] G. Rainò, M. A. Becker, M. I. Bodnarchuk, R. F. Mahrt, M. V Kovalenko, and T. Stöferle, "Superfluorescence from lead halide perovskite quantum dot superlattices.," *Nature*, vol. 563, no. 7733, pp. 671–675, Nov. 2018, doi: 10.1038/s41586-018-0683-0.

[3] B. M. *et al.*, "Coupling and Entangling of Quantum States in Quantum Dot Molecules," *Science (80-.).*, vol. 291, no. 5503, pp. 451–453, Jan. 2001, doi: 10.1126/science.291.5503.451.

[4] A. L. Ravindranath, M. S. Shariatdoust, S. Mathew, and R. Gordon, "Colloidal lithography double-nanohole optical trapping of nanoparticles and proteins.," *Opt. Express*, vol. 27, no. 11, pp. 16184–16194, May 2019, doi: 10.1364/OE.27.016184.

Nanoaperture optical fiber tweezers fabricated with a low-cost colloidal pattern transfer method

Michael Dobinson[1,2], Reuven Gordon[1,2]

1. Department of Electrical and Computer Engineering, University of Victoria, Victoria, BC, V8P 5C2, Canada
2. Centre for Advanced Materials and Related Technology (CAMTEC), University of Victoria, Victoria, BC, V8P 5C2, Canada
E-mail: rgordon@uvic.ca

Optical trapping using nanoapertures such as double nanoholes (DNHs) is a useful technique for analysing proteins and other small particles which unfortunately is inaccessible for many due to the complicated optical setup and nanofabrication requirements [1]. Integrating a DNH aperture on the tip of an optical fiber greatly simplifies the technique as it allows for fully fiber-based trapping systems which require only minimal optics experience. Previous works have demonstrated nanoaperture optical fiber tweezers, but fabrication has been based on expensive top-down approaches [2–4]. This work presents a method to fabricate nanoaperture optical fiber tweezers by colloidal pattern transfer with a low-cost pattern fabricated using colloidal lithography. Results of optical trapping using a fabricated nanoaperture fiber tweezer with a polystyrene nanoparticle size standard are also presented.

A gold film pattern of DNH apertures is first produced using colloidal lithography as previously presented by our group [5]. This pattern contains single, double, and multiple nanoholes in the gold film. Scanning electron microscopy or polarization analysis [6] can be used to find suitable DNHs, where they are separated by more than the fiber core radius, 4.1 μm. A cleaved single-mode fiber is aligned to the DNH by monitoring transmission through the fiber. The face of the optical fiber is coated with UV-cured optical adhesive and moved to contact the gold surface. The glue is cured using UV light and the fiber is lifted to detach the gold from the glass substrate. Fig. 1a shows a schematic of the final device with the DNH affixed to the tip of the optical fiber.

A fiber nanoaperture optical tweezer was used with a fiber laser to optically trap a 40 nm polystyrene nanoparticle by dipping the tip of the fiber into solution. Fig. 1b shows the transmission through the aperture which shows trapping with a 0.5% increase in the transmission as well as 2.4% increase in the signal variation, measured by the full width at half maximum of a Gaussian fit. The laser is turned off at 85 s and back on at 110 s which shows a return to the low variation state, indicating that the particle was released. Fiber-based nanoaperture tweezers simplify trapping with nanoapertures and the colloidal pattern transfer fabrication method presented here shows a low-cost route to producing these devices.
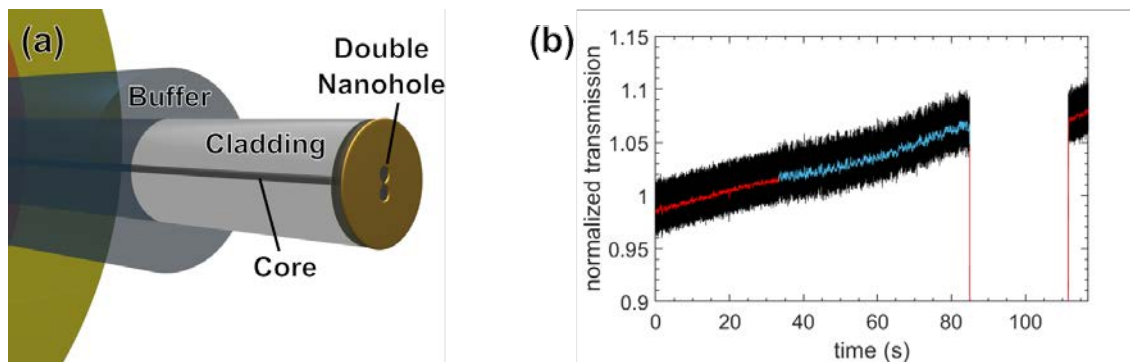

Fig. 1. Nanoaperture optical fiber tweezers. (a) Schematic drawing of the structure at the tip of a cleaved optical fiber. (b) Normalized transmission signal (black) through the aperture with 40 nm polystyrene nanoparticles. The signal is filtered and shown before trapping in red, and during trapping in blue.

References
[1] Gordon, R. 2019. *Opt. & Laser Tech.*, vol. 109, pp. 328–335.
[2] Gelfand, R.M., Wheaton, S., and Gordon, R. 2014. *Opt. Let.*, vol. 39, no. 22, pp. 6415–6417.
[3] Ehtaiba, J.M. and Gordon, R. 2019. *Opt. Express*, vol. 27, no. 10, pp. 14112–14120.
[4] Berthelot, J., Aćimović, S., Juan, M., Kreuzer, M.P., Renger, J., and Quidant, R. 2014. *Nature Nanotech*, vol. 9, pp. 295–299.
[5] Ravindranath, A.L., Shariatdoust, M.S., Mathew, S., and Gordon, R. 2019. *Opt. Express*, vol. 27, no. 11, pp. 16184–16194.
[6] Hajisalem, G., Babaei, E., Dobinson, M., Iwamoto, S., Sharifi, Z., Eby, J., Synakewicz, M., Itzhaki, L.S., and Gordon, R. 2022. *Opt. Express*, vol. 30, no. 3, pp. 3760–3769.

Breakdown of spin-to-helicity locking at the nanoscale in topological photonic crystal edge states

Sonakshi Arora[1], **Thomas Bauer**[1], **René Barcyzk**[2], **Nikhil Parrapurath**[2], **Ewold Verhagen**[2], **Kobus Kuipers**[1],

1 Kavli Institute of Nanoscience, Delft University of Technology, 2600 GA Delft, The Netherlands

2. Center for Nanophotonics, AMOLF, Science Park 104, 1098 XG Amsterdam, The Netherland

E-mail: s.arora@tudelft.nl

Topological photonics recently gained widespread attention due to its potential for robust information transport, with on-chip photonic modes protected by a given topological invariant, or pseudo-spin [1] and near-unity far field helicity [2]. Unidirectional emission is achieved, in general, by strong coupling of a quantum emitter with circularly polarized dipole moment to the local polarization state of a photonic mode. In our work [3], we use a photonic crystal based approach emulating quantum spin-Hall (QSHE) [4] resulting in symmetry-protected edge states present at the interface of topologically different photonic crystal lattices. With near-field microscopy we quantitatively investigate the photonic edge eigenstates and their transport properties.

We investigate the properties of the topologically-protected edge states at the interface of topologically non-equivalent photonic crystals lattices: shrunken and expanded (top left inset Fig. 1.). The interface supports counter-propagating topological states that mimic the QSHE (Fig. 1). By directly measuring the individual in-plane field components, we obtain signatures of the underlying photonic spin-orbit coupling, manifested by spatially-varying spin densities (right inset Fig. 1). These observations are in striking contrast to the far-field helicity of the edge state which is uniquely linked to its pseudo-spin.

Fig. 1 Measured near-field amplitude map of a QSHE edge state that lies below the light line. Inset: SEM image of the two lattices, 'shrunken' and 'expanded'. Dashed box shows the experimentally measured z-component of the spin density Sz ∝ $\Im(E^*\times E)z$, normalized to the maximum absolute value shown in the image.

The contrast between near- and far-field observations can be understood from the measured and calculated band structure of the edge states (see dispersion relation in Fig. 2; [5]).The Bloch harmonic within the first Brillouin zone also called the fundamental harmonic contributes to unambiguous near-unity spin (S_{FF}) in the far-field. This is the only Bloch harmonic interrogated in far-field measurements (Fig.2 (b)). However, as the higher-order Bloch harmonics are added to construct the actual Bloch mode, the global spin S_{NF} is reduced by a factor of 30 and for certain frequencies, S_{NF} is even flipped compared to the pseudo-spin measured in the far-field S_{FF}. We experimentally reveal the influence of higher-order Bloch harmonics in spin inhomogeneity, leading to a breakdown in the coupling between local helicity and global spin.
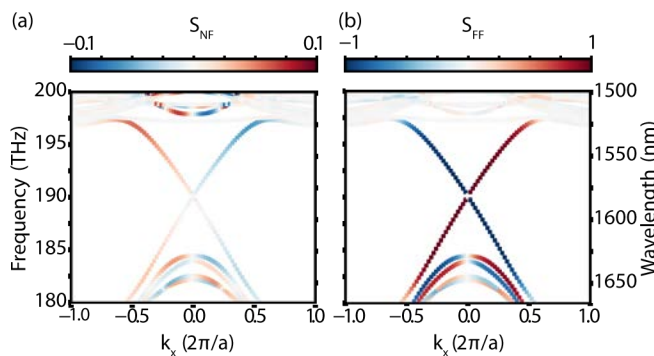

Fig. 2 Numerically simulated dispersion relation where the edge state eigen frequencies are color coded with the estimated (a) near-field and (b) far-field optical spin S.
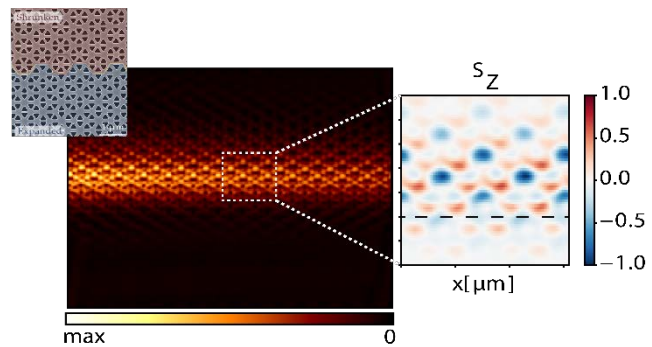
Our findings demonstrate that in order to employ these systems for unambiguous spin-dependent photon transport from coupled chiral emitters, the local structure of the edge state's spin density must be taken into account. This has profound consequences on the design of topological photonic quantum networks and provides a route towards engineering more robust topologically protected chiral interfaces. A detailed study of this spin-to-helicity breakdown might furthermore lead to novel concepts in understanding dissipative mechanisms in electronic topological insulators.

References

[1] Lu, L., Joannopoulos, J. D., & Soljačić, M. (2014). Topological photonics. Nature photonics, 8(11), 821.

[2] Christiansen, R., Wang, F., Sigmund, O. & Stobbe, S. (2019). Nanophotonics, 8(8), 1363-1369.

[3] Arora, S., Bauer, T., Parappurath N.,, Barczyk R.,, Verhagen, E., Kuipers L. (2022) arXiv:2202.04402v1 [cond-mat.mes-hall]

[4] Wu L.-H. and Hu, X. Phys. Rev. Lett. 114, 223901 (2015).

[5] Parappurath, N., Alpeggiani, F., Kuipers, L., & Verhagen, E. (2020). Science Advances, 6(10), eaaw4137.

Plasmon-excited near-field luminescence of semiconductor light sources

Vlastimil Křápek[1], **Petr Dvořák**[1], **Lukáš Kejík**[1], **Zoltán Édes**[1], **Michal Kvapil**[1], **Michal Horák**[1], **Petr Liška**[1], **Jan Krpenský**[1], **Tomáš Šikola**[1]

1. Brno University of Technology, Technická 2, CZ-61669 Brno, Czechia

E-mail: krapek@vutbr.cz

On-chip integration of semiconductor light sources is hindered by the fact that the wavelength of the light is considerably larger than the physical dimensions of the emitter. Therefore, near-field handling of the emission with a deeply subwavelength spatial resolution would be of great importance. Here we present a fully near-field photoluminescence study of semiconductor light sources (CdSe/ZnS quantum dots), with a surface plasmon interference device (SPID) used for the excitation and scanning near-field optical microscopy (SNOM) for the collection.

The SPID consists of an opaque metallic layer (gold or silver with a thickness of about 200 nm) on a glass substrate with thin slits fabricated using focused-ion-beam milling [1,2,3]. The subwavelength thickness (below 100 nm) of the slits ensures that only surface plasmon polaritons (SPP) can propagate through the slits while the far-field radiation is blocked. The SPID is illuminated from the bottom while the metallic layer blocks the impinging wave. SPP are generated at the slits, propagate through the slit, and form a standing wave on the top interface, where the distribution of the field is characterized by SNOM. With a semiconductor light source positioned directly at the top interface, luminescence can be generated [Fig. 1(a)]. The luminescence near field at the top of the SPID is again characterized by a SNOM. The optical signal is collected with the aperture-type probe and guided through the optical fiber to the spectrometer. Details of the setup are provided in Ref. [2].

We have demonstrated the plasmon-excited far-field and near-field luminescence of CdSe/ZnS quantum dots [Fig. 1(b,c)]. We have observed a rather weak effect of the excitation mechanism on the emission energy and intensity. This makes the plasmon-excited luminescence a suitable tool for the on-chip integration of semiconductor light sources, as well as a characterization technique with the subwavelength spatial resolution.
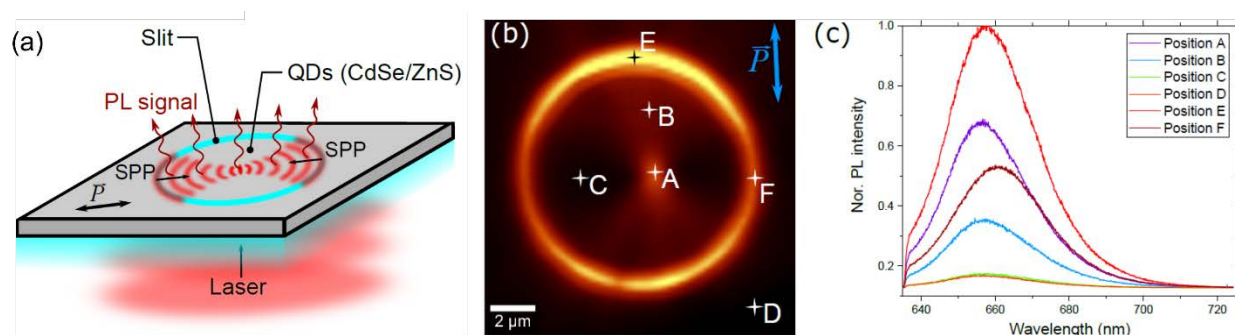

Fig. 1 (a) Scheme and operation principle of SPID. (b) Spatial map of the luminescence from quantum dots excited with SPP. (c) Spectral of the luminescence recorded at selected areas of SPID indicated in panel (b).

References

[1] Dvořák P., Neuman T., Břínek L., Šamořil T., Kalousek R., Dub P., Varga P, Šikola T. 2013. *Nano Lett.*, 13, 2558–2563.

[2] Dvořák P., Édes Z., Kvapil M.., Šamořil T., Ligmajer F., Hrtoň M., Kalousek R., Křápek V., Dub P., Spousta J., Varga P, Šikola T. 2017. *Opt. Express*, 25, 16560–16573.

[3] Dvořák P., Kvapil M., Bouchal P., Édes Z., Šamořil T., Hrtoň M., Ligmajer F., Křápek V., Šikola T. 2018. *Nanoscale*, 45, 21363–21368.

Correlative electron and optical spectroscopy of strongly-coupled mid-infrared plasmon and phonon polaritons

Pavel Gallina[1], Andrea Konečná[1], Michal Kvapil[1,2], Jiří Liška[1,2], Vlastimil Křápek[1,2], Radek Kalousek[1,2], Juan Carlos Idrobo[3], and Tomáš Šikola[1,2]

1. CEITEC BUT, Brno University of Technology, Purkyňova 123, 612 00 Brno, Czech Republic
2. Institute of Physical Engineering, Brno University of Technology, Technická 2, 616 69 Brno, Czech Republic
3Center for Nanophase Materials Sciences, Oak Ridge National Laboratory, Oak Ridge, Tennessee 37831, USA
E-mail: michal.kvapil@ceitec.vutbr.cz

Plasmonic or generally nanophotonic systems have been usually investigated by optical and electron beam spectroscopic methods. However, as a rule, each of them have been applied for individual samples separately without direct comparison of their results. In this presentation we take up this challenge and report on the correlative electron and optical spectroscopy applied for an exploration of fundamental phenomena associated with nanostructured systems possessing both infrared phonon polaritons (PhPs) and plasmon polaritons (PPs). More specifically, we have studied an electromagnetic coupling between MIR PhPs in a silicon dioxide membrane and low-energy localized surface plasmon (LSP) modes formed by the confinement of PPs in micrometer-long gold antennas. We have found that far-field IR spectra can be substantially different from EEL spectra, which we confirm by experiments supported by numerical simulations and analytical modeling. We show that by precisely positioning the electron beam, the coupling between the polaritonic excitations can selectively trigger either uncoupled PhPs or coupled LSPs/PhPs. Based on our understanding of the focused-beam excitation of the polaritonic system, we also present a post-processing analysis in the EEL spectra that facilitates identification of the new hybrid modes and allows an easier comparison to the far-field optical spectra [1].

In addition to this study, we will present a complementary analysis of the electromagnetic coupling between localized surface plasmons in gold rectangular antennas and MIR PhPs in a silicon dioxide thin film on a semi-infinite silicon substrate. Even though the underlying principles in this system have been previously described [2, 3], we complement these results by a detailed analysis of the resultant hybrid modes based on a coupled oscillator model, realistic SiO2 dielectric function, as well as on the calculation of the Hopfield mixing coefficients [4].
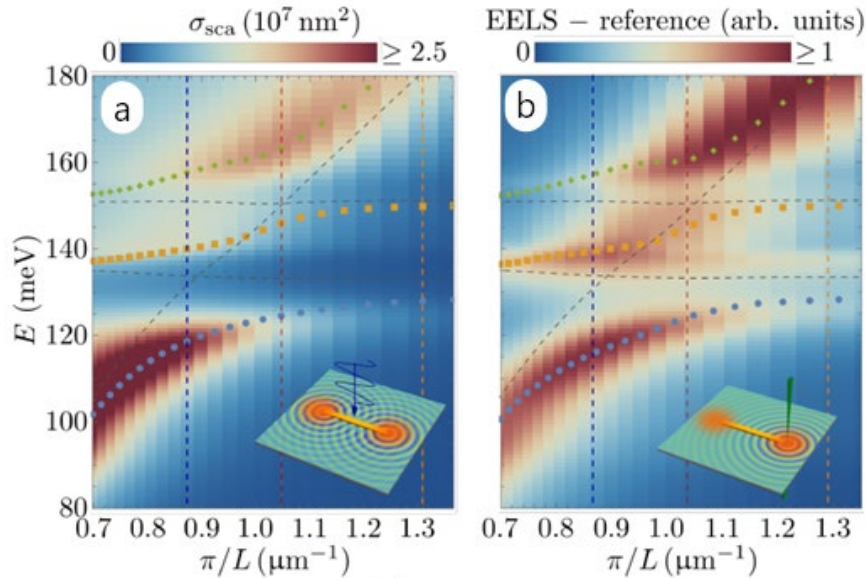

Fig. 1 Coupled system response as a function of the plasmonic antenna length. Simulated pseudo-dispersions for (a) optical scattering and (b) reference-subtracted EEL spectra.

References

[1] Gallina, P. et al., arXiv:2112.12832 (2021), https://arxiv.org/pdf/2112.12832.pdf
[2] Huck, C; Vogt, J.; Neuman, T.; Nagao, T.; Hillenbrand, R.; Aizpurua, J.; Pucci, A.; and Neubrech, F., Strong coupling between phonon-polaritons and plasmonic nanorods, 2016, Opttics express 24, 25528.
[3] Shelton, D.J.; Brener, I.; Ginn, J.C.; Sinclair, M.B.; Peters, D.W.; Coffey, K.R.; and Boreman, G.D., Strong coupling between nanoscale metamaterials and phonons, 2011, Nano letters 11, 2104.
[4] Gallina P. et al., arXiv:2112.07767v1 (2021), https://arxiv.org/pdf/2112.07767.pdf

Far-field photonic spin texture of thermal radiation from a non-isothermal nano-antenna

Parry Y. Chen[1], **Roy Ayash**[1], **Chinmay Khandekar**[2], **Yonatan Sivan**[1], **Z. Jacob**[2]

1. School of Electrical and Computer Engineering, Ben-Gurion University; 2. School of Electrical and Computer Engineering, Purdue University

E-mail: zjresearchgroup@gmail.com

The fluctuational electrodynamic analysis of thermal radiation from non-equilibrium or non-isothermal bodies remains largely unexplored because it is computationally cumbersome due to the requirement of volume integration over the fluctuating currents inside the emitter. Here, we put forth a formalism combining fast calculations based on complex permittivity mode expansion (also known as generalized normal modal expansion, GENOME) [1] and fluctuational electrodynamics to accelerate research at this frontier. Our formulation enables a complete characterization of the emission which for systems with a uniform temperature, require only knowledge of the permittivity eigen modes and eigenfunctions, thus, making our approach significantly simpler and accurate than any previous approach.

We then employ our formalism to predict that temperature gradients in an experimentally relevant long silica wire can generate thermal emission with a non-zero spin that extends into the far-field, is constant in direction and sign, and is perpendicular to the direction of power flow [2]. Such nonequilibrium spin texture of heat radiation is non-intuitive and quite unexpected since the previously known origins of spin emission rely on the use of exotic chiral, nonisotropic or magnetic materials, mechanical rotations or magnetic fields and is limited to the near-field.
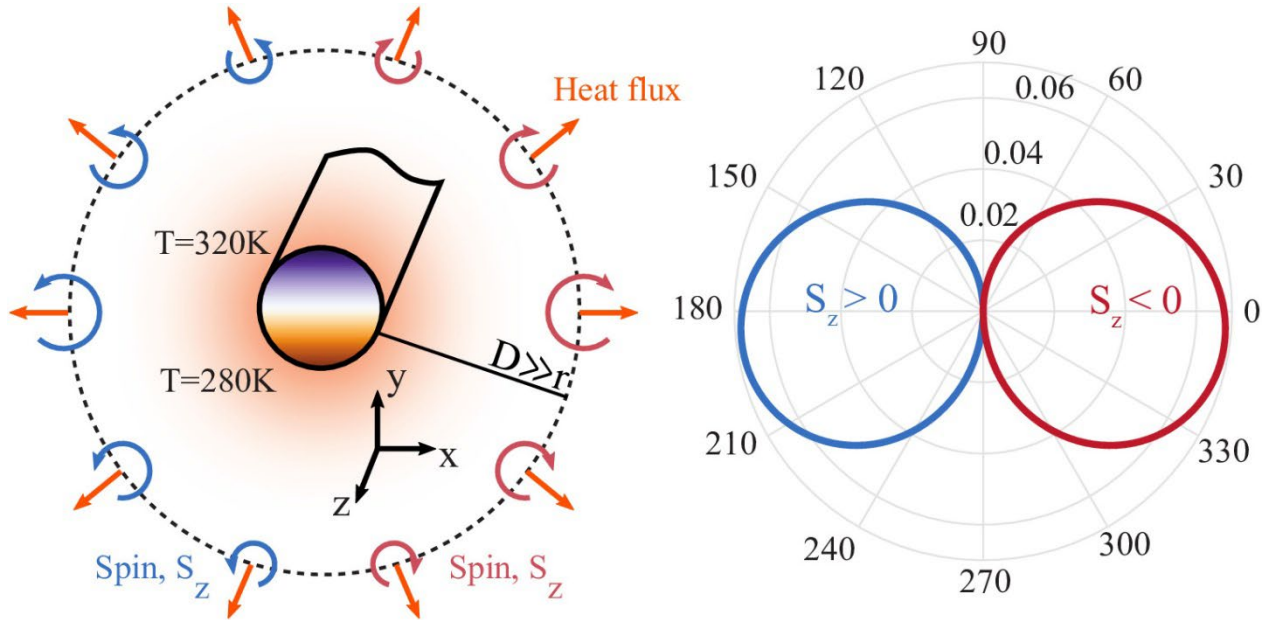

Fig. 1 (Left) An example geometry that can be treated by our formalism for non-equilibrium fluctuation electrodynamics. A temperature gradient is maintained across the cross-section of a circular silica rod, which extends infinitely along the z-direction. Heat flux, characterized by Poynting's vector, is generated along the radial direction. More notably, spin fields are generated that are in-plane, characterized by a spin vector which is perpendicular to both the plane and the Poynting vector. (Right) The spin extends into the far-field, D >> r, where r is the radius of the cylinder and D is the radius of the far-field contour. The normalized spin converges to the displayed non-zero values. The sign and the magnitude of the far-field spin vector changes as a function of the in-plane polar angle, but does not substantially change at scales of the order of the wavelength.

References

[1] Chen, P. Y., Bergman, D. J., Sivan, Y., (2019*), Phys. Rev. Appl.* 11, 044018.
[2] Chen, P. Y., Ayash, R., Khandekar, C., Jacob, Z., Sivan, Y., (2022*), submitted.*

Optical phase control in strongly driven infrared nanoresonators assisted by molecular vibrations

Felipe Herrera[1,2]**, Mauricio Arias**[3]**, Johan F. Triana**[1]

1. *Departamento de Física, Universidad de Santiago de Chile, Santiago, Chile*
2. *ANID-Millennium Institute for Research in Optics, Chile*
3. *Departamento de Física, Universidad de Concepción, Concepción, Chile*
E-mail: felipe.herrera.u@usach.cl

Open infrared nanoresonators are ideal platforms for studying room temperature cavity QED with organic materials. Nanotips can be used for imaging the coupled near field with a spatio-temporal resolution that is currently unavailable with conventional diffraction-limited cavities [1]. We propose and numerically demonstrate a novel type of ultrafast infrared blockade effect assisted by molecular vibrations that can be used for manipulating the temporal response of pulse-driven vibration-resonator systems. Using strong femtosecond infrared pulses, near-field IR photons and molecular vibrations become transiently detuned due to the natural anharmonicity of higher vibrational levels. This effective vibrational blockade imprints a coherent phase shift on the free induction decay signal that can be measured using tip nanoprobes. We predict infrared phase shifts of a few radians with short (~100 fs) pulses that can bleach the vibrational ground state by 10% or more. The phase shift depends nonlinearly with the pulse power [2]. In contrast with other blockade mechanisms in cavity QED, our scheme does not rely on light-matter entanglement and is suitable for weak coupling scenarios. Possible applications in optical state preparation in the mid-infrared are discussed.

References

[1] B. Metzger, E. Muller, J. Nishida, B. Pollard, M. Hentschel, and M. B. Raschke. 2019. *Phys. Rev. Lett*. 123, 153001
[2] J.F. Triana, M. Arias, F. Herrera et. Al. 2021. *arXiv*:2110.07371.

Compact 750-µJ, 75-W, sub-40-fs laser for efficient THz light sources driven by a two-color scheme

Christian Grebing[1], Fabian Stutzki[1], Sven Breitkopf[1], Oliver Herrfurth[1]
Joachim Buldt[2], <u>Tino Eidam</u>[1,*] and Jens Limpert[1,2,3,4]

1. Active Fiber Systems GmbH, Ernst-Ruska-Ring 17, 07745 Jena, Germany.
2. Institute of Applied Physics, Abbe Center of Photonics, Friedrich Schiller University Jena, Albert-Einstein-Str. 15, Germany.
3. Fraunhofer Institute for Applied Optics and Precision Engineering, Albert-Einstein-Str. 7, 07745 Jena, Germany
4. Helmholtz-Institute Jena, Fröbelstieg 3, 07743 Jena, Germany
Author e-mail address: publications@afs-jena.de

The THz spectral range attracted a lot of interest during recent years due to the growing number of applications in various fields including fundamental research [1], material research [2], imaging [3] or quality control [4] in production processes. For many of these applications, more output power of the THz source is demanded. In principle, this need can be satisfied by higher input power of the driving light source, however, it is often limited by the damage threshold of the THz-generation material. This can be circumvented when gas-based THz generation in a plasma is utilized [5].

In this contribution, we present a state-of-the-art ultrafast fiber-based chirped-pulse amplifier (FCPA) system emitting 800µJ laser pulse at 1030 nm wavelength and 100kHz repetition rate to drive a THz-generation scheme as depicted in Figure 1.

Figure 1: Schematic view of the laser-based THz generation as published in reference [5].

The FCPA is used to drive a multipass cell (MPC) that enables efficient pulse compression to sub-40-fs pulse duration. More than 90% of the input laser power is preserved during compression due to our recent advances in multipass cells [6]. The MPC enables pulse compression to less than 40fs as shown by the autocorrelation signal in Figure 2 (left). The compressed pulses are then used for second-harmonic generation. Both the fundamental mode and its second harmonic can then be focussed into gas for plasma-based THz generation. The presented THz-driver source features excellent long-term power stability over more than 8 hours at 75W average power with 0.2% standard deviation as depicted in Figure 2 (right).
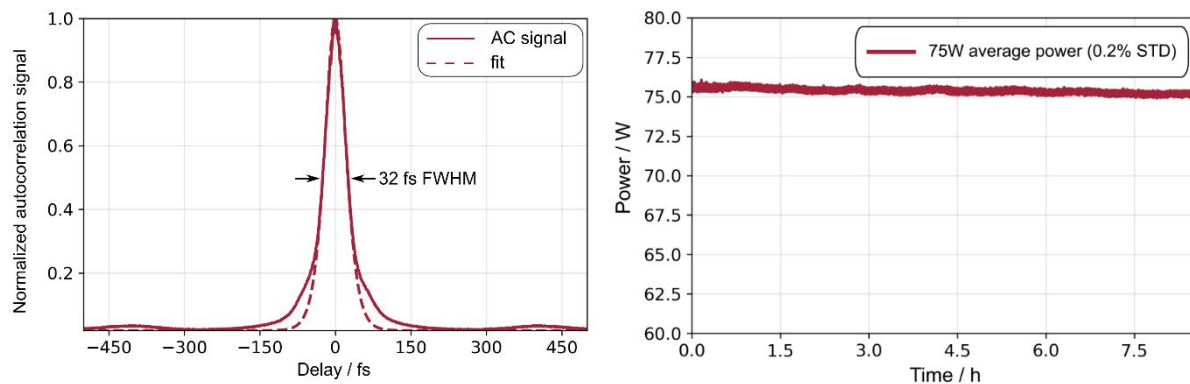

Figure 2: (left) Autocorrelation measurement (solid line) and sech2 fit (dashed line) of the compressed laser pulses featuring 32 fs pulse duration at 75W average power. (right) Corresponding long-term power-stability measurement of the compressed laser pulses over more than 8 hours.

References
[1] O. Schubert et al., "Sub-cycle control of terahertz high-harmonic generation by dynamical bloch oscillations",
 Nat. Photonics **8**, 119–123 (2014)
[2] Daniele Nicoletti and Andrea Cavalleri, "Nonlinear light–matter interaction at terahertz frequencies," Adv. Opt. Photon. **8**, 401-464 (2016)
[3] C. Jansen et al., "Terahertz imaging: applications and perspectives," Appl. Opt. **49** 19, E48–E57 (2010).
[4] M. Tonouchi, Cutting-edge terahertz technology. Nat. Photonics 1, 97–105 (2007)
[5] J. Buldt et al., "Gas-plasma-based generation of broadband terahertz radiation with 640 mW average power", Opt. Lett. **46**, 20 (2021).
[6] C. Grebing et al., "Kilowatt-average-power compression of millijoule pulses in a gas-filled multi-pass cell", Opt. Lett. **45**, 22 (2020).

Time-resolved Cathodoluminescence in a TEM

S. Meuret*[1], L. H.G. Tizei[2], F. Houdellier[1], S. Weber[1], Y. Auad[2], M. Tencé[2], H.-C. Chang[3], M. Kociak[2] and A. Arbouet[1]

1 - CEMES-CNRS Université de Toulouse 29 rue Jeanne Marvig 31055 Toulouse France
2 - Université Paris-Saclay, CNRS, Laboratoire de Physique des Solides, 91405, Orsay, France
3 - Institute of Atomic and Molecular Sciences, Academia Sinica, Taipei 106, Taiwan

*sophie.meuret@cemes.fr

Cathodoluminescence is the emission of visible light when an electron interacts with matter. It is a powerful technique to study the luminescence properties of semiconductors below the diffraction limit of visible light. The development of time-resolved Cathodoluminescence (TR-CL) in a scanning electron microscope (SEM) enabled the measurement of the lifetime of excited states in semiconductors with a sub-wavelength spatial resolution. It was used for example to measure the influence of stacking faults on the GaN exciton lifetime [1], to probe the role of a silver layer on the dynamics of a YAG crystal [2] or to show the influence of stress on the optical properties of ZnO nanowires [3]. These results demonstrate that TR-CL is essential to study the correlation between semiconductor optical and structural properties (composition, defects, strain…). Despite giving precious information, TR-CL in a SEM is still limited in spatial resolution. CL in the *transmission* electron microscope (TEM) could dramatically improve the spatial resolution with respect to SEM-CL, in addition to give access to multiple complementary analysis tools (from atomic scale imaging to electron energy loss spectroscopy).

In this presentation, we will discuss the first experimental demonstration of time-resolved cathodoluminescence within a TEM [4]. It was performed in a unique femtosecond pulsed TEM, with a cold-FEG electron gun [5]. This technology allows among other things sub-ps temporal resolution while preserving a spatial resolution of a few nanometers, essential for the study of nanophotonic materials. We will present the first lifetime maps acquired in a TEM both on nano-diamonds and InGaN quantum wells and discuss the unique features and opportunities of this technique.
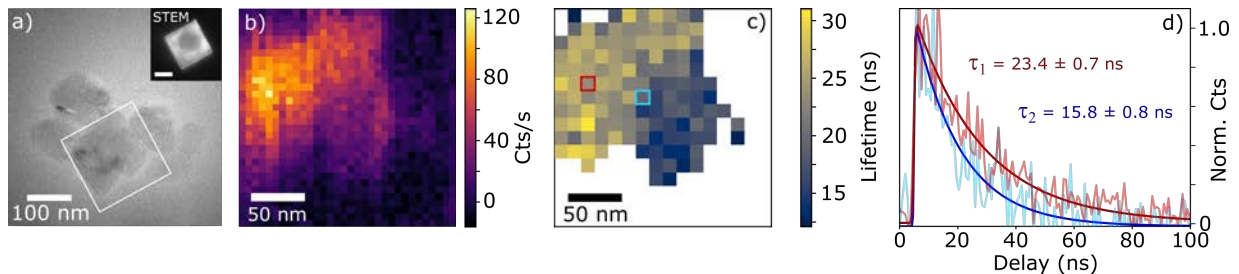

Figure 1: a) TEM image of a nano-diamond cluster containing a high density of nitrogen vacancy color center. b) CL Intensity map (whit square in a). c) Lifetime extracted from the decay trace at each pixel. d) Example of two decay traces form two different pixels.

References

[1] P. Corfdir *et al.*, "Exciton localization on basal stacking faults in a-plane epitaxial lateral overgrown GaN grown by hydride vapor phase epitaxy," *J. Appl. Phys.*, vol. 105, no. 4, p. 043102, 2009.

[2] R. J. Moerland, I. G. C. Weppelman, M. W. H. Garming, P. Kruit, and J. P. Hoogenboom, "Time-resolved cathodoluminescence microscopy with sub-nanosecond beam blanking for direct evaluation of the local density of states," *Opt. Express*, vol. 24, no. 21, p. 24760, 2016.

[3] X. Fu *et al.*, "Exciton Drift in Semiconductors under Uniform Strain Gradients: Application to Bent ZnO Microwires," *ACS Nano*, vol. 8, no. 4, pp. 3412–3420, 2014.

[4] S. Meuret *et al.*, "Time-resolved cathodoluminescence in an ultrafast transmission electron microscope," *Appl. Phys. Lett.*, vol. 119, no. 6, p. 6, 2021.

[5] F. Houdellier, G. M. Caruso, S. Weber, M. Kociak, and A. Arbouet, "Development of a high brightness ultrafast Transmission Electron Microscope based on a laser-driven cold field emission source," *Ultramicroscopy*, vol. 186, pp. 128–138, 2018.

Slot-bridge nanobeam cavities for high Q/V ratios

Joshua Fabian[1,2], **Xiruo Yan**[1,3], **Adan Azem**[1,2], **Donald Witt**[1,2], **Kashif Awan**[1], **Matthew Mitchell**[1],
Andreas Pfenning[1], **Lukas Chrostowski**[1,2], **and Jeff F. Young**[1,3]

1. Steward Blusson Quantum Matter Institute, University of British Columbia, 2355 East Mall, Vancouver, BC V6T 1Z4, Canada
2. Department of Electrical and Computer Engineering, University of British Columbia, 5500-2332 Main Mall, Vancouver, BC V6T 1Z4, Canada
3. Department of Physics and Astronomy, University of British Columbia, 325-6224 Agricultural Road, Vancouver, BC V6T 1Z1, Canada
E-mail: jfabian@ece.ubc.ca

Optical resonators that enhance the coupling between individual optically active elements and photonic modes are a central element in quantum information technologies based on spin-photon interactions, see Refs. [1-4]. These resonators should simultaneously have low losses (i.e., a high Q factor) and a small optical mode volume (to increase the coupling strength). Based on a design proposal by Choi et al. [5], we demonstrate a silicon photonic crystal nanobeam cavity that provides extreme dielectric light confinement within a tiny bridge structure with a mode volume down to $V \approx 0.0093\ \lambda_0^3$ while keeping a high quality factor of $Q \approx 15$ k.

Figure 1 (a) shows a SEM image of the fully under-etched cavity. From the SEM images, we extract the exact device dimensions such as a bridge width of only 45 nm (indicated by a white arrow). Based on the experimentally determined device dimensions, we have calculated the mode profiles for the lowest three supported resonant modes using a three-dimensional finite difference time domain (3D-FDTD) solver. The simulated mode volumes for the first, second, and third order mode are found to be $V_1 \approx 0.0093\ \lambda_0^3$, $V_2 \approx 0.0092\ \lambda_0^3$, and $V_3 \approx 0.011\ \lambda_0^3$, respectively, and are also shown in Figure 1 (a). The first order mode is particularly well suited for enhanced coupling schemes due to its field maximum which is strongly localized within the bridge area. Figure 1 (b) shows the measured transmission spectrum with a closer view of the first order mode in linear scale. The second order mode is strongly damped by the grating couplers used to couple light into the chip, whereas the third order mode is completely suppressed. Using a Lorentzian fit function, we extract $Q_1 \approx 15$ k, and $Q_2 \approx 3$ k, respectively.
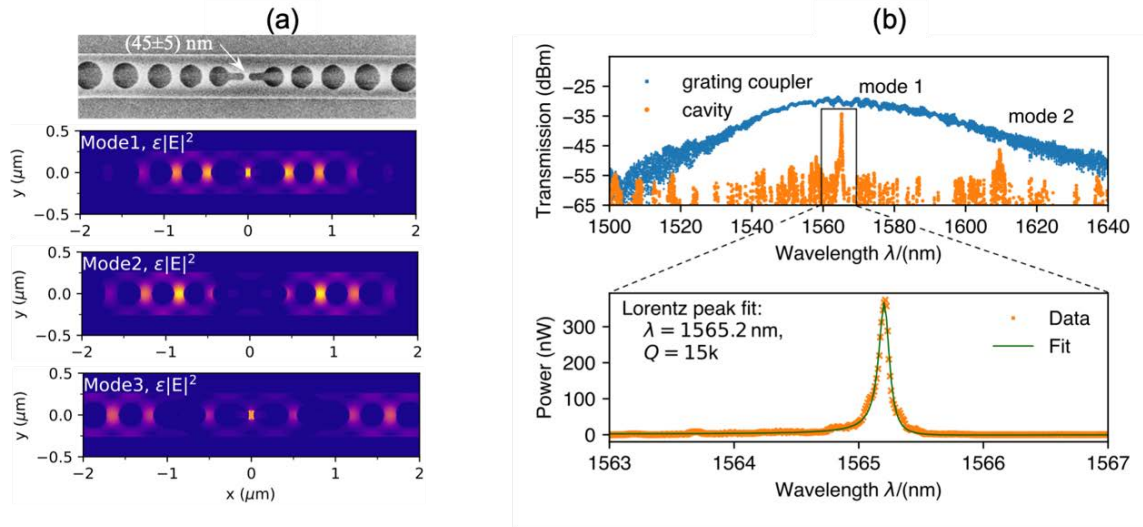

Fig. 1. (a) SEM image of the fabricated slot-bridge nanobeam cavity and simulated mode profiles of the lowest 3 supported modes. The cavity is formed by holes in a free-floating silicon nanobeam with a slot connecting the two innermost holes. The bridge (indicated by a white arrow) spans the slot at the center of the cavity and has a width of 45 nm. The simulated mode volumes are $V_1 \approx 0.0093\ \lambda_0^3$, $V_2 \approx 0.0092\ \lambda_0^3$, and $V_3 \approx 0.011\ \lambda_0^3$, respectively. (b) Measured transmission spectrum with zoom-in on the first order mode in linear scale. The Lorentz peak fit yields a high quality factor of 15 k at a wavelength of 1565.2 nm. The second and third order mode are suppressed by the grating coupler used to couple light into the chip.

References
[1] Nemoto, K. *et al.* 2014. *Phys. Rev. X* **4**, 031022.
[2] Morse, K. J. *et al.* 2017. *Sci. Adv.* **3**, e1700930.
[3] Yan, X. *et al.* 2020. *Adv Quantum Tech* **3**, 2000011.
[4] Yan, X. *et al.* 2021. *APL Photonics* **6**, 070901.
[5] Choi, H., Heuck, M. & Englund, D. 2017. *Phys. Rev. Lett.* **118**, 223605.

iSCAT in Nanofluidic Channels: A Physical Model

Philippe Marc Nicollier[1], **Armin Knoll**[1]

1. IBM Research Europe - Zurich, Säumerstrasse 4, 8803 Rüschlikon, Switzerland

E-mail: phn@zurich.ibm.com

Interferometric Scattering Microscopy (iSCAT) has emerged in the last 20 years as a method of choice to achieve label-free, high-speed imaging and characterization of nanoparticles [1]. The interferometric nature of the technique leads to a favorable scaling of contrast with particle volume. The contrast depends linearly on the scattered and reference field amplitudes |Es| and |Er|, as well as on their phase difference θ:

$$C \approx \frac{|Es|}{|Er|}\cos\theta$$

To reach sensitivities and signal-to-noise ratios necessary to visualize biological species such as single proteins [2], optimized set-ups and image processing procedures have been implemented. Among them, particles are generally immobilized on the coverslip interface to provide a defined focal plane and to allow for frame averaging. However, it is also desirable to image freely diffusing particles in nanofluidic channels [3]. Many parameters play a role when imaging diffusing particles in nanofluidic channels, such as the geometry of the slits, the thin film structure of the confining walls, the position of the particle in the gap, as well as the focus position of the imaging beam [4]. It is thus crucial to have a robust description of the imaging contrast to be expected for a particular particle in a certain nanofluidic channel geometry.

Various models have been proposed in the last years to describe the contrast and point spread function in iSCAT imaging [5-8]. However, a comprehensive physical model taking into account near-field effects, as well as considering the presence of multiple dielectric interfaces, is yet to be published.

Building on existing models, we propose a physical description of the interference contrast and point spread function for the general case of diffusing particles in multilayered nanofluidic slits. We are in the process of validating the simulations with experimental data acquired on our dedicated experimental set-up, the nanofluidic confinement apparatus (NCA) [9]. The NCA allows us to perform experiments in nanofluidic gaps of varying wall composition, gaps and focal positions. Thus, we can explore a wide parameter space to validate the model. This will allow us to predict the optimal imaging contrast as a function of layer parameters and illumination conditions.

References

[1] Young, G., Kukura, P., 2019, *Ann. Rev. Phys. Chem.*, 70, 301-322
[2] Piliarik, M., Sandoghdar, V., *Nat. Comm.*, 2014, 5, 4495, 1-8
[3] Spackova et al., *Nat. Methods,* 2022, 1-8
[4] Mojarad, N., Sandoghdar, V., Krishnan, M., *Opt. Exp.*, 2013, 21, 8, 9377-9389
[5] Fringes, S., Skaug, M., Knoll, A., *J. Appl. Phys.*, 2016, 119, 2, 024303
[6] Sevenler, D., Avci, O., Ünlü, S., *Biomed. Opt. Exp.,* 2017, 8, 6, 2976-2989
[7] Mahmoodabadi, R., et al., *Opt. Exp.,* 2020, 28, 18, 25969-25988
[8] He, Y., et al., *J. Phys. D.: Appl. Phys.* 2021, 54, 274002
[9] Fringes, S., Holzner, F., Knoll, A., *Beilstein J. Nanotech.,* 2016, 9, 1, 301-310

iSCAT Microscopy for Imaging the Interactions of Polymer Dots with HeLa Cells

Eric Boateng, **Bruno Luppi, William Primrose, Luke Melo, Zachary Hudson, and Edward Grant**

Department of Chemistry, University of British Columbia, Vancouver, BC V6T 1Z1 Canada

eboateng@chem.ubc.ca

Semiconducting polymer dots (Pdots) have emerged as powerful nanoscale probes for bioimaging, sensing, and photodynamic therapy. Characterized by high brightness, resistance to photobleaching, and tunable surface chemistry, Pdots can enable imaging and analysis on the scale of single nanoparticles. Pdots are water-dispersed nanoparticles composed of >50% organic semiconducting polymer, ideally with strong absorbance and high emission quantum yield [1–3].

Here we aim to image the biological effects of Pdot-cell interactions using interferometric scattering (iSCAT) microscopy. We have studied the iSCAT kinetics of diblock copolymer nanoparticles composed of a water-soluble polyethylene glycol-based block and a rigid organic semiconductor block.

Initial experiments have applied the methodologies we have developed to gauge size distributions of gold nanoparticles [4] to record iSCAT mass photometry signals from HeLa cells and pure Pdots in aqueous suspension. These Pdots had an estimated mean diameter of 100 nm, with a standard deviation σ of about 30 nm. HeLa cells were incubated at 37°C and maintained in a cell medium until imaging. Figure 1A is an iSCAT image of individual HeLa cells attached on poly-D-lysine (PDL) derivatized glass coverslip. Figure 1C shows a single frame of a typical ratiometric image of Pdots landing on the PDL coverslip. A comparison in Figure 1D shows the changes in the HeLa cell image when altered by interaction with Pdots. This observation is a typical mechanism of cell lysis recorded when HeLa cells take up polymer nanoparticles.
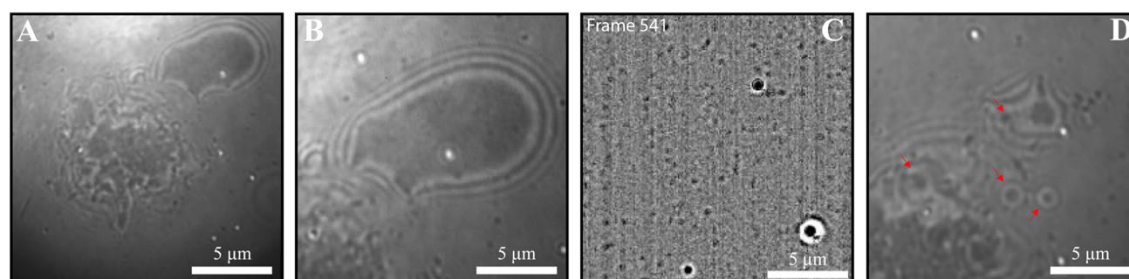

Fig. 1. **(A)** iSCAT image of single HeLa cells. **(B)** Close-up view of the HeLa cell showing very well-resolved membrane as the specific site for Pdots penetration. **(C)** Ratiometric image of polymer dots landing on a poly-D-lysine coverslip recorded at a single frame. **(D)** Changes in HeLa cell image observed when polymer dots penetrate. This shows a typical mechanism of cell lysis, red arrows indicate remains of the cell-penetrating polymer dots in the host cell.

References

[1] Rong, Y et al. 2013. Multicolor Fluorescent Semiconducting Polymer Dots with Narrow Emissions and High Brightness. *ACS Nano*, 7 (1), 376–384.

[2] Yuan, Y.; Hou, W.; Qin, W.; Wu, C. 2021. Recent Advances in Semiconducting Polymer Dots as Optical Probes for Biosensing. *Biomaterial. Science* 9:328-346

[3] Christopherson C.J.; Paisley N.R.; Xiao Z.; Algar, W.R.; Hudson, Z.M. 2021. Red-Emissive Cell-Penetrating Polymer Dots Exhibiting Thermally Activated Delayed Fluorescence for Cellular Imaging. *Jam. Chem. Soc.* 143:13342-9.

[4] Melo, L.; Hui, A.; Kowal, M.; Boateng, E.; Poursorkh, Z.; Rocheron, E.; Wong, J.; Christy, A.; Grant, E. 2021. Size distributions of colloidal gold nanoparticles measured in solution by single-particle mass photometry. *J. Phys. Chem. B*, 125:12466−12475

iSCAT as a high-throughput, accurate and reproducible probe of size distribution in solution-phase suspensions of cellulose nanocrystals

Hooman Tavakolizadeh,[1] Mahfuzul Hoque,[2] Luke Melo,[1] Johan Foster[2] and Edward Grant[1]

[1]Department of Chemistry, University of British Columbia, Vancouver, BC V6T 1Z3, Canada
[2]Department of Chemical and Biological Engineering, University of British Columbia, Vancouver, BC V6T 1Z3, Canada
E-mail: hooman.tzn@gmail.com

The innovative use of nanocellulose materials (NCMs) and cellulose nanocrystals (CNCs) in particular, calls for readily applicable methods that can characterize morphology and size distributions, as well as dispersion-agglomeration state in solution. Transmission electron (TEM) and atomic force (AFM) microscopy yield structurally detailed fixed images, but require low-throughput, labor-intensive processes of analysis that are prone to inconsistency [1,2]. Dynamic light scattering (DLS) operates on solution-phase dispersions, but suffers well-known limitations in accuracy and dynamic range.

Interferometric scattering microscopy (iSCAT) offers a direct high-throughput means of sampling nanoparticles from solution [3]. In this technique, the light scattered by every particle as it binds to a coverslip interferes with a reflected reference field to form a diffraction-limited image with a contrast that scales linearly with the mass of the particle. Here, we demonstrate the application of iSCAT to measure the size distribution of CNCs with a throughput as high as 1,000 particles per minute.

Figure 1(a) shows one frame in a sequence of ratiometric images. Particles that appear as point-spread functions in Figure 1(a) fade to one as the background advances to include them. Figure 1(b) shows the distribution of contrast formed by the measurement of 2574 particles in a 3 minute experiment. The particle size distribution derived from many TEM images such as Figure 1(c) calibrates contrast to determine the CNC mass distribution.
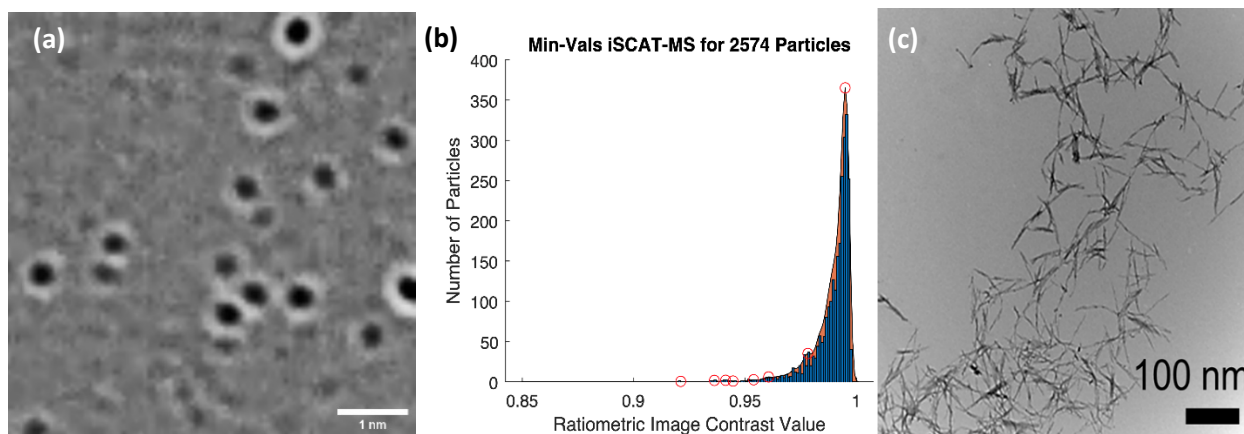

Figure 1 (a) Ratiometric iSCAT image of single CNCs landing and receding into the background. (b) Distribution of contrast for 2574 particles acquired in a 3 minute experiment. (c) TEM micrograph of CNCs.

References

[1] Balea, A., Blanco, A., Delgado-Aguilar, M., Monte, M., Tarres, Q., Fuente, E., Mutje, P., & Negro, C. 2021. *BioResources, 16*(2), 4382-4410
[2] Foster J, Moon RJ, Agarwal UP, Bortner MJ, Bras J, et al. 2018. *Chem. Soc. Rev.*,47, 2609-2679
[3] Melo L, Hui A, Kowal M, Boateng E, Poursorkh Z, Rocheron E, et al. 2021. *J Phys Chem B*, 125(45):12466-12475.

The Solution Transport Limit of Non-Langmuir iSCAT Adsorption

Edène Rocheron[1], **Luke Melo**[1], Jake Wong[1], Edward Grant[1]

1. University of British Columbia, Department of Chemistry, 2036 Main Mall, Vancouver, BC, Canada, V6T 1Z1

E-mail: lmelo@chem.ubc.ca

Specialized applications of nanoparticles often call for particular, well-characterized particle size distributions in solution, but this property can prove difficult to measure. Recent work has exploited interferometric scattering (iSCAT) mass photometry advantages of high-throughput and large dynamic range to quickly infer size distributions in colloidal suspensions of gold nanoparticles [1]. Other applications have measured the kinetics of binding reactions to gauge the concentration of reactants in solution [2]. The most straightforward analysis of experimental measurements assumes in both cases that the rate of transport in the bulk exceeds the depletion of particles in the solution immediately adjacent to the plane of measurement.

We have found evidence for 5, 10 and 15 nm gold nanoparticles that the observed rate of binding to a poly-D-lysine coated coverslip decreases much faster than deposition decreases the bulk concentration of nanoparticles in solution [3]. The fall-off in deposition rate clearly fails to conform with a Langmuir adsorption model. The evident size selectivity of this non-Langmuir behaviour seems to suggest a deposition process that is limited by the transport properties of nanoparticles in quiescent solutions.

We computationally model the molecular dynamics of 10 nm gold nanoparticles in solution to track concentration as a function of distance from the coverslip at observed deposition rates for reasonable values of diffusion coefficient. Our results indicate the formation of a depletion layer above the surface of the coverslip, creating a concentration gradient that grows with time. (**Fig. 1A**). Particles that remain in solution when the rate plateaus remain available to replenish the deposition when we stir the solution. (**Fig. 1B**)
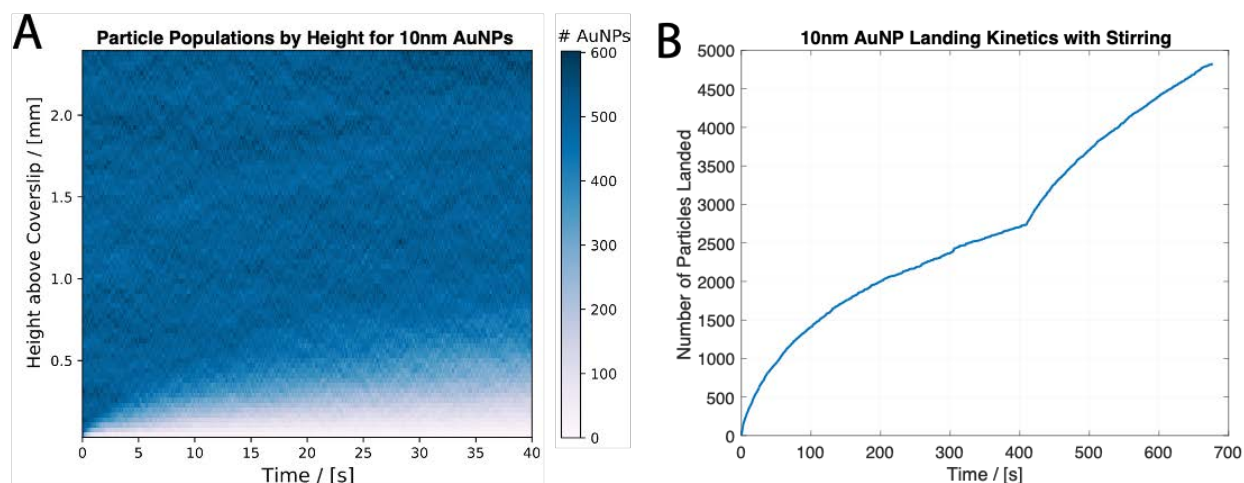

Fig. 1 (A) As time progresses, the depletion of particle concentration rises through the height of the bulk. (B) As time progresses, the rate of deposition decreases. However, upon stirring the solution, the deposition rate increases again corresponding to a replenished depletion layer.

References

[1] Young, G., Hundt, N., Cole, D., Fineberg, A., Andrecka, J., Tyler, A., Olerinyova, A., Ansari, A., Marklund, E. G., Collier, M. P., Chandler, S. A., Tkachenko, O., Allen, J., Crispin, M., Billington, N., Takagi, Y., Sellers, J. R., Eichmann, C., Selenko, P., … Kukura, P. (2018). Quantitative mass imaging of single biological macromolecules. *Science*, *360*(6387), 423–427.

[2] Young, G., & Kukura, P. (2019). Interferometric Scattering Microscopy. Annual Review of Physical Chemistry, 70(1), 301–322.

[3] Melo, L., Hui, A., Kowal, M., Boateng, E., Poursorkh, Z., Rocheron, E., Wong, J., Christy, A., & Grant, E. (2021). Size Distributions of Gold Nanoparticles in Solution Measured by Single-Particle Mass Photometry. *Journal of Physical Chemistry B*, *125*(45), 12466–12475.

Detection of Nanoplastics in Mixed Solutions using Interferometric Scattering Microcopy

Matthew D. Kowal, Teresa M. Seifried and Edward Grant

Department of Chemistry, University of British Columbia, Vancouver, BC V6T 1Z1

E-mail: mdkowal@chem.ubc.ca

Synthetic polymers, produced and discarded for nearly a century, ultimately degrade to form small plastic particles now found in every sphere of the environment. Measurements have detected evidence for airborne microplastics in Arctic and Antarctic snow [1]. Microplastic discharged from terrestrial sources pollute natural aquatic environments in all parts of the world [2].

Accurate assessments of the extent of microplastic pollution face a number of fundamental materials challenges. Real environmental systems contain natural particulate matter in abundance. Assays must distinguish microplastics from mineral dust and natural organic particles. Microplastics span a very broad distribution in size, from tens of millimeters to tens of nanometers. Though rarely detected, particles at the small end of this range dominate in number, and may well present the greatest cause for pathological concern [3].

Here we describe an approach using interference microscopy to count individual nanoplastic particles as they land and bind to poly-D-lysine and other derivatized coverslips. Small plastic particles generally support a negative surface charge at near-neutral pH [4]. Microplastic zeta potentials generally exceed those of mineral particles [5]. Thus, conditions exist under which functionalized coverslips can differentially bind suspended microplastics, enabling methods of iSCAT microscopy to measure abundance and relative size [6].
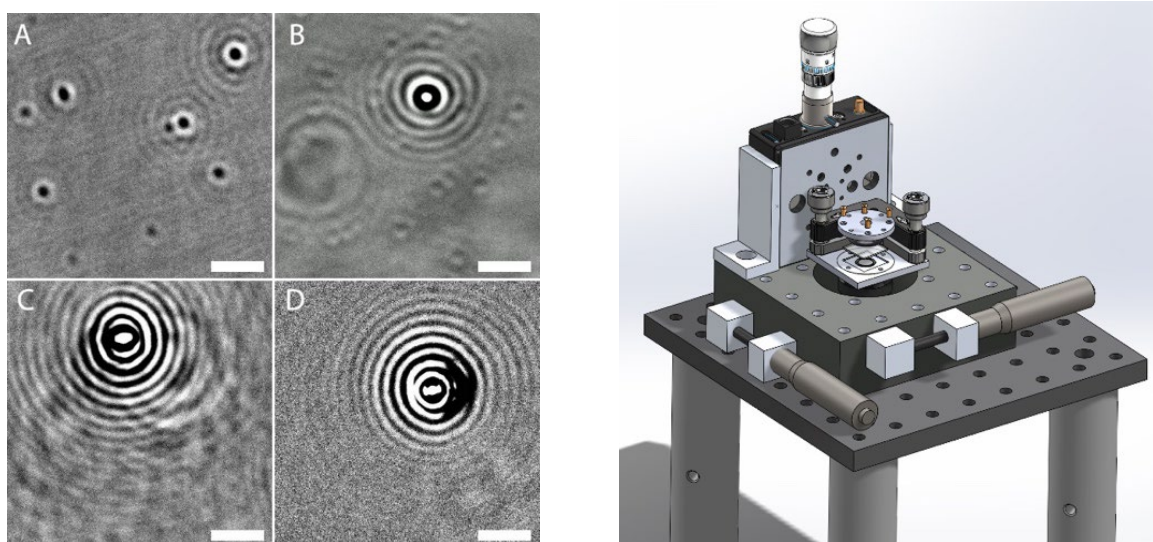

Fig. 1 Left, Interferometric scattering images of polystyrene nanobeads in (A) 50 nm, (B) 100 nm, C) 200 nmm D) 350 nm diameters. Scale bar: 2 μm. Right, 3D model of the microscope sample stage

References

[1] Aves AR, Revell LE, Gaw S, Ruffell H, Schuddeboom A, Wotherspoon NE, LaRue M, McDonald AJ. First evidence of microplastics in Antarctic snow. *The Cryosphere Discussions*. 2022 Jan 4:1-31.

[2] Bergmann M, Gutow L, Klages M. *Marine anthropogenic litter*. Springer Nature; 2015.

[3] Lim X. Microplastics are everywhere—but are they harmful?, *Nature* 2021 **593**, 22-25

[4] Wang Y, Xu L, Chen H, Zhang M. Retention and transport behavior of microplastic particles in water-saturated porous media. *Science of The Total Environment*. 2022 **808** 152154.

[5] Berg JM, Romoser A, Banerjee N, Zebda R, Sayes CM. The relationship between pH and zeta potential of~ 30 nm metal oxide nanoparticle suspensions relevant to in vitro toxicological evaluations. *Nanotoxicology*. 2009 **1** 276-83.

[6] Melo, L., Hui, A., Kowal, M., Boateng, E., Poursorkh, Z., Rocheron, E., Wong, J., *Size Distributions of Gold Nanoparticles in Solution Measured by Single-Particle Mass Photometry*, The Journal of Physical Chemistry B 2021, **125** 12466-12475

High-throughput synthesis and characterization of compositionally-graded films

Shahram Moradi[1], Makhsud Saidaminov[1,2]
1. Department of Electrical & Computer Engineering, University of Victoria, 3800 Finnerty Rd, Victoria, BC V8P 5C2, Canada
2. Department of Chemistry, University of Victoria, 3800 Finnerty Rd, Victoria, BC V8P 5C2, Canada
E-mails: msaidaminov@uvi.ca
Shahrammoradi@uvic.ca

New materials are conventionally searched by synthesizing and studying a limited number of compositions. However, this approach is fragmentary and unfortunately misses a significant fraction of material alloys. This fragmentary approach my delay or even disable the discovery of potential 'magic' compositions.

Here we report a method for fabricating compositionally gradient films to synthesize all possible alloys from binary systems in a single shot in less than 1 min. We use our approach to study an applied challenge – the stability of halide perovskites, a promising and fast-growing class of semiconductors for various optoelectronic applications. We synthesize over 200 possible phases from a binary system of MAPbI3 and MAPbBr3, and then study their optical properties in a high-throughput manner (Fig. 1). We find that perovskite alloys experience three different degradation mechanisms depending on halogen content: Br-rich perovskites degrade through hydration, while I-rich perovskites – through the loss of organic component; all other intermediate alloys degrade through segregation to Br-rich perovskite and lead iodide. The proposed method of fabricating composition gradient film paves avenues for discovering new materials and processing parameters for a broad range of applications that rely on compositional engineering.
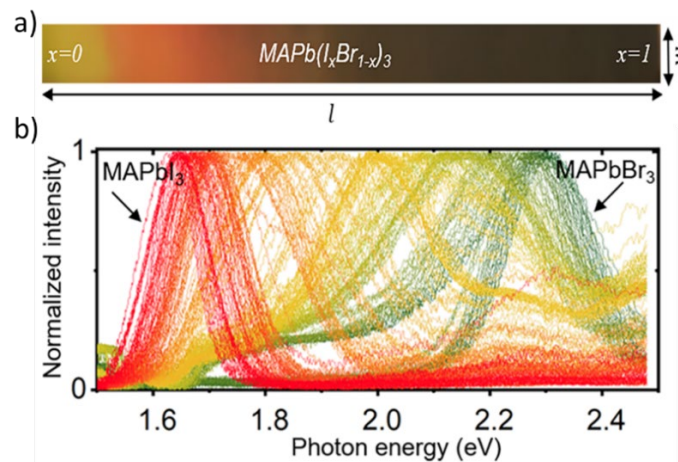

Fig. 1 Optical properties of MAPb(IxBr1-x)3

References

[1] S. Moradi et. al. "High-throughput exploration of halide perovskite compositionally-graded films and degradation mechanisms", Just acceptedCommunications Materials.

Defocus Phase Contrast in Photon-Induced Near-field Electron Microscopy

John H. Gaida[1,2], **Hugo Lourenco-Martins**[1,2], **Sergey V. Yalunin**[1,2], **Armin Feist**[1,2], **Murat Sivis**[1,2],

Thorsten Hohage[3], **F. Javier García de Abajo**[4,5], **and Claus Ropers**[1,2]

1. Max Planck Institute for Multidisciplinary Sciences, Am Faßberg 11, 37077 Göttingen, Germany
2. 4th Physical Institute, University of Göttingen, Friedrich-Hund-Platz 1, 37077 Göttingen, Germany
3. Institute of Numerical and Applied Mathematics, University of Göttingen, Lotzestraße 16-18, 37083 Göttingen, Germany
4. ICFO-Institut de Ciencies Fotoniques, Av. Carl Friedrich Gauss, 308860 Castelldefels (Barcelona), Spain
5. ICREA-Institució Catalana de Recerca i Estudis Avançats, Passeig Lluís Companys 23, 08010 Barcelona, Spain
john.gaida@mpinat.mpg.de

Electron microscopy encompasses a variety of techniques to study the nanoscale optical properties of materials and devices. Spontaneous inelastic electron-light scattering (IELS), resulting in cathodoluminescence and electron-energy loss, is frequently used to spectroscopically characterize the photonic density of states with high spatial resolution over a broad optical bandwidth [1]. In addition, stimulated scattering in the presence of optical illumination of the sample, allows for mode- and polarization-selective quantitative measurements of optical near fields in the form of Photon-Induced Near-field Electron Microscopy (PINEM) [2, 3]. In this technique, inelastic scattering produces sidebands in the electron kinetic energy spectrum corresponding to energy gains and losses in multiples of the photon energy. The number of populated sidebands is a direct measure of the near-field strength [1], and since the scattering process is coherent in nature, the spatial distribution of the optical near-field phase is imprinted onto the electron wave function. Here, we use Fresnel-mode defocus imaging to reveal electron phase contrast induced by stimulated IELS.
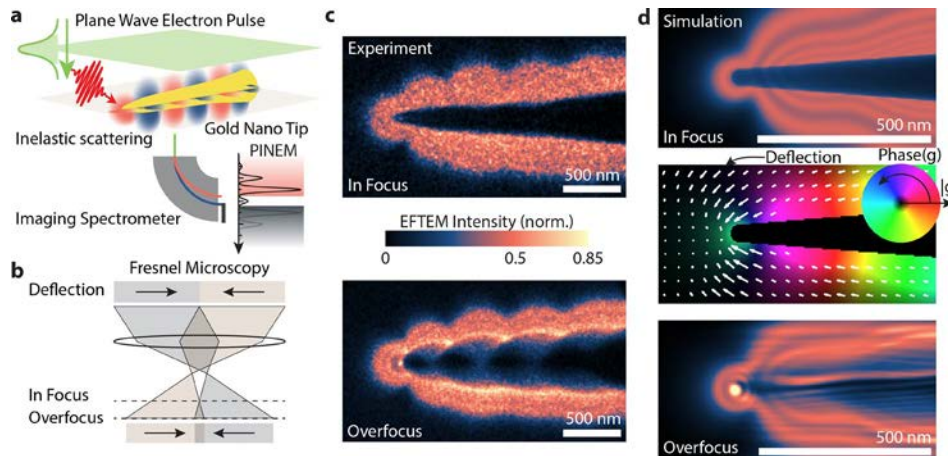

Fig. 1 a, Sketch of the PINEM experiment with IELS and energy-filtered imaging. b, Schematic of Fresnel microscopy. c, EFTEM micrographs reveal the amplitude and deflections of the optical near-field under in-focus and overfocus imaging conditions, respectively. d, Simulated amplitude and phase of the near-field interaction g and resulting in focus and overfocus EFTEM images.

The experiments are carried out at the Göttingen Ultrafast Transmission Electron Microscope (UTEM) operated with a laser-triggered field emission electron gun delivering electron pulses of high spatial coherence. Here, a gold nanotip is excited by femtosecond laser pulses shown in Fig. 1 a. Collimated electron pulses are used for PINEM, imaging individual sideband amplitudes of the electron wave function Ψ_N (N photon order). To this end, we employ a single-electron-sensitive detector behind an imaging electron spectrometer with a controllable slit for energy selection. Figure 1 c presents an in-focus image collected from all electrons experiencing energy loss, exhibiting the shadow image of the nanotip and a standing wave pattern resulting from interference between surface plasmons excited on the conical tip and far-field radiation scattered at the tip-supporting shaft. A corresponding simulation of the near-field interaction near the tip apex is displayed in Fig. 1 d and shows general agreement. In the absence of aberrations, the image intensity in focus is independent of the phase of the coupling parameter g. However, gradients in the phase of g result in electron beam deflections, which can be revealed using phase-contrast imaging. Specifically, we employ Fresnel-mode Lorentz imaging, a phase-contrast technique that is widely used to characterize in-plane magnetic fields. As illustrated in Fig. 1 b, defocus imaging translates locally varying beam deflections into amplitude modulations. In the specific geometry in study, strong phase gradients are induced near the apex of the tip (cf. simulation of phase gradients in Fig. 1 d, center). Working under overfocus conditions modifies the energy-filtered image, producing a bright spot of enhanced intensity near the tip apex, and caustics along the shaft in both experiment (Fig. 1 c, bottom) and simulation (Fig. 1 d, bottom). In the presentation, we will compare differences in imaging contrast using energy gain and loss sidebands, coupled by the relation $\Psi_{-N} = \overline{\Psi_N}$ and, thus, exhibiting opposite deflections and phase gradients. Moreover, we will explore algorithmic near-field phase reconstruction and polarization-dependent imaging.

References
[1] García de Abajo, F. J. and Kociak, M. *Phys. Rev. Lett.* **100**, 106804 (2008).
[2] Barwick, B., Flannigan, D. J. & Zewail, A. H. *Nature* **462**, 902–906 (2009).
[3] Harvey, T. R. *et al. Nano Lett.* **20**, 4377–4383 (2020).

Photon pair directly produced into the guided modes of nonlinear waveguides via down-conversion

Álvaro Rodríguez Echarri[1], Joel D. Cox[2,3] and F. Javier García de Abajo[1,4]

1. ICFO – Institut de ciències fotòniques, The Barcelona Institute of Science and Technology, 08860 Castelldefels, Barcelona, Spain
2. Center for Nano Optics, University of Southern Denmark, Campusvej 55, DK-5230 Odense M, Denmark
3. Danish Institute for Advanced Study, University of Southern Denmark, Campusvej 55, DK-5230 Odense M, Denmark
4. ICREA – Institució Catalana de Recerca i Estudis Avançats, Passeig Lluís Companys 23, 08010 Barcelona, Spain
alvaro.rodriguez@icfo.eu

During the last decades great advances have been made to consolidate the field of quantum communications, in which the entanglement of particles and photons plays a key role. Up until now, there have been many strategies proposed to generate entangled photon pairs that encode the information carried by photons in their polarization or orbital angular momentum degrees of freedom. However, additional difficulties are found to steer and manipulate the generated photons to use them in practical applications, and therefore efforts have been made to integrate on-chip sources of entangled photons. In this work, we introduce a direct illumination scheme to generate entangled photons encoded in the optical mode states of a lossless fiber [1] (see Fig. 1a). We study this scheme of pair production by employing a rigorous theoretical method to down-convert a direct incident electric field into guided modes, where energy and momentum conservation restricts the allowed excited modes (see Fig. 1b). In order to quantify the production rate, we compute the reverse process of frequency sum for which two photons up-convert and emit into the far field, and based on the reciprocity theorem, both processes have the same probability. We demonstrate that for optical fibers made of a suitable nonlinear material such as $LiNbO_3$, the rate of photon pair production can be $\sim 10^5$ under attainable illumination condition, thus supporting the feasibility of this disruptive approach to directly generate entangled and waveguided photon pairs. We thus envision that these findings can stimulate experimental ventures in quantum optics to entangle light with a predictable degree of fidelity and help alleviate practical issues related to the coupling of quantum light sources to optical components required in emerging quantum information technologies.
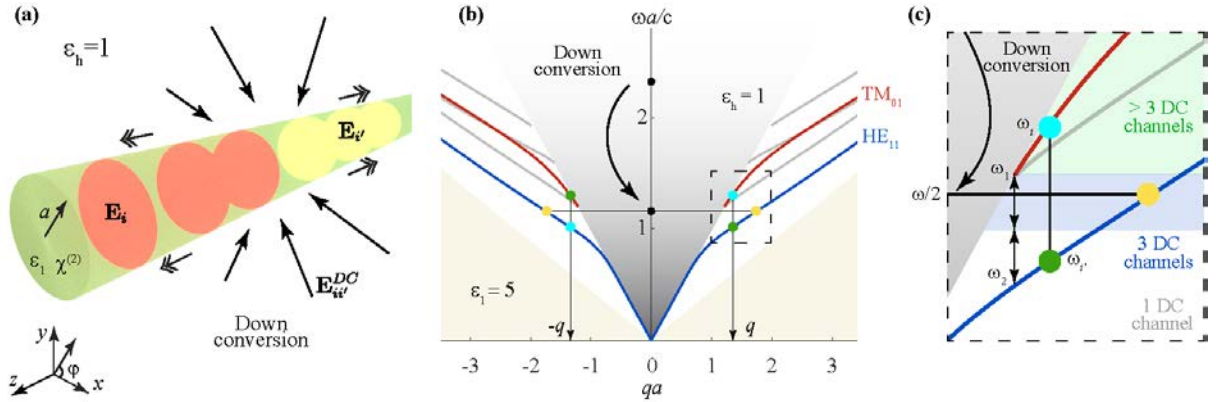

Figure 1. Generation of waveguided entangled photon pairs by down-conversion in an optical fiber. (a) Illustration of a cylindrical fiber (radius a, material permittivity ϵ_1, host permittivity ϵ_h) subject to normal illumination. Each incident photon can be down-converted via the second-order nonlinear response of the fiber material (susceptibility $\chi^{(2)}$) to produce two waveguided photons within modes i and i' of fields $\mathbf{E}_i$ and $\mathbf{E}_{i'}$, frequencies ω_i and $\omega_{i'}$, and wave vectors q_i and $q_{i'}$ satisfying $q_i + q_{i'} = 0$. (b) Dispersion diagram of waveguide modes (normalized frequency $\omega a/c$ as a function of normalized wave vector qa) for $\epsilon_1 = 5$ and $\epsilon_h = 1$. The light cones in the waveguide and host materials (white and grey areas, respectively) limit the existence of the modes. We highlight the two lowest-order modes that possess nonzero longitudinal field components (HE_{11} and TM_{01}, see labels) and enable down-conversion with a small number of emission photon-pair channels: one symmetric (yellow circles) and two asymmetric (blue and green circles) channels. (c) Detail of these channels, showing the threshold frequency of the TM_{01} mode ω_1, the frequency ω_2 of the HE_{11} mode with the same wave vector, and the number of down-conversion channels available depending on the incident photon frequency ω (1, 3, and >3 in white blue and green areas). Each channel has $\pm q$ and $\pm m$ degeneracies.

References

[1] Álvaro Rodríguez Echarri, Joel D. Cox, and F. Javier García de Abajo, "*Direct generation of entangled photon pairs in nonlinear optical waveguides*", Nanophotonics (2022).

Sizing single quantum dots in solvent using nano-tweezers

Hao Zhang[12], **Parinaz Moazzezi**[123], **Brett Henderson**[23], **Cristina Cordoba**[24], **Arthur Blackburn**[24], **Makhsud I. Saidaminov**[123], **Irina Paci**[23] and **Reuven Gordon**[12]

1. Department of Electrical and Computer Engineering, University of Victoria, 3800 Finnerty Road, Victoria, V8P 5C2, British Columbia, Canada
2. Centre for Advanced Materials & Related Technologies (CAMTEC), University of Victoria, 3800 Finnerty Road, Victoria, V8P 5C2, British Columbia, Canada
3. Department of Chemistry, University of Victoria, 3800 Finnerty Road, Victoria, V8P 5C2, British Columbia, Canada
4. Department of Physics and Astronomy, University of Victoria, 3800 Finnerty Road, Victoria, V8P 5C2, British Columbia, Canada

E-mail: rgordon@uvic.ca

Cesium lead halide perovskite quantum dots (PQDs) promising solution-based optical materials because of their outstanding photonic performance [1]. With the great breakthroughs in studying PQDs, many applications have been developed (e.g., single-photon emitters [2], improved solar cells [1]). Based on the quantum confinement, the emission wavelengths from PQDs vary with size [3]. Producing and measuring the dots with uniform and controllable size has been a goal to improve the performance in device applications. Several groups have refined the fabrication processes to obtain good size uniformity; however, this usually involves transmission electron microscope analysis a posteriori, which is not convenient for characterization. Sizing PQDs insolvent would be a good approach when producing PQDs with uniform size [3], allowing for in-situ monitoring.

In this paper, we present an approach to characterize in-situ the size of **individual** quantum dots and correlate this with their optical spectrum to see the impact of quantum confinement. We observe and analyze the heterogeneity of PQDs insolvent by using optical tweezers with DNH aperture. From the Brownian motion characteristic signal collected by an avalanche photodiode, we calculate the standard deviation and autocorrelation time constant of each single trapping event, as is shown in Fig. 1(a), which has a slope of -0.67 on a log-log plot, as expected from theory. With the linear relationship between the standard deviation and emission spectrum, as is shown in Fig. 1(b), we can analyze and estimate the physical size of the single dot in solution. By using a simple calculation model of the Schrödinger equation, we calculate the bandgap as a function of particle size, which has a good agreement with our experiment result.
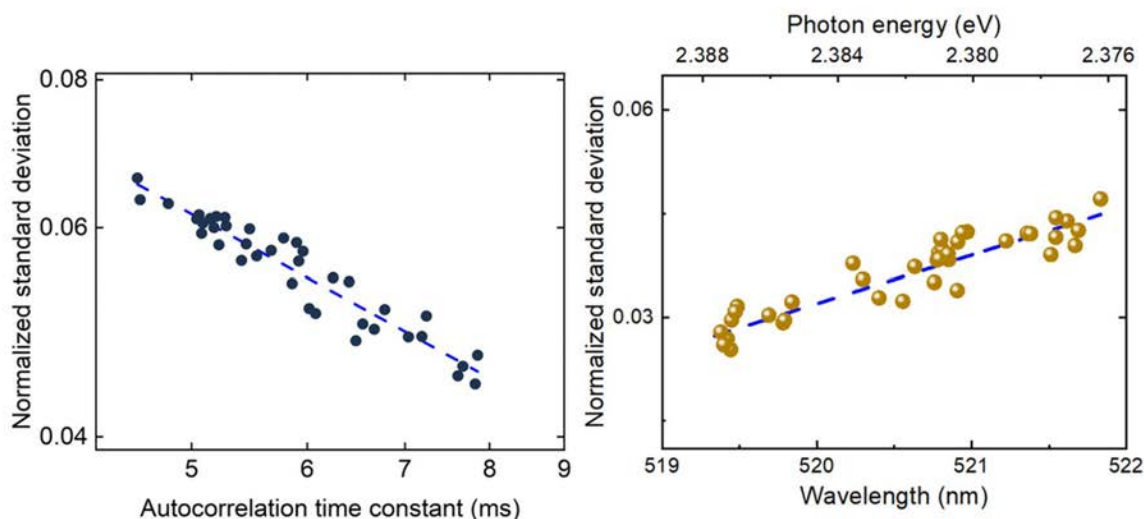

Fig. 1 (a) The standard deviation against the autocorrelation time constant of single PQD trapping collected by using DNH optical tweezer. The curve of standard deviation against autocorrelation time constant is about the power of -0.68 with the best fit, which has a good agreement with the theoretical calculation in our previous work [4]. (b) The standard deviation from the trapping event has a linear relationship with the emission wavelength of the single PQD. The single PQD's size can be estimated by a simple calculation.

References

[1] Stranks, S. D., Snaith, H. J. (2015). Metal-halide perovskites for photovoltaic and light-emitting devices. Nature nanotechnology, 10(5), 391-402.
[2] Morozov, S., Vezzoli, S., Myslovska, A., Di Giacomo, A., Mortensen, N. A., Moreels, I., & Sapienza, R. (2021). Purifying single-photon emission from a CdSe/CdS colloidal quantum dot. arXiv preprint arXiv:2111.09090.
[3] Dong, Y., Qiao, T., Kim, D., Parobek, D., Rossi, D., & Son, D. H. (2018). Precise control of quantum confinement in cesium lead halide perovskite quantum dots via thermodynamic equilibrium. Nano letters, 18(6), 3716-3722.
[4] Wheaton, S., Gordon, R. (2015). Molecular weight characterization of single globular proteins using optical nanotweezers. Analyst, 140(14), 4799-4803

Tip-Enhanced Strong Coupling (TESC):
Quantum coherent control of single emitters at room temperature

Benjamin G. Whetten[1], Kyoung-Duck Park[2], Molly A. May[1], Matthew Pelton[3], and Markus B. Raschke[1,*]

1. Department of Physics and JILA, University of Colorado, Boulder, CO 80303, USA
2. Department of Physics, School of Natural Sciences, Ulsan National Institute of Science and Technology, 50 UNIST-gil, Eonyang,-eup, Ulju-gun, Ulsan, South Korea
3. Department of Physics, UMBC (University of Maryland, Baltimore County), Baltimore, Maryland, 22150, USA
E-mail: markus.raschke@colorado.edu

Emerging quantum technologies with applications in sensing, metrology, and information processing rely on the coherent control of quantum states which can be achieved through optical cavities with hybridization and control of light-matter interaction. Traditionally, micro-cavities such as photonic crystals have been used to reach strong coupling of photons to single quantum emitters. However, because of the diffraction limited mode volume of micro-cavities, cryogenic temperatures are required to overcome decoherence. In contrast, plasmonic nano-cavities confine light to orders of magnitude smaller dimensions with nanometer-scale mode volumes, opening pathways to quantum control of solid-state emitters even at room temperature.

Here, we demonstrate and apply tip-enhanced strong coupling (TESC), to induce, image, and control single quantum emitters in the strong coupling regime. Using a shear force atomic force microscope, we position a plasmonic nano-tip with sub-nm precision above a metallic substrate to form a plasmonic pico-cavity with controllable mode volume and position (**Fig. 1a**). Unlike static plasmonic nano-cavities, the scanning probe in TESC enables imaging and spectroscopy of different quantum emitters at tunable coupling strengths all within the same cavity. We demonstrate strong coupling with Rabi splitting up to 160 meV in 8 nm CdSe/ZnS quantum dots (QDs) coated in a 0.5 nm layer of Al_2O_3 [1,2]. By controlling the nano-tip position, we reversibly control the coupling behavior of the cavity-emitter system with sub-nm precision (**Fig. 1b**). Furthermore, by probing QDs of different resonant energies, we observe an anti-crossing in the hybridized energy levels with splitting up to 100 meV (**Fig. 1c**).
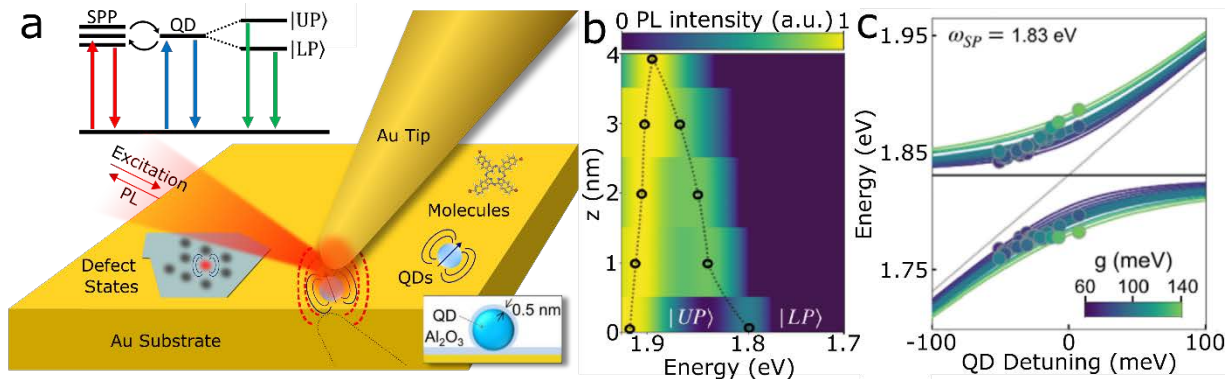

Fig. 1 (a) Tip enhanced strong coupling (TESC) of various quantum emitters in the pico-cavity formed between the nano-tip and mirror substrate. The cavity resonance (SPP) hybridizes with the quantum emitter energy levels to form strongly coupled polariton states. (b) Rabi splitting of the quantum emitter photoluminescence as a function of tip-emitter distance showing sub-nm precision control. (c) Anti-crossing of the hybridized energy levels as a function of quantum dot detuning from the cavity.

To obtain pico-cavity mode volumes, we extend TESC to sub-nm height emitters such as excitons and defects in two-dimensional (2D) materials. The reduced dimensionality of 2D materials allows the preparation of stable quantum emitters in few-layer samples that enable smaller mode volumes and thus higher coupling strengths. Here, we first investigate defects such as nitrogen vacancies in hexagonal boron nitride which exhibit strong photoluminescence across a range of wavelengths [3,4]. We further discuss the extension of pico-cavity control of competing relaxation pathways by distance control and modeling of coupled radiative and non-radiative pathways in heterostructures of transition metal dichalcogenides [5].

TESC thus offers unprecedented control of coherent interactions with quantum emitters in the strong coupling regime at room temperature. The generalization of TESC to a variety of single emitters will further enable the development of a wide array of quantum sensing and information devices for operation in ambient conditions.

References
[1] K. D. Park, et al., "Tip-enhanced strong coupling spectroscopy, imaging, and control of a single quantum emitter," Sci. Adv. **5**, (2019).
[2] M. A. May, et al., "Nano-Cavity QED with Tunable Nano-Tip Interaction," Adv. Quantum Technol. **3**, 1900087 (2020).
[3] T. T. Tran, et al., "Quantum emission from hexagonal boron nitride monolayers," Nat. Nanotechnol. 2015 111 **11**, 37–41 (2015).
[4] Y. Chen, et al., "Solvent-Exfoliated Hexagonal Boron Nitride Nanoflakes for Quantum Emitters," ACS Appl. Nano Mater. **4**, 10449–10457 (2021).
[5] M. A. May, et al., "Nanocavity Clock Spectroscopy: Resolving Competing Exciton Dynamics in WSe2/MoSe2Heterobilayers," Nano Lett. **21**, 522–528 (2021).

FRET-mediated Collective Blinking of Self-Assembled Stacks of Semiconducting Nanoplatelets

Zakarya Ouzit[1], **Jiawen Liu**[1], **Juan Pintor**[1], **Lilian Guillemeney**[2], **Benoît Wagnon**[2], **Benjamin Abécassis**[2], **Laurent Coolen**[1]

1. Sorbonne Université, CNRS, Institut des NanoSciences de Paris, INSP, F-75005 Paris, France
2. Université de Lyon, CNRS, Ecole Normale Supérieure de Lyon, Laboratoire de Chimie UMR 5182, F-69007 Lyon, France
E-mail: zakarya.ouzit@sorbonne-universite.fr

The synthesis of quasi-2D semiconducting nanoplatelets is common and easily achievable after years of study and development. Because of their particular shape, they present interesting optical properties: large oscillator strength, low Stokes shift and negligible inhomogeneous line width. The behavior of single nanoplatelets has been widely studied and different applications are investigated nowadays. Electronic devices (LEDs, field effect transistors…) or optical sources based on semiconducting nanoplatelets can be proposed as potential applications. In most cases, the particles are not used as individual emitters, but as ensembles in packed layers. To that extent, understanding the effects of nanoparticles on one another and their interactions is a topical issue in order to anticipate their collective behavior as a stack. Studies on films of close-packed semiconducting nanoplatelets showed the particles interact through FRET (Förster Resonance Energy Transfer), a non-radiative energy transfer by electromagnetic dipole-dipole interaction, widely studied used in biophysics and imaging.

Our latest interests were focused on linear self-assembled chains of CdSe nanoplatelets (TEM image in fig 1a) [1,2]. They play the role of a model system for the study of the platelet-platelet interactions. Indeed, the self-assembly protocol allows us to obtain a well-ordered stack with a homogeneous particle to particle spacing. Their length varies from one chain to another, from several 100 nm to 3-4 μm. We showed that in such stacks, nanoplatelets interact through FRET, leading to exciton diffusion along the chains with a characteristic diffusion length of around 500 nm [3].
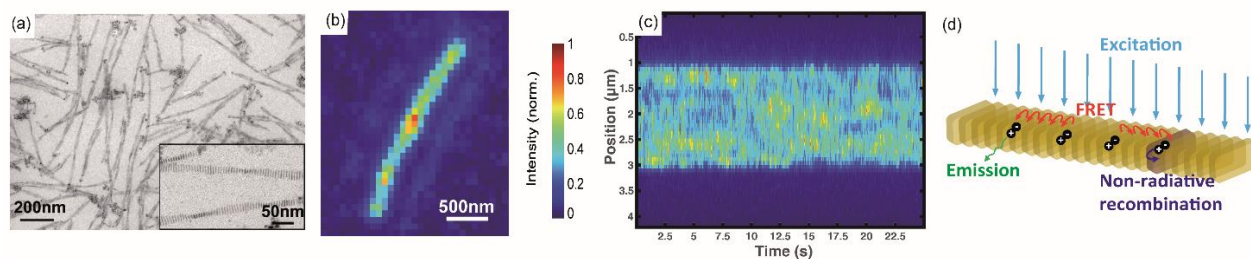

Fig. 1. (a) TEM image of CdSe nanoplatelets chains. (b) Fluorescence image with deconvoluted PSF of a typical single platelet chain under wide-field mercury lamp excitation. (c) Time-position diagram of the intensity along the chain of Fig.1b showing collective intensity fluctuations (same colorbar for both Fig. 1b and 1c). (d) Schematic representation of FRET-mediated collective blinking induced by a quenching nanoplatelet along a platelet chain under uniform excitation.

Here, we study the fluorescence fluctuations of self-assembled chains of CdSe nanoplatelets by imaging them through a micro-photoluminescence setup. We show on fig. 1b the fluorescence image of a single chain under wide-field mercury lamp excitation after deconvoluting the PSF of the imaging system. We acquired movies of the chains that showed fluctuations of the intensity. On fig. 1c, we plotted the time-position fluorescence diagram of the chain shown on fig 1b, showing the intensity profile along the y-axis evolving over time. One can spot "bright" states of emission and also "dark" ones where tens of nanoplatelets are switched off at the same time. Even stacked, it appears that the platelets blink as if they were single but collectively. We propose on fig 1d a mechanism to explain this collective blinking. We argue that FRET-diffusion and quenching nanoplatelets, being the site of fast non-radiative exciton recombination, drive this collective blinking: the excitons created along the chains would be diffused by FRET to the quenching sites and recombine non-radiatively. A 1D-random-walk model for the excitons diffusion supports our hypothesis.

References

[1] Abécassis, B., "Three-dimensional Self Assembly of Semiconducting Colloidal Nanoparticles: from fundamental forces to collective optical properties", *Chem Phys Chem*, **17**, 618-631 (2016)
[2] Guillemeney, L. et al, "Curvature and Self-Assembly of Semiconducting Nanoplatelets", *Comm Chem* **5**, 7 (2022)
[3] Liu, J. et al, "Long Range Energy Transfer in Self-Assembled Stacks of Semiconducting Nanoplatelets", *Nano Lett*, **20**, 3465–3470 (2020)

A scalable route to single-photon sources at low-loss wavelengths by anchoring nanocrystals with a single Er^{3+} dopant

Adriaan L. Frencken[1], **Michael Dobinson**[2], **Reuven Gordon**[2], **Frank C. J. M. van Veggel**[1]

1. Department of Chemistry, University of Victoria, Victoria, British Colombia V8W 2Y2, Canada
Centre for Advanced Materials & Related Technologies (CAMTEC), University of Victoria, Victoria, British Columbia V8W 2Y2, Canada
2. Department Electrical and Computer Engineering, University of Victoria, Victoria, British Columbia V8W 2Y2, Canada
Centre for Advanced Materials & Related Technologies (CAMTEC), University of Victoria, Victoria, British Columbia V8W 2Y2, Canada
E-mail: adriaanfrencken@uvic.ca

Quantum information science is a rapid growing scientific field, involving computation using quantum states with the goal to outcompete classical computation. A promising candidate for this is the photonic qubit and scalable fabrication of a single photon source is highly sought after.[1][2] Previously, our groups have demonstrated the isolation of single photon sources using optical traps to isolate nanoparticles (NPs) doped with a single Er^{3+} ion.[3][4] We are currently developing methods to anchor these NPs permanently in order to develop a scalable route for the fabrication of single photon sources.

Here we present an anchoring method based on the photo-removal of thiol protecting groups on the NP surface, allowing formation of a bond between the sulfur and the gold surface of the trapping aperture. Oleate-capped NaYF$_4$(:Er^{3+}) NPs of ca. 20 nm were coated with thiol functionalised phospholipids that were subsequently treated with the photo-removable protecting group (PG) 2-bromo-4'-hydroxyacetophenone. Succesful protection and photo-triggered deprotection were demonstated using thiol detecting agents.

For the anchoring demonstration, a 980 nm laser was used to trap the nanoparticles in a double nanohole (DNH) aperture optical tweezer in a 70 nm thick gold film with a 7 nm Ti adhesion layer. After verification of successful trapping, light from a 340 nm LED was used to trigger the release of the PGs and allow reaction of the sulfur groups with the gold surface. This process is demonstrated schematically in Fig. 1 (left). EM was used to show the presence of NPs after removal of the sample from the trapping optical beam, Fig. 1 (right).
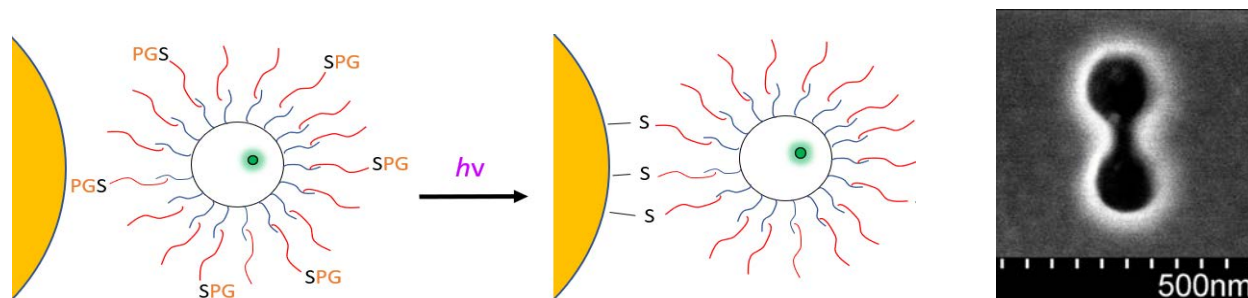

Fig. 1. (Left) Schematic representation of light triggered anchoring of NaYF$_4$ NPs doped with a sinle Er^{3+} ion. (Right) SEM image of a single NP anchored on the wall of a DNH gold aperture.

With our upcoming experiments, we aim to demonstrate emission from anchored NPs doped with a single Er^{3+} ion in the absence of the trapping beam. The single photon nature of the emission from the anachored NPs can then be verified, and the method can be used to up-scale the isolation of single Er^{3+} doped NPs for mass fabrication of single photon sources for photonic qubits.

References

[1] Dibos, A. M., et al. (2018). "Atomic Source of Single Photons in the Telecom Band." Phys. Rev. Lett., 120(24), 243601.
[2] Eisaman, M. D. et al. (2011). "Invited Review Article: Single-Photon Sources and Detectors." Review of Scientific Instruments, 82(7), 071101.
[3] Alizadehkhaledi, A., et al. (2020). "Isolating Nanocrystals with an Individual Erbium Emitter: A Route to a Stable Single-Photon Source at 1550 nm Wavelength." Nano Letters 20(2): 1018-1022.
[4] Sharifi, Z.., et al. (2021). "Isolating and Enhancing Single-Photon Emitters for 1550 Nm Quantum Light Sources Using Double Nanohole Optical Tweezers." J. Chem. Phys., 154(18), 184204.

Strong coupling dynamics and multi-photon correlations in waveguide QED using three coupled qubits

Sofia Arranz Regidor and Stephen Hughes

Queen's University, 99 University Avenue, Kingston, ON, K7L 3N6, Canada

E-mail: 18sar4@queensu.ca

The interaction between light and atoms and resonant materials has been a critical field of study in quantum mechanics for decades, leading to new quantum protocols and technologies. Photons coupled to atoms and resonant few-state systems present a fundamental model system in quantum optics, and when implemented on photonic chips, quantum circuits enabled through waveguide quantum electrodynamics (QED) are becoming an important field of research in nanophotonics and quantum optics. In waveguide QED, the interaction between quantum emitters (e.g., quantum dots or qubits) in the presence of a radiation channel is quasi one-dimensional, where the qubits are coupled to a continuum of quantized field modes. These hybrid systems show several new phenomena that are unique to the waveguide geometry. For example, in the presence of a time-delayed coherent feedback, qubits in a waveguide gives rise to interesting effects such as long-lived vacuum Rabi oscillations and multi-photon-matter entangled states [1].

Partly motivated by recent experimental work that realized qubit *strong coupling* behavior with atom-like mirrors [2], we explore three coupled qubits in a waveguide environment [Fig 1(a)]. We fully account for multi-photon effects and non-Markovian dynamics of the qubits, by implementing a Matrix Product State (MPS) approach [3], a powerful quantum model to represent the product state of many photons and qubits. In Fig. 1(b), we show example qubit dynamics, for a target qubit (center qubit, initially excited) as well as the mirror qubits, including the effects of chirality and delay time between the mirrors. We show how cavity-like phenomena (mediated by the mirror qubits), such as vacuum Rabi oscillations, can have their performance significantly improved through non-Markovian feedback.
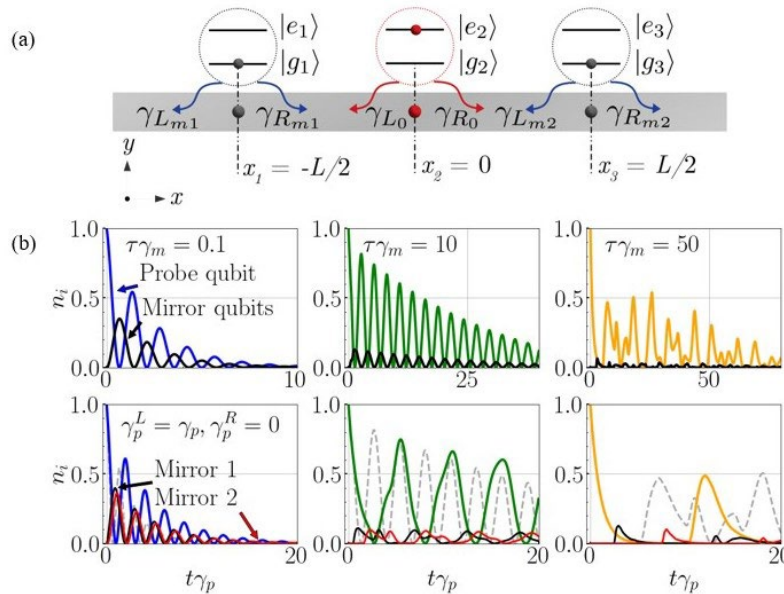

Fig. 1 (a) Schematic of three qubits (quantum dots or two-level systems) in a waveguide-QED system. The probe qubit is in the center. (b) Probe and mirror population dynamics for three different delay times, scaled by the nominal radiative decay rate for the target qubit into the waveguide (L means left scattering and R means right scattering rate). The top figures show symmetric coupling while the bottom ones explore chiral qubit behavior (where the dashed grey line compares to the symmetric results).

To more fully explore the quantum statistics of light, we also calculate the multi-photon quantum correlation functions for the three-qubit waveguide system, as well as the emitted spectrum, which show interesting phenomena when multi-photon resonances come into play. In the presence of a nonlinear pump field, we will demonstrate how well this quantum nonlinear system mimics a cavity-QED system and when it offers a significant departure, with some major advantages for exploring and controlling non-classical states of few photons and matter.

References

[1] Arranz Regidor, S., and Hughes, S. 2021, "Cavitylike strong coupling in macroscopic waveguide QED using three coupled qubits in the deep non-Markovian regime", *Phys. Rev. A* 104, L031701.

[2] Mirhosseini, M., Kim, E., Zhang, X., Sipahigil, A., Dieterle, P. B., Keller, A. J., Asenjo-Garcia, A., Chang, D. E., and Painter, O. 2019, "Cavity quantum electrodynamics with atom-like mirrors", *Nature* 569, 692-697.

[3] Arranz Regidor, S., Crowder, G, Carmichael, H.J, and Hughes, S. 2021, "Modeling quantum light-matter interaction in waveguide QED with retardation, nonlinear interactions, and a time-delayed feedback: Matrix product states versus a space-discretized waveguide model", *Phys. Rev. Research,* 3 023030.

Quantum Many-Body Study of Hybrid Plasmon–Exciton Systems at the Subnanometer Scale: Influence of Electronic Orbital Coupling

Antton Babaze[1,2], **Ruben Esteban**[1,2], **Andrei G. Borisov**[3], **and Javier Aizpurua**[1,2]

1. Materials Physics Center CSIC-UPV/EHU, Paseo Manuel de Lardizabal 5 20018 Donostia-San Sebastián, Spain
2. Donostia International Physics Center DIPC, Paseo Manuel de Lardizabal 4 20018 Donostia-San Sebastián, Spain
3. Institut des Sciences Moléculaires d'Orsay, UMR 8214 CNRS-Université Paris-Saclay Bât. 520, 91405 Orsay Cedex, France
E-mail: anttonbabaze@dipc.org

Due to the excitation of plasmonic resonances, metallic nanoparticles (MNPs) strongly enhance the amplitude of the incident electromagnetic field at optical frequencies and thus can excite very efficiently electronic transitions in quantum emitters (QEs) located nearby. Coupled QE–MNPs systems have been extensively exploited in many spectroscopy and microscopy techniques and, parallel to the experimental progress, substantial theoretical effort has been devoted to describe the optical response of such systems. Typical simulations based e.g. on classical or quantum electrodynamics only account for the *electromagnetic coupling* between QEs and MNPs, and are often able to successfully reproduce experimental results in situations of relatively large QE–MNPs separation [1]. However, at subnanometric distances, quantum phenomena associated with the *electronic coupling* between the orbitals of the QE and the MNP can play a crucial role. In such a situation, a quantum many-body treatment of the problem is essential to describe the optical response of the system. In this context, recent works based on time-dependent density functional theory (TDDFT) have shown that a QE bridging two MNPs can trigger charge-transfer processes due to the electronic coupling between the QE and MNPs at subnanometric distances [2,3].

In this work, we use TDDFT simulations to study the influence of electronic coupling on the optical interaction between QEs and MNPs [4]. The studied system consists of a QE supporting a single HOMO–LUMO transition placed within the nanogap formed by two spherical MNPs (Figure 1a). The gap separation and the QE transition energy are varied to study different regimes of QE−MNPs electronic coupling and identify the onset of quantum effects that strongly affect the optical response of the system. The TDDFT calculations reveal that the hybridization between the electronic states localized at the QE and at the MNPs produces a drastic quenching of the LUMO at (sub)nanometric gap separations that hinders the excitation of the HOMO–LUMO transition in the QE. As a consequence, the coupling strength between the QE and light is dramatically reduced, and thus, the optical response obtained within TDDFT significantly deviates from the classical electromagnetic prediction (Figure 1b). Further, our work demonstrates that electronic coupling can frustrate strong coupling between QEs and MNPs in situations where the system would be classically in the strong-coupling regime. This work thus shows the importance of electronic coupling between the orbitals localized at the QE and at the MNPs for subnanometric separations and stress the need to go beyond the electromagnetic interaction picture usually adopted to describe these systems.
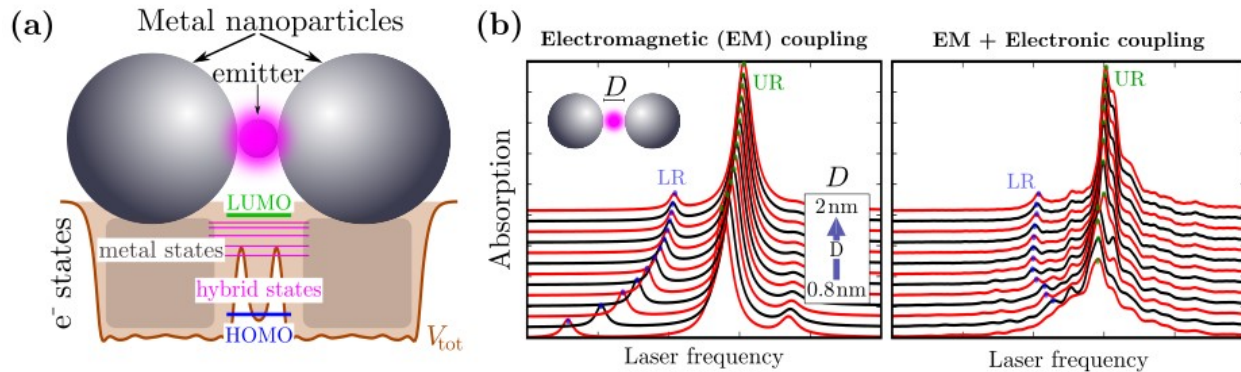

Fig. 1: (a) Sketch of the system under study. A quantum emitter (QE) is placed at the nanogap formed by two spherical metallic nanoparticles (MNPs). The HOMO and LUMO of the isolated QE electronically hybridize with the electronic states of the MNPs. **(b)** Absorption cross-section spectra of the coupled QE–MNPs system calculated within two different frameworks. Left: a classical electromagnetic model only accounting for the electromagnetic (EM) coupling. Right: TDDFT accounting for both the EM and the electronic coupling.

References

[1] Zhang, Y. *et al.* 2017. *Nat. Commun*. 8, 15225.
[2] Song, P. *et al*. 2011. *J. Chem. Phys.*134, 74701.
[3] Kularni, V. *et al*. 2015. *ACS Photonics*, 2, 987.
[4] Babaze, A. *et al*. 2021. *Nano Lett.*, 21, 8466.

Electrically-pumped QD emission from single plasmonic nanoantennas

Junyang Huang, Shu Hu, Dean Kos, Jeremy J Baumberg

NanoPhotonics Centre, Cavendish Laboratory, Department of Physics, University of Cambridge, Cambridge, CB3 0HE, United Kingdom

E-mail: jh2002@cam.ac.uk

Spontaneous emission from semiconductor quantum dots (QDs) at room temperature is attractive for nanophotonic applications due to wavelength-tunable emission, high radiative quantum efficiency, and ease of integration with devices. Here we integrate single/few QDs into plasmonic nanocavities for electrically pumped emission, showing strong coupling is reliably obtained.

Plasmonic nanoantennas support highly localized field enhancement ($I/I_0 \approx 10^6$) [1], a Purcell-enhanced photonic density of states ($F_P = \gamma_{sp}/\gamma_{sp}^0 \approx 10^3$), and broadband resonances (Q factor $\approx$ 10-30), making them desirable resonators for tailoring QD emission at room temperature [2,3]. The substantial Purcell enhancement in self-assembled plasmonic cavities boosts the fluorescence intensity and accelerates the intrinsically slow emission of the QDs ($\tau_{QD} \approx$ 1-20 ns), matching ultrafast optoelectronic devices needing emission rates >100 GHz. Moreover, the optical modes defined by the nanoantenna geometry impose directionality to QD emission, offering the opportunity to optimize the coupling efficiency into photonic devices. Despite increasing interest in the integration of colloidal QDs into plasmon-enhanced antennas, electrically-driven emission from such metal junctions has yet to be demonstrated.

Here, we demonstrate a self-aligned and robust electrically-contacted plasmonic junction for QD optoelectronics (Fig.1a), where a near-perfect monolayer of CdSe QDs is sandwiched between a flat Au surface electrode and a single gold nanoparticle (AuNP) [5]. Embedding this nanoparticle-on-mirror (NPoM) geometry in a cross-bar junction device [4] facilitates electrical excitation of QD excitons and their Purcell-enhanced photoemission, typically quenched close to metal surfaces. Driving emission at a bias of 2 V allows us to follow fluctuations of the intensity and the spectral shape of the QD electroluminescence (Fig.1b). Tuning the optimal coupling to the band-edge exciton in these extremely compact cavities with ultrasmall mode volumes $\sim$50nm^3, we observe Rabi splitting in the electroluminescence spectrum (Fig.1c). Now controlling the number of QDs within the cavity makes a variety of room-temperature quantum-optical effects open to experimental investigation in a reliable route.
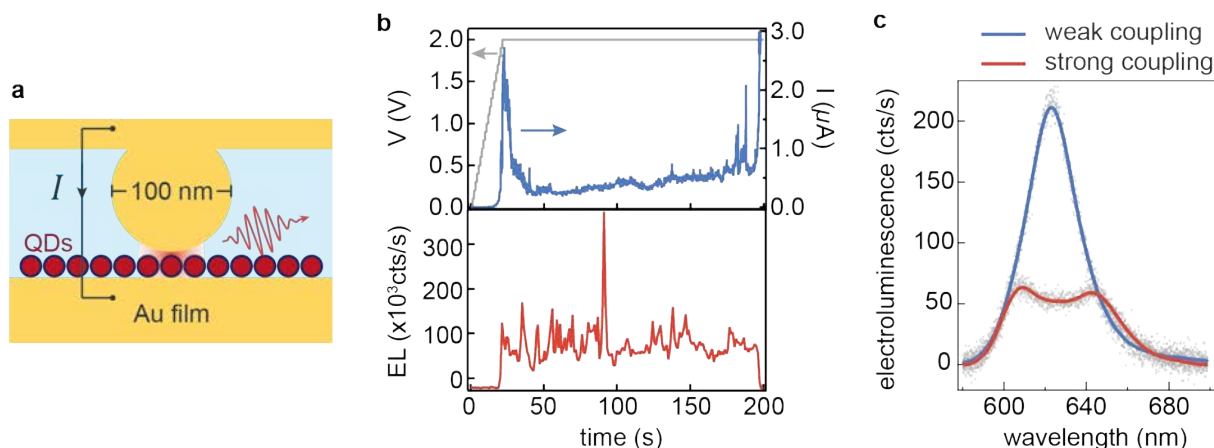

Fig. 1 a, Electrically-pumped photoemission from monolayer of CdSe QDs sandwiched between a single Au nanoparticle and a Au bottom electrode. **b**, Evolution of electrical current (blue) and electroluminescence intensity (red) from a single plasmonic junction as a result of bias applied (grey). **c**, Spectra of nanoantenna-dressed QD electroluminescence in weak (blue) and strong (red) coupling regimes.

References

[1]   Huang, J.; Grys, D.-B.; Griffiths, J.; de Nijs, B.; Kamp, M.; Lin, Q.; Baumberg, J. J. Tracking Interfacial Single-Molecule PH and Binding Dynamics via Vibrational Spectroscopy. *Science Advances* **2021** 7, eabg1790.

[2]   Hoang, T. B.; Akselrod, G. M.; Argyropoulos, C.; Huang, J.; Smith, D. R.; Mikkelsen, M. H. Ultrafast Spontaneous Emission Source Using Plasmonic Nanoantennas. *Nat Commun* **2015**, *6* (1), 7788.

[3]   Huang, J.; Ojambati, O. S.; Chikkaraddy, R.; Sokołowski, K.; Wan, Q.; Durkan, C.; Scherman, O. A.; Baumberg, J. J. Plasmon-Induced Trap State Emission from Single Quantum Dots. *Phys. Rev. Lett.* **2021**, *126* (4), 047402.

[4]   Kos, D.; Assumpcao, D. R.; Guo, C.; Baumberg, J. J. Quantum Tunneling Induced Optical Rectification and Plasmon-Enhanced Photocurrent in Nanocavity Molecular Junctions. *ACS Nano* **2021**, *15* (9), 14535–14543.

[5]   Huang, J.; Hu, S; Kos, D; Baumberg, JJ; submitted (2022)

Addressing the correlations of photons emitted from an ultrastrongly coupled system

Álvaro Nodar[1], **Ruben Esteban**[1], **Unai Muniain**[2], **Javier Aizpurua**[1,2], **Mikołaj Kajetan Schmidt**[1,2,3]

1. Centro de Física de Materiales CFM (CSIC-UPV/EHU), Paseo Manuel de Lardizabal, 5, 20018, Donostia, Spain
2. Donostia International Physics Center DIPC, Paseo Manuel de Lardizabal, 4, 20018, Donostia, Spain
3. Macquarie University Research Centre for Quantum Engineering (MQCEQ), MQ Photonics Research Centre, School of Mathematical and Physical Sciences, Macquarie University, NSW 2109, Sydney, Australia
E-mail: alvaro_nodar001@ehu.eus

Intensity correlations describe the statistical properties of photons emitted by a coupled system and help to determine its dynamics and whether the nature of the emitted light is classical or quantum. In this work, we study the intensity correlations of an incoherently-driven two-level system (TLS), such as an electronic transition of a quantum well, interacting with an electromagnetic cavity. We focus on the ultrastrong coupling regime, where the coupling strength g_0 is comparable to the natural energies of the system. In this regime, the system strongly deviates from the simplified, Jaynes-Cummings model (see Fig. 1), leading to the emergence of novel features in the emission spectra and statistics [1,2].

We use two different descriptions to model the cavity-TLS interaction, based on cavity quantum electrodynamics (cavity-QED): (i) the Jaynes-Cummings model and (ii) the gauge-fixed (GF) Rabi model [3-5]. The Jaynes-Cummings model is widely used to describe the dynamics of coupled systems and correctly describes the interaction in many practical configurations of cavity-enhanced light emission but fails in the ultrastrong coupling regime. Fig. 1 shows the intensity correlations ($g^{(2)}$) obtained within this model (red line) for different coupling strengths ranging from the weak coupling to the ultrastrong coupling regime. The intensity correlations exhibit anti-bunching ($g^{(2)}<1$), indicating non-classical emission. On the other hand, the recently developed GF Rabi model accurately describes the TLS-cavity interaction also in the ultrastrong coupling regime [3-5]. The resulting intensity correlations (blue line in Fig. 1) are very similar to those obtained with the Jaynes-Cummings model for weak and moderate coupling strengths. However, the GF Rabi model indicates that the photons become highly bunched in the ultrastrong coupling regime ($g^{(2)}>1$), deviating from the Jaynes-Cummings results. To analyze this difference, we calculate the correlations obtained after filtering the emitted light to select pairs of photons of particular frequencies (two-color correlation maps). This approach allows for gaining additional information about the processes involved in the light emission [6]. Understanding the changes in the statistical nature of the light emitted in cavity-coupled systems provides important information to fully characterize light emission from quantum devices in the strong and ultrastrong coupling regimes.
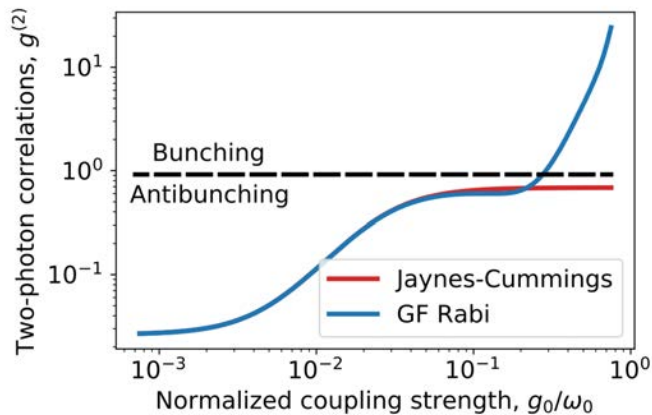

Fig. 1 Intensity correlations ($g^{(2)}$) of a cavity coupled to a two-level system (TLS) as a function of the normalized coupling strength (g_0/ω_0, with $\omega_0=1$ eV the natural frequency of the TLS and of the cavity). The red and blue lines correspond to the Jaynes-Cummings and the gauge-fixed (GF) Rabi calculations, respectively. The dashed line corresponds to $g^{(2)}=1$ and separates the regions where bunching ($g^{(2)}>1$) and antibunching ($g^{(2)}<1$) are found. For these calculations, the TLS is pumped incoherently with a rate $P_\sigma=1$ meV, and the losses of the cavity and of the TLS are $\kappa=50$ meV and $\gamma=0.1$ meV, respectively.

References

[1] Forn-Díaz P., *et. al.*, 2017 *Nat. Phys.* 13, 39
[2] Kockum A. F., et al., 2019, Nat. Rev. Phys. 1, 19
[3] Salmon W., *et al.*, 2021, arXiv:2102.12055
[4] Settineri A., *et al.,* 2021, Phys. Rev. Research 3, 023079
[5] Di Stefano O., *et al.,* 2019 Nat. Phys. 15, 803
[6] Schmidt M. K., *et al.* 2021 Quantum Sci. Technol. 6, 034005

First-principles study of plasmon-molecule coupling and charge transfer in Ag nanoparticle dimers

Bruno Candelas[1], Nerea Zabala[2], Daniel Sánchez-Portal[1], Javier Aizpurua[1]

1. CFM-MPC, Centro mixto CSIC-UPV/EHU, and DIPC, Manuel de Lardizabal 5, 20018, Donostia, Spain
2. Department of Electricity and Electronics, FCT-ZTF, UPV/EHU, Bº Sarriena s/n, 48940 Leioa, Spain
bcandelas001@ikasle.ehu.eus

When an organic molecule is placed inside a plasmonic cavity formed by two metallic nanoparticles (MNPs) under illumination, the electronic transitions of the molecule couple to the electromagnetic modes of the cavity, so that, in the strong-coupling regime, two hybrid light--matter modes called polaritons emerge [1]. Atomistic ab-initio methods accurately describe the coupling between MNPs and molecules at this nanometer scale [2]. In this work, we study the optical absorption spectra of porphyrin molecules coupled to silver nanoparticle dimers from first-principles, by using the ab-initio SIESTA software to obtain the ground state of the system in the Kohn-Sham scheme with a basis set of numerical atomic orbitals [3], and the TDDFT code PyNAO [4, 5], which uses its own iterative scheme to obtain the linear response using a linear combination of atomic orbitals as basis set, to compute the optical excitations. The results show the splitting of the plasmonic resonance in two distinct polaritons, a characteristic feature of the strong light-matter coupling regime. We analyse the dependence of the coupling strength on the geometrical features of the system, such as the separation between the MNPs or their relative orientation. For certain gap morphologies, our simulations reveal the existence of a Charge Transfer Plasmon at lower frequencies, a state which is predicted to emerge when the molecular energy level is resonant with the Fermi level of the MNPs [6]. Moreover, we show that the strength of the charge transfer modes can be tuned by artificially shifting the molecular energy levels relative to those of the MNPs.
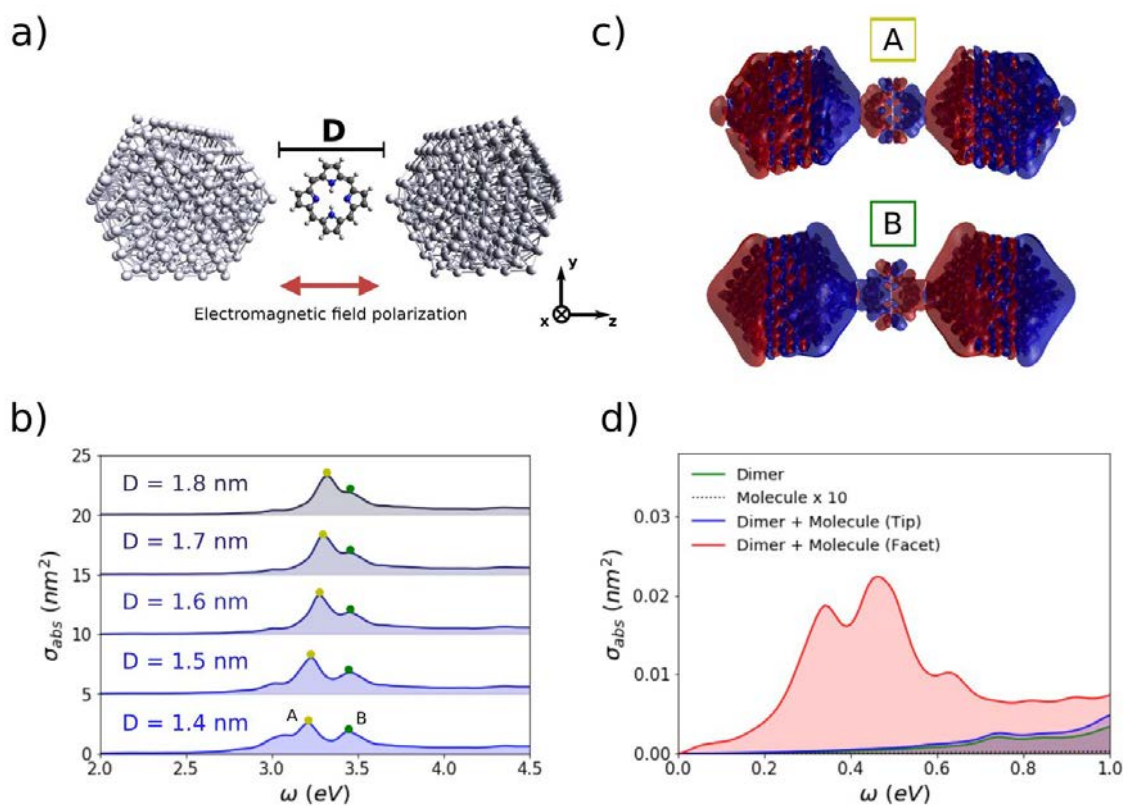
he system under study, composed of two icosahedral Ag309 nanoparticles with a 2,3-Dihydroporphyrin molecule placed in the gap between them. The system is displayed in the tip-to-tip configuration, with a gap size D=1.5 nm. The system is excited by light polarized along the dimer axis direction. b) Absorption spectra of the complete system for gap size values in the range between D=1.4 nm (bottom) and D=1.8 nm (top). The new emerging Lower and Upper Polaritons are marked by yellow and green dots, respectively. c) Isosurfaces of induced density at the emerging resonances for D=1.4 nm. d) Low energy part of the absorption spectrum for the bare dimer (green), the isolated porphyrin molecule (dotted black), and the complete system in both the tip to tip (blue) and facet to facet (red) configurations, with D=1.4 nm.

References
[1] García-Vidal, F. J.; Ciuti, C.; Ebbesen, T. W. 2021 . *Science*, 373, eabd0336.
[2] Rossi, T. P.; Shegai, T.; Erhart, P.; *Antosiewicz, T.* 2019. *Nat. Commun.,* 10, 3336.
[3] Soler, J. M.; Artacho, E.; Gale, J. D.; García, A.; Junquera, J.; Ordejón, P.; Sánchez-Portal, D. 2002. *J.Phys.: Condens. Matter*, 14, 2745.
[4] Koval, P.; Barbry, M.; Sánchez-Portal, D. 2019. *Comput. Phys. Commun.* , 236, 188.
[5] Barbry, M.; Koval, P.; Marchesin, F.; Esteban, R.; Borisov, A. G.; Aizpurua, J.; Sánchez-Portal, D. 2015. *Nano Lett..,* 15, 5, 3410-3419.

Quantum Surface Effects in a Plasmonic Nanoantenna–Emitter System: Time-Dependent Density Functional Theory vs. Semiclassical Approach

Antton Babaze[1,2], **Eduardo Ogando**[3], **P. Elli Stamatopoulou**[4], **Christos Tserkezis**[4], **N. Asger Mortensen**[4,5], **Javier Aizpurua**[1,2], **Andrei G. Borisov**[6], and **Ruben Esteban**[1,2]

1. Materials Physics Center CSIC-UPV/EHU, Paseo Manuel de Lardizabal 5 20018 Donostia-San Sebastián, Spain
2. Donostia International Physics Center DIPC, Paseo Manuel de Lardizabal 4 20018 Donostia-San Sebastián, Spain
3. Department of Physics, University of the Basque Country UPV/EHU, Paseo de la Universidad 7 01006 Vitoria-Gasteiz, Spain
4. Center for Nano Optics, University of Southern Denmark, Campusvej 55, DK-5230 Odense M, Denmark
5. Danish Institute for Advanced Study, University of Southern Denmark, Campusvej 55, DK-5230 Odense M, Denmark
6. Institut des Sciences Moléculaires d'Orsay, UMR 8214 CNRS-Université Paris-Saclay Bât. 520, 91405 Orsay Cedex, France
E-mail: anttonbabaze@dipc.org

The electromagnetic coupling between quantum emitters (QEs) and plasmonic metallic nanoparticles (MNPs) has attracted great interest in the field of nanophotonics due to the ability of MNPs to strongly enhance the absorption and emission rate of QEs located in close proximity. Typically, the electromagnetic QE–MNPs interaction is addressed using the classical local-response approximation (LRA) of metals, which has successfully described many physical phenomena of interest when the size of the MNPs and the QE–MNPs distance are relatively large. However, quantum phenomena such as electron spill in/out at the metallic interface, surface-enabled Landau damping, or nonlocal dynamical screening can significantly influence the electromagnetic interaction in practical QE–MNPs configurations involving small QE–MNPs separation distances [1]. In this context, time-dependent density functional theory (TDDFT) is well suited to naturally account for all quantum phenomena occurring in the QE–MNPs interaction [2]. Moreover, computationally less-demanding semiclassical approaches such as the Feibelman model have been also used to capture some of these quantum effects [3]. The Feibelman formalism incorporates *ab initio* quantum surface-response corrections at metallic interfaces in the solution of classical Maxwell's equations by means of the $d_\perp(\omega)$ parameter, which accounts for the position of the centroid of the induced charges at frequency ω with respect to the classical metallic boundary [4].

This work explores the influence of quantum-mechanical effects in the electromagnetic interaction between QEs and MNPs using TDDFT calculations within the jellium model. We first use TDDFT to study the Green's function that describes the electric field experienced by a QE due to its self-interaction in the presence of a spherical MNP (Figure 1a), and then compare the results with those obtained within the Feibelman model. The QE is described as a point dipole of amplitude p_d. The analysis of the TDDFT and Feibelman results confirms that the spill out of the induced charges and surface-enabled Landau damping produces a redshift and broadening of plasmonic resonances, not present within the LRA results (Figure 1b). Furthermore, the good agreement between the TDDFT and Feibelman results for most QE–MNPs separations validates the use of the Feibelman approach in many nanoscale systems. However, we identify situations of very small QE–MNP distance where the current implementation of the Feibelman model is not accurate. Our study thus provides a fundamental description of quantum effects influencing the electromagnetic interaction between QEs and MNPs and establishes the validity range of the semiclassical Feibelman formalism.
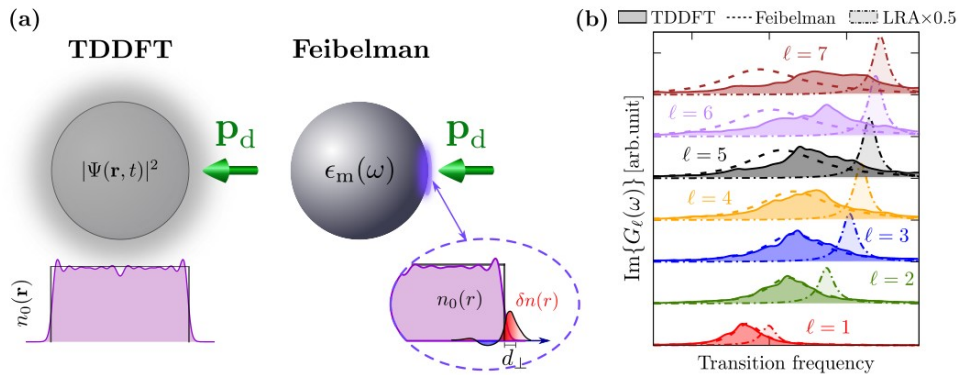

Fig. 1: (a) Sketch of the system under study consisting of a quantum emitter (QE), modeled as a point dipole of amplitude p_d**,** located in front of a spherical metallic nanoparticle (MNP). The MNP is described within the quantum TDDFT by calculating the time evolution of the electron density $n_0(r)$ (left), and within the semiclassical Feibelman formalism by incorporating quantum surface-response corrections with the use of the $d_\perp(\omega)$ parameter (right). **(b)** Contribution of the first seven plasmonic modes to the imaginary part of the self-interaction Green's function obtained within the three models employed in this work. Solid lines: TDDFT. Dashed lines: Feibelman formalism. Dashed-dotted lines: Local-response approximation (LRA).

References
[1] Gonçalves, P. *et al*. 2020. *Nat. Commun.,* 11, 366.
[2] Babaze, A. *et al*. 2021. *Nano Lett.,* 21, 8466.
[3] Mortensen, N. A. 2021. *Nanophotonics,* 10, 2563.
[4] Feibelman, P. J. 1982. *Prog. Surf. Sci.* 12, 287.
[5] Babaze, A. *et al*. 2022. *In preparation.*

Interference-based Wide-range Dynamic Tuning of the Plasmonic Color of Single Gold Nanoparticles

Bokusui Nakayama[1], **Hiroki Endo**[1], **Yuki Hiruta**[1] and **Toshiharu Saiki**[1]

1. Graduate School of Keio University / 3-14-1 Hiyoshi, Kohoku-ku, Yokohama-shi, Kanagawa 223-8522 Japan

E-mail: bokusui.nakayama@saiki.elec.keio.ac.jp

Coloration in natural and artificial materials is rich in variety. Surface plasmon resonance and interference can explain these colorations and lead to ink-free color production. In particular, plasmonic coloring using metal nanoparticles has advantages of high resolution, low energy consumption, high brightness, and large viewing angle, as well as color tunability through variation of the material, size, shape, and environment. Researchers have devoted great effort to developing a high-resolution dynamic display that operates via fast tuning of plasmonic and interference effects. They have used electrical, chemical, mechanical, and thermal modulation of the environment because of the difficulties of tuning the material itself in real-time. Among these methods, each of which has advantages and disadvantages in terms of speed, tunable range, and power consumption, mechanical tuning using stimuli-responsive polymers is promising because of its potential to satisfy the requirements of a specific application.

Such stimuli-responsive polymers have also exhibited advantages in the dynamic modulation of color. Ding *et al*. demonstrated modification of the surface plasmon gap mode between an Au nanoparticle (AuNP) and an Au-coated substrate by utilizing the volume change of a hydrogel with temperature [1]. At low temperatures, where the hydrogel was swelled, the gap between an AuNP embedded in the hydrogel and the substrate was large and the AuNP appeared green under dark-field microscopic observation. When the temperature was increased, the gap was substantially reduced to the sub-10 nm range to induce a color change of the AuNP from green to orange. Although this approach enables reversible, repeatable, and high-speed modulation at a single-particle level by using focused laser heating, the coverage of the color space is narrow and far from that required for color displays.

In the present paper [2], we demonstrate dynamic nanoscale coloration using single AuNPs by hybridizing plasmon-based and interference-mode approaches. Under back-scattering white-light observation of single AuNPs, interference between the scattered light from the AuNPs and the reflected light from the substrate gives rise to various colorations depending on the distance between the AuNPs and the substrate (Figure 1). We experimentally examined the coverage of the color-space diagram and compared the color range with theoretical calculations. We also attempted to dynamically control the color of the AuNPs by precisely tuning their distance from the substrate via the volume change of a temperature-responsive hydrogel (Figure 2).
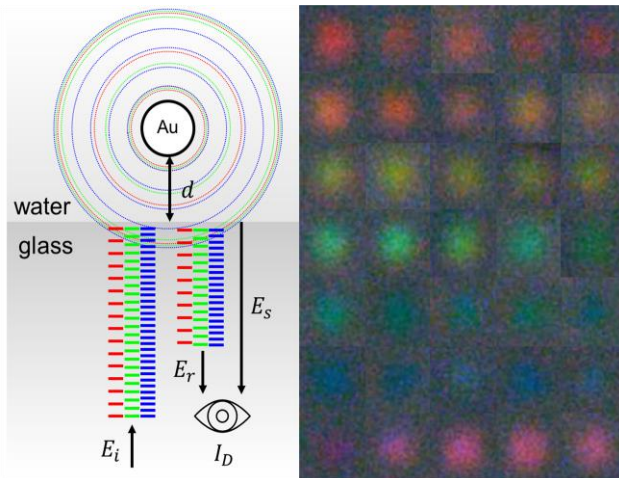

Fig. 1 Schematic model of our system and a set of color images of AuNPs. Scattered light E_s from an AuNP interferes with reflected light E_r from the substrate/solution interface.
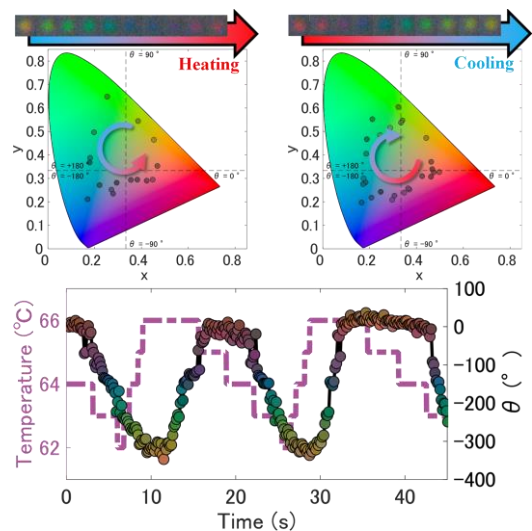

Fig. 2 Time-sequence snapshots and color plots visualizing in color of an identical AuNP by heating and cooling processes, respectively, to induce the volume change of the hydrogel.

References

[1] T. Ding, *et. al.*, *Adv. Opt. Mater.* **4**(6), 877-822 (2016).
[2] B. Nakayama, *et. al.*, *Opt. Express.* **29**(10), 15001-15012 (2020).

Furthering nano-optic techniques through the simultaneous integration of heterodyned-tapping-mode AFM

Kevin W.C. Kwock[1], Thomas Darlington[2], Emanuil S. Yanev[2], Natalie Fardian-Melamed[2], Benedikt Ursprung[2], James C. Hone[2], P. James Schuck[2]

1. Department of Electrical Engineering, Columbia University
2. Department of Mechanical Engineering, Columbia University
E-mail: kwk2118@columbia.edu, pjs2191@columbia.edu

Scanning tip-enhanced spectroscopy techniques such as tip-enhanced Raman scattering (TERS) and tip-enhanced photoluminescence (TEPL) are powerful tools for investigation of opto-electronic properties of materials surfaces. However, the improved resolution comes at the significant expense optical signal, requiring the use of higher excitation powers which can be detrimental to samples and nano-optical probes.[1-2] This leads to the current paradigm of 'hit-or-miss' in tip-enhanced measurements where success is heavily dependent on of fabrication of extraordinary nano-optical probes that can simultaneously tolerate high excitation densities and greatly enhance the signal of interest for a measurement's duration. Methods to increase signal/noise throughput in a system without high photon fluences on the sample/tip are thus greatly needed for imaging typically weak optical interactions, such as many Raman scattering signals as well as nonlinear optical interactions such nano-second harmonic generation.

In this study, we present on our current efforts to improve our nano-optical studies through the incorporation of lock-in detection of tip-enhanced signals using the oscillation of an AFM-cantilever mounted nano-optical probe, through interaction of fast single photon sensitive avalanche photo diodes and time-correlated single photon counting electronics, a system first demonstrated by Gerton et al.[3] We show that this technique can successfully image the nano-PL nanobubble in monolayer WSe_2 on Au, achieving resolutions below 20 nm. Our results show the viability for lock-in detection in tip-enhanced spectroscopic and show a potentially path for true on-demand nano-optical measurements.

References

[1] Neacsu, C.C., van Aken, B.B., Fiebig, and Raschke, M.B. 2005. *Phys. Rev. B* **79**, 100107.
[2] Yao, K., Zhang, S., Yanev, E., McCreary, K., Chuang, H., Rosenberger, M.R., Darlington, T., Krayev, A., Jonker, B.T., Hone, J.C., Basov, D.N., and Schuck, P.J. 2022. arXiv:2111.06955.
[3] Gerton, J.M., Wade, L.A., Lessard, G.A., Ma, Z., and Quake, S.R. 2004. *Phys. Rev. Lett.* **93**, 180801.
[4] Darlington, T.P. *et. al. 2020.* Imaging strain-localized excitons in nanoscale bubbles of monolayer WSe2 at room temperature, Nature Nanotechnology, **15**(10), 854-860.

ULF TERS imaging –a novel technique for assessing the layer interaction in vertical heterostructures of 2D semiconductors.

Alvaro Rodriguez[1], <u>Andrey Krayev</u>[2], Matěj Velický[1], Peng Chen[3], Xiangfeng Duan[4], Patrick El-Khoury[5], Otakar Frank[1]

1. J. Heyrovský Institute of Physical Chemistry, Czech Academy of Sciences, Dolejškova 2155/3, 182 23 Prague, Czech Republic
2. HORIBA Scientific, 359 Bel Marin Keys Blvd, Suite 18, Novato CA, 94949, USA
3. School of Microelectronics, Southern University of Science and Technology; 1088 Xueyuan Avenue, Shenzhen 518055, China
4. Department of Chemistry and Biochemistry and California NanoSystems Institute, University of California, Los Angeles, USA
5. Physical Sciences Division Pacific Northwest National Laboratory, P.O. Box 999, Richland, WA, 99352, USA
E-mail: andrey.krayev@horiba.com

Tip enhanced Raman scattering (TERS) and tip enhanced photoluminescence (TEPL) are effective tools for the assessment of nanoscale heterogeneity in mono- and a few- layer 2D semiconductors and their heterostructures. Due to their non-destructive nature, TERS and TEPL imaging can be cross-correlated with other images conveniently recorded using scanning probe microscopy (SPM), such as topography, surface potential, photocurrent etc, which further improves our understanding of 2D semiconductors. Recent interest of the community in vertical heterostructures of graphene and transition metal dichalcogenides (TMDs) with precise control of the twist angle between the layers motivated us to apply and extend TERS imaging to the characterization of the WS_2-WSe_2 vertical heterostructures.

WS_2-WSe_2 heterobilayer samples were exfoliated to PDMS and then transferred to a gold-coated silicon wafer and were confirmed to feature large areas (tens of microns across) showing the presence of a lattice-like Moire pattern with 6-8 nm pitch. Additionally, as it almost inevitably occurs with the stacked layers exfoliated in air, large number of nanobubbles were present in the samples. TERS imaging of larger bubbles with 785 nm excitation revealed extreme heterogeneity of the TERS response across the bubble- at the outer edges we observed strong bands coming from WSe_2 and additionally- a predominant ultralow frequency (ULF) TERS peak at around 23 cm^{-1} that arises from the interlayer phonon mode was observed. To the best of our knowledge this is the first time demonstration of ULF TERS that track low frequency inter-layer phonons, and therefore, directly report on local structure with nanometer spatial resolution. Interestingly, this peak disappeared towards the center of the bubble, while an A'/A_{1g} peak of WS_2 simultaneously appeared at ~416 cm^{-1}. Careful correlation analysis of the recorded spectral nano-images showed that this WS_2–like peak was correlated to a local exciton. The same analysis paints a unique picture about the two layers in the bubble region, which seems to be comprised of WS_2-WSe_2 bilayers that are separated at the apex of the nanobubble. It's a rather remarkable observation taking into account that the lateral spatial extent of this decoupling took place on the 10's of nm length scale.

Again, somewhat surprisingly, TERS response of the areas in between the larger bubbles looked patchy showing great similarity to the response from larger bubbles which indicates that the sample had a developed network of smaller and larger nanobubbles that inevitably affected the electronic band structure of WS2-WSe2 vertical heterostructures, which brings us to the conclusion that any far field Raman spectra obtained on exfoliated vertical heterostructures should be taken with certain caution unless a solid proof of the lack of nanobubbles in the investigated sample is provided.

Finally, we should note that despite the demonstrated utility for characterization of the layer interaction in vertical heterostructures, ULF TERS of 2D semiconductors requires significant work for proper understanding of the resonant effects and the resulting band assignments. Unlike the case of conventional ULF Raman response in TMDs, ULF TERS response changes quite dramatically as the excitation laser wavelength changes, both the intensity and the spectral position-wise. Examples of this apparently resonant behavior will also be presented.

TERS Characterization of Functionalized Gold Nanostructures for Improved Biosensors.

JF Bryche[1], **M. Vega**[1,2], **A. Tempez**[3], **T. Brulé**[3], **T. Carlier**[3], **J. Moreau**[1,2],
P.G. Charette[1], **M. Chaigneau**[3], **M. Canva**[1,2]

1. Laboratoire Nanotechnologies Nanosystèmes (LN2 – IRL 3463) – CNRS/ Institut Interdisciplinaire d'Innovation Technologique (3IT) /Université de Sherbrooke, Sherbrooke, Canada.
2. Laboratoire Charles Fabry (LCF), Université Paris-Saclay, Institut d'Optique Graduate School, CNRS, Palaiseau, France.
3. Horiba FRANCE SAS, Palaiseau, France
E-mail: jean-francois.bryche@usherbrooke.ca

Plasmonic gold nanostructures are being used to develop high-performance biosensors. The confinement of electromagnetic fields far beyond the diffraction limit has led in recent design to single-molecule detection through surface-enhanced Raman spectroscopy (SERS) [1]. Tip-Enhanced Raman Spectroscopy (TERS) characterization, which has emerged as a powerful analytical technique providing high chemical sensitivity for surface molecular mapping with nanoscale spatial resolution, can provide nano-spatially resolved response and help in designing highly sensitive and high-resolution biosensing structures.

This work examined the TERS performance of functionalized gold nanodisk arrays on a gold-coated glass substrate. These samples have shown results in SERS [2] upon coupled plasmonic modes: the gold layer sustains propagative surface plasmons while the nanostructures sustain localized surface plasmon resonances. Coupling between them can occur in specific conditions and give rise to hybrid modes [3]. Nano-resolved TERS response distribution from grafted thiophenol molecules on nanodisks of 110 and 220 nm diameter feature strong signal localization on the periphery of the nanostructures, in agreement with numerical modeling [4]. This highlights the importance of grafting molecules on high electric field locations to optimize detection sensitivity and speed at low molecular concentrations.
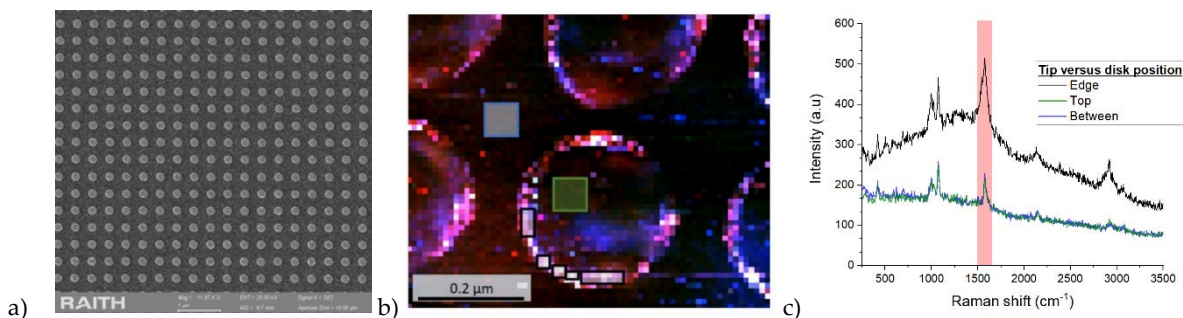

Fig. 1 a) SEM picture of gold nanodisk arrays on gold film with 220nm diameters and 400nm periods. b) TERS mapping of 220 nm gold nanodisks with a 638 nm laser. In the TERS image, the pixel size is 10×10 nm². c) Raman signal for three identified regions of the sample: Top – Edge – Between. Each zone has the same size area (16 pixels).

References
[1] A. Bhattarai, K. T. Crampton, A. G. Joly, L. Kovarik, W. P. Hess, P. Z. El-Khoury, J. Phys. Chem. Lett., vol. 9, no. 24, 7105 (2018).
[2] J.-F. Bryche, R. Gillibert, G. Barbillon, P. Gogol, J. Moreau, M. Lamy de la Chapelle, B. Bartenlian, M. Canva, Plasmonics, vol. 11, no. 2, 601 (2015).
[3] M. Sarkar, M. Besbes, J. Moreau, J.-F. Bryche, A. Olivéro, G. Barbillon, A.-L. Coutrot, B. Bartenlian, M. Canva, ACS Photonics, vol. 2, no. 2, 237(2015).
[4] J.-F. Bryche, M. Vega, A. Tempez, T. Brulé, T. Carlier, J. Moreau, M. Chaigneau, P. G. Charette, M. Canva, Submitted to Nanomaterials

Novel integrated III-V/silicon AFM active optical probe for combined AFM/NSOM/TERS measurements

Alexander A. Ukhanov, Fei-Hung Chu, Gennady A. Smolyakov, Kevin J. Malloy

Actoprobe LLC, 800 Bradbury SE, Suite 160, Albuquerque, NM 87106
E-mail: aukhanov@actoprobe.com

Actoprobe LLC has been developing a novel class of AFM active optical probes (AAOPs) fabricated entirely from GaAs-based or similar semiconductor laser materials, including the semiconductor laser source, the cantilever with the tip on its end, and the probe base, all monolithically integrated into a semiconductor chip for combined AFM/NSOM/TERS measurements [1,2]. As important as it was for establishing the general concept of AAOP, this approach is not economical in utilizing relatively expensive III/V material, which makes the final product rather costly. At the same time, in terms of their mechanical properties, GaAs-based cantilever AFM probes are typically inferior to standard silicon cantilever AFM probes. To take full advantage of both the III/V semiconductor laser technology and the established silicon microfabrication techniques of the standard technology of AFM tip/cantilever manufacturing, we propose a novel concept of integrated III-V/silicon AAOP.

The innovation is accomplished by integrating a III-V semiconductor laser source into a silicon cantilever AFM probe using a promising III-V silicon integration approach [3] based on metal bonding the III-V gain medium section to the SOI silicon substrate for direct optical coupling (edge- or butt coupling) between the III-V gain section and the silicon layer of the SOI waveguide (Fig. 1). The light is delivered to the end of the cantilever where it is redirected vertically from the silicon waveguide into the probe tip using a folding mirror. The gold-coated tip acts as an output laser mirror in the special intracavity design of the AAOP. The light reflected from the gold-coated tip is coupled back into the silicon waveguide and, eventually in the laser chip active region. This light feedback mechanism has to be sufficiently strong to make sure that the probe tip is supplied with intracavity high-intensity laser light.
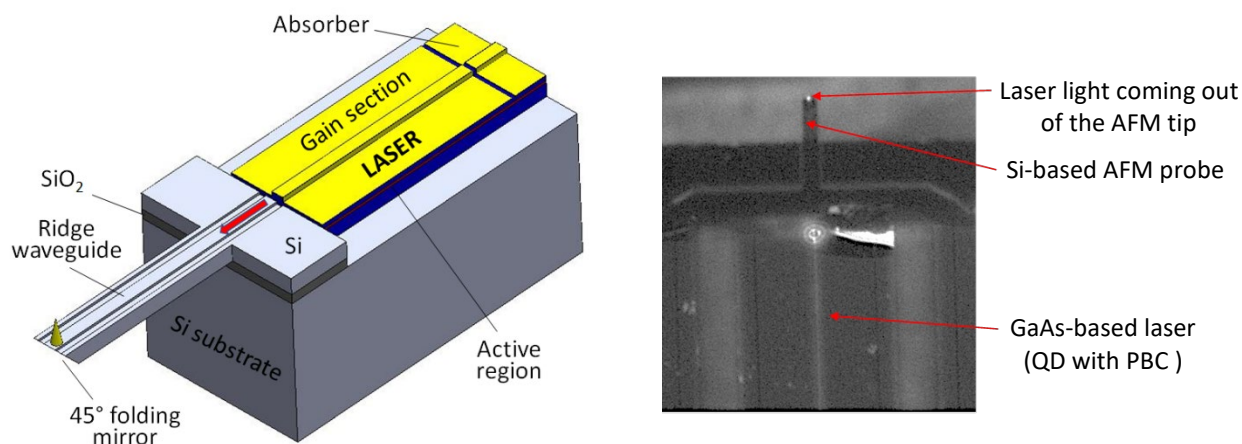

Fig. 1. Integrated III-V/silicon AAOP concept (left) and silicon-integrated AAOP with laser chip bonded to a silicon probe (right).

So far, a simpler concept of integrated III-V/silicon AAOP with free-space illumination of the probe tip has been demonstrated. The concept is based on integrating a semiconductor laser source into a cantilevered silicon AFM probe in such a way that the free propagating light from the integrated laser source can be used to illuminate the probe tip and carry out AFM, NSOM, and TERS measurements. Using lithography and ICP dry etching, a standard silicon AFM probe was patterned and etched to a depth of 150 µm to accommodate a thick laser chip with photonic-band-crystal (PBC) waveguide structure for improved vertical divergence [4]. The active region of the laser chip was aligned with the probe tip, so that the free propagating light from the integrated laser source was used to illuminate the probe tip and carry out AFM and NSOM measurements.

In conclusion, we have proposed a novel concept of integrated III-V/silicon AAOP that takes full advantage of both the III/V semiconductor laser technology and the established silicon microfabrication techniques of the standard technology of AFM tip/cantilever manufacturing. The first prototype of integrated III-V/silicon AAOP with free-space illumination of the probe tip has been demonstrated with confirmed AFM and NSOM performance.

References

[1] Ukhanov, A. A., Smolyakov, G. A., "Atomic force microscopy active optical probe", Patent No. US 9482691, issued November 01, 2016.
[2] Ukhanov, A. A., Smolyakov, G. A., Chu, F. H., Wang, C., "Monolithic atomic force microscopy active optical probe", Patent No. US 11,016,119, issued May 25, 2021.
[3] Creazzo, T., Marchena, E., Krasulick, S. B., et al. 2013. *Opt. Express* 21, 28048-28053.
[4] Liu, L., Qu, H., Liu, Y, et al. 2014. *Appl. Phys. Lett.* 105, 231110.

Infrared nano-spectroscopy of antenna coupled intra-molecular vibrational interactions and dynamics

Jun Nishida[1,†], Roland Wilcken[1,†], Johan F. Triana[2], Aurelian John-Herpin[3], Hatice Altug[3], Felipe Herrera[2,4], and Markus B. Raschke[1,*]

1. Department of Physics and JILA, University of Colorado, Boulder, 2000 Colorado Ave, CO 80309, USA
2. Department of Physics, Universidad de Santiago de Chile, Av. Victor Jara 3493, Santiago, Chile
3. Institute of Bioengineering, École Polytechnique Fédérale de Lausanne (EPFL), Lausanne 1015, Switzerland
4. ANID-Millennium Institute for Research in Optics, Chile
E-mail: *markus.raschke@colorado.edu   †: These authors contributed equally

Intramolecular vibrational coupling and energy transfer in polyatomic molecules not only defines nuclear motion during chemical processes but is also the fundamental limit to vibrational coherence. Intramolecular coupling can be resolved by two-dimensional infrared (2D-IR) spectroscopy. However, with diffraction-limited cavity mode volumes and probing large heterogeneous molecular ensembles, the approach precludes a controlled modification of coupled vibrational coherence in small molecular ensembles as desirable for, e.g., new photochemical pathways.

To address this outstanding challenge, we pursue selective modification of the *intrinsic* intramolecular vibrational coupling and energy transfer by *extrinsic* antenna coupling of molecular vibrations. In femtosecond infrared nano-spectroscopy of molecular-monolayer functionalized length-tunable IR-resonant nano-wire antennas we resolve vibrational coupling with sensitivity down to 10's of molecules. Exemplary, we use a metal organic complex Re(bpy)(CO)$_3$Cl (bpy = 2,2'-bipyridine) surface bound by click-chemistry (**Fig. 1a**) with its three long-lived CO asymmetric $\overline{v}_{A'(2)}$ = 1900 cm^{-1} and $\overline{v}_{A''}$ = 1940 cm^{-1} (spectrally unresolved), and symmetric $\overline{v}_{A'(1)}$ = 2020 cm^{-1} stretch modes [1,2] (**Fig. 1b**). Tuning the antenna resonance across the vibrational modes, on resonant excitation of the symmetric stretch A'(1) with $\overline{v}_{ant} = \overline{v}_{A'(1)}$, the signal amplitude increases and yhe lifetime $T_2(\overline{v}_{A'(1)})$ is reduced from 760 fs to 300 fs (**Fig. 1 c,e**) due to Purcell enhancement as described previously [3,4]. Significantly, we also observe a reduction in $T_2(\overline{v}_{A'(1)})$ by tuning the nanoantenna on resonance with A'(2) and A'' (**Fig. 1e**). This behavior is a direct signature of intramolecular vibrational coupling and energy transfer. We model the results based on a semi-empirical quantum approach we recently developed [5] to describe the multispectral interplay between antenna-mediated and intramolecular coupling strength g_l (see **Fig. 1d**). We further observe spatial variations in $T_2(\tilde{v}_{A'(1)})$ depending on tip-antenna position (data not shown), which we model as interfering pathways of vibrational coherence.

In conclusion, vibrational mode-selective infrared nanoantenna coupling can resolve intramolecular interaction and energy transfer in linear spectroscopy – information otherwise only accessible through coherent 2D spectroscopy.
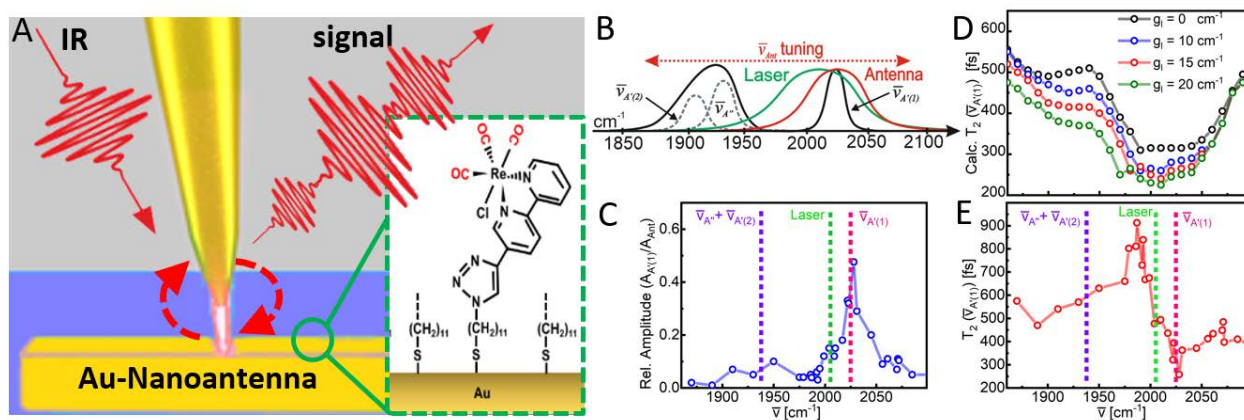

Fig. 1. (a) IR resonant nanoantenna coated by a monolayer of a Re-metal carbonyl complex to investigate the intra- and antenna-mediated vibrational energy transfer by nano-probe spectroscopy. (b) Scheme of the CO stretch modes and the laser and antenna frequencies. (c) Relative lifetime of the vibrational to the antenna signal. (d) Calculated T_2 lifetime of the A'(1) mode with changing antenna resonance in dependence on the intramolecular coupling g_l. (e) Measured T_2 lifetime of the A'(1) mode

References

[1] C. Yan et al., "Unraveling the dynamics and structure of functionalized self-assembled monolayers on gold using 2D IR spectroscopy and MD simulations", *PNAS.* **2016**, *113*, 4929–4934. [2] L. M. Kiefer et al., *Acc. Chem. Res.* **2015**, *48*, 1123-1130. [3] B. Metzger et al., "Purcell-Enhanced Spontaneous Emission of Molecular Vibrations", *Phys. Rev. Lett.* **2019**, *123*, 153001. [4] E. A. Muller et al., "Nanoimaging and Control of Molecular Vibrations through Electromagnetically Induced Scattering Reaching the Strong Coupling Regime", *ACS Photonics* **2018**, *5*, 3594–3600. [5] J. F. Triana et al., "Semi-empirical Quantum Optics for Mid-Infrared Molecular Nanophotonics", arxiv:2110.07371, **2021**

Intraparticle Heat Transfer inside Cross-shaped Nanoparticles
Revealed by Femtosecond Transient Spectroscopy

M. Vega[1,2], **JF Bryche**[1], **P. Bresson**[1,2], **PL Karsenti**[1], **M. Besbes**[2], **J. Moreau**[1,2],
P. Gogol[1], **D. Morris**[1], **P.G. Charette**[1], **M. Canva**[1,2],

1. Laboratoire Nanotechnologies Nanosystèmes (LN2 – IRL 3463) – CNRS/ Institut Interdisciplinaire d'Innovation Technologique (3IT) /Université de Sherbrooke, Sherbrooke, Canada.
2. Laboratoire Charles Fabry (LCF), Université Paris-Saclay, Institut d'Optique Graduate School, CNRS, Palaiseau, France.
E-mail: marlo.vega@usherbrooke.ca

Nanoparticles (NP) can release the energy absorbed under light excitation into heat. To fully exploit these heat nanosources in applications such as medicine, catalysis or photonic switch, the dynamics of heat distribution inside NPs must be better understood and modelled. It remains a challenging task regarding the time and space scales involved in the photothermal process (femtosecond and nanometer scales).

In this work, we realized femtosecond transient spectroscopy measurement on cross-shaped gold nanoparticles and then compared the data with our extended two-temperatures model [1]. This NP geometry is known to support polarization-dependent localized plasmonic resonances (LSPR) along each branch. By selectively exciting one LSPR, a single branch can be heated, with the energy carried by non-thermalized electrons and electron-phonon coupling to the other branch in a few 100 fs. The thermal distribution inside the cross-shaped NP can be determined by measuring the time delay between the shifts in spectral responses in each branch. In addition, the spatiotemporal dynamics of the electronic and lattice temperatures inside the NP can be determined by fitting the experimental data to the numerical model. Good agreement was found between simulations and experiments.

The pump-probe setup is based on a Ti-sapphire femtosecond (~75 fs HWHM) laser centered at 795 nm. The pump frequency is tuned through an OPA to a wide range of wavelengths from the UV to the IR. A fraction of the 795 nm laser source is sent through a non-linear crystal to generate the white light continuum probe. The samples consist of gold crosses fabricated by E-Beam lithography on a 30 nm gold film, atop a 2 nm titanium adhesive layer and BK7 substrate. The dimensions of the crosses are: 300/410 nm branch lengths, 60 nm height, 60 nm width and 520/640 nm period along the short/long branch axes.

An illustration of the optical excitation configuration is shown in Figure 1.a. The pump is used to resonantly heat one branch of the cross and the probe to measure the optical responses of both branches. Figure 1.b shows a simulation of the resulting electronic temperature (Te) reached inside the nano cross a few femtoseconds after the excitation, where the asymmetric electronic temperature distribution inside the cross can be seen. Figure 1.c shows the measured optical response delay between the longitudinal and transverse LSPR.
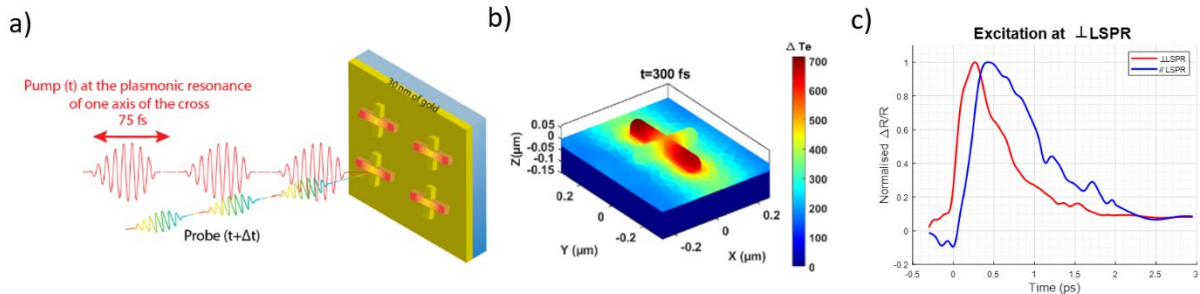

Fig. 1. a) schema of the pump-probe experiment on gold cross-shaped nanoparticles. b) Numerical simulation of the electronic temperature distribution inside the nanoparticles at 300fs after the pulsed light excitation. c) Spectral profiles of ΔR/R for each LSPR associated to each branch.

To go further, we then exploit this mechanism through reversible polarization control to manage heat repartition and time delay inside the nanoparticle.

References

[1] Bresson, P. et al., "Improved two-temperature modeling of ultrafast thermal and optical phenomena in continuous and nanostructured metal films," Phys. Rev. B, vol. 102, no. 15, Oct. 2020.

Correlation effects of electrons emitted from needle tips
by strongly confined ultrashort optical pulses

Stefan Meier, Jonas Heimerl, Peter Hommelhoff

Department of Physics, Friedrich-Alexander-University Erlangen-Nürnberg (FAU), Staudtstraße 1, 91058 Erlangen, Germany, EU
E-mail: stefan.m.meier@fau.de

Optical field enhancement on metallic nanostructures allows the measurement of nonlinear light-matter interactions with moderate laser pulse intensities. In the case of metal needle tips, strongly confined optical near-fields at the tip apex allow triggering ultrashort electron emission by few-cycle laser pulses. Measuring the resulting kinetic energy of these electron pulses enables deep insights in the nonlinear emission process in combination with the subsequent electron dynamics of the electron in the optical near-field. Thus the electron energy spectra intrinsically serve as probe for the optical near-field at these tips [1]. These processes have been well investigated within the past decade. For example, the quenching of the electron quiver motion in the near-field has been shown by the laser wavelength dependence of the electron spectra [2]. By taking advantage of the carrier-envelope phase of the optical laser field, the electron emission can even be controlled on the attosecond timescale [3].

Besides the fundamental insights gained on light-matter interactions, the resulting electron pulses exhibit excellent properties to serve in ultrafast electron devices. We could recently show that the spatial coherence of such an electron beam is as good as its DC equivalent, namely field-emitted electrons from the same tip [4]. In the present study, we go one step further and investigate the spatial coherence properties as function of the average number of electrons per pulse. As the electrons are highly confined in space and time when they are emitted, they are interacting with each other by Coulomb interaction [Fig. 1 (a)]. We show an exponential decrease in the visibility of electron interference measurements [Fig. 1 (b)] depending on the number of emitted electrons per pulse. Example electron interference images are shown in Fig. 1 (c) and 1 (d). The observed reduction of spatial coherence corresponds to an increase in effective source size, as supported by numerical point-particle simulations [5]. We will discuss the implications for important ultrafast electron beam properties.
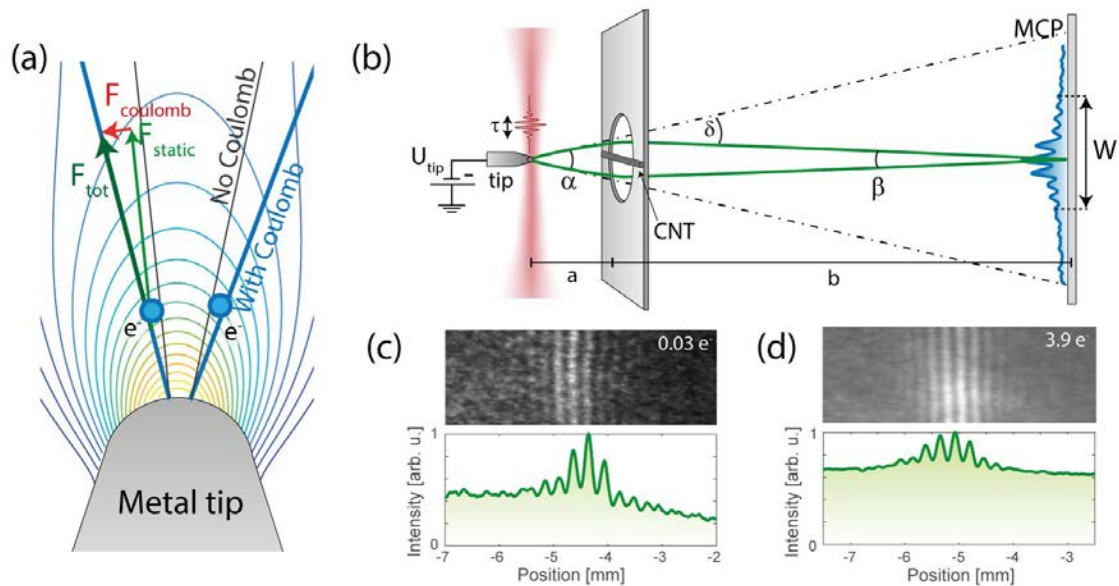

Fig. 1 (a) Illustration of a metal tip with an optical near-field that is triggering the emission of multiple electrons. The electrons interact via Coulomb interaction. (b) Sketch of the experimental setup: few-cycle laser pulses are focused on a biased tungsten needle tip. The resulting electron pulses are passing by a carbon nanotube (CNT), acting as an electrostatic biprism. The electron wave packets interfere and are detected at a micro-channel plate (MCP). (c) Interferogram of the electron beam at low number of electrons per pulse. (d) Interferogram at more than one electrons per pulse. Due to Coulomb interactions, the contrast of the interference pattern is reduced.

References
[1] Thomas, S., Krüger, M., Förster, M., Schenk, M., Hommelhoff, P.. Probing of optical near-fields by electron rescattering on the 1 nm scale. Nano Letters **13**, 4790 (2013)
[2] Herink, G., Solli, D. R., Gulde, M., Ropers, C.. Field-driven photoemission from nanostructures quenches the quiver motion. Nature **483**, 190-193 (2012)
[3] Krüger, M., Schenk, M., Hommelhoff, P.. Attosecond control of electrons emitted from a nanoscale metal tip. Nature **475**, 78-81 (2011)
[4] Meier, S., Higuchi, T., Nutz, M., Högele, A., Hommelhoff, P.. High spatial coherence in multiphoton-photoemitted electron beams. Applied Physics Letters **113**, 143101 (2018)
[5] Meier, S. Hommelhoff, P.. Manuscript under review.